

AD-A089 278

NEW MEXICO UNIV ALBUQUERQUE ERIC H WANG CIVIL ENGINE--ETC F/6 18/3
COMPUTATIONAL MODELING OF SIMULATION TESTS.(U)

JUN 80 6 LEIGH, W CHOWN, B HARRISON

F29601-76-C-0015

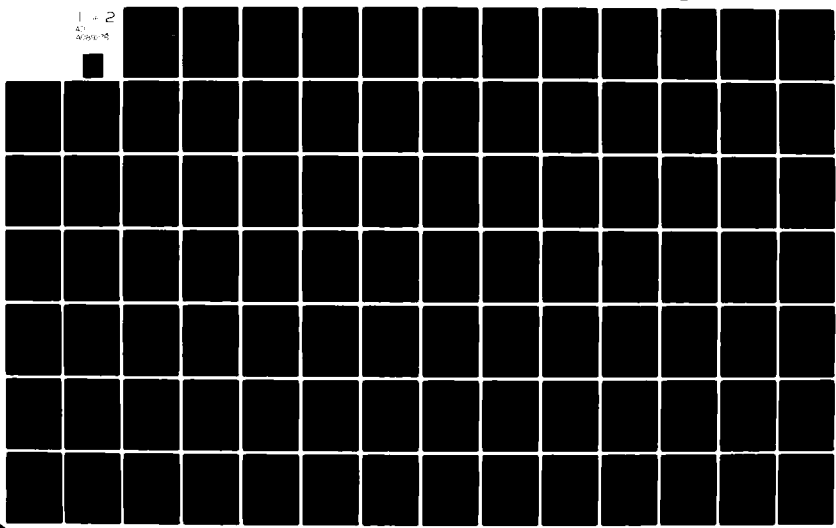
UNCLASSIFIED

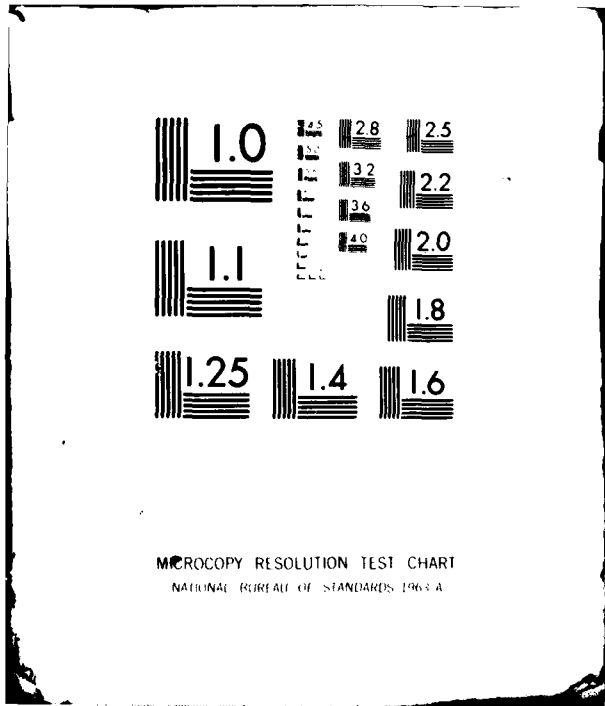
LMM/CERF-AST-86

NL

1 + 2

AD-A089 278





MICROCOPY RESOLUTION TEST CHART
NATIONAL BUREAU OF STANDARDS 1963-A

AFWL-TR-79-128

LEVEL

12
B.S.

AFWL-TR-79-128

AD A089278

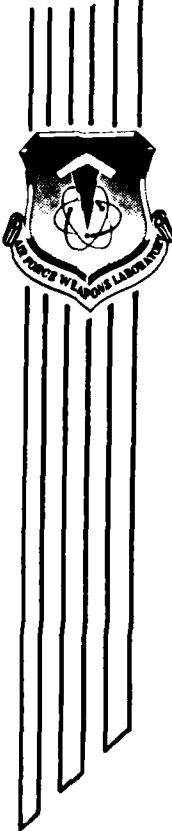
COMPUTATIONAL MODELING OF SIMULATION TESTS

G. Leigh
W. Chown
B. Harrison

Eric H. Wang Civil Engineering Research Facility
University of New Mexico
Albuquerque, NM 87131

June 1980

DTIC
SEP 19 1980



Final Report

Approved for public release; distribution unlimited.

This research was sponsored by the Defense Nuclear Agency under Subtask H35KASXS355, Work Unit 18, Work Unit Title: "0703 Shelter Concept Development."

Prepared for
Director
DEFENSE NUCLEAR AGENCY
Washington, DC 20305

AIR FORCE WEAPONS LABORATORY
Air Force Systems Command
Kirtland Air Force Base, NM 87117

DDC FILE COPY

80 9 19 007

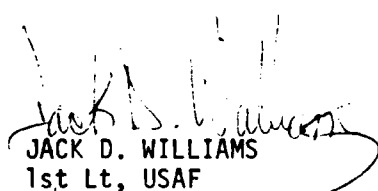
This final report was prepared by the Eric H. Wang Civil Engineering Research Facility, University of New Mexico, Albuquerque, New Mexico, under Contract F29601-76-C-0015, Job Order WDNS3520 with the Air Force Weapons Laboratory, Kirtland Air Force Base, New Mexico. Lieutenant Jack D. Williams (NTED) was the Laboratory Project Officer-in-Charge.

When US Government drawings, specifications, or other data are used for any purpose other than a definitely related Government procurement operation, the Government thereby incurs no responsibility nor any obligation whatsoever, and the fact that the Government may have formulated, furnished, or in any way supplied the said drawings, specifications, or other data, is not to be regarded by implication or otherwise, as in any manner licensing the holder or any other person or corporation, or conveying any rights or permission to manufacture, use, or sell any patented invention that may in any way be related thereto.

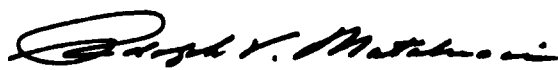
This report has been authored by a contractor of the United States Government. The United States Government retains a nonexclusive, royalty-free license to publish or reproduce the material contained herein, or allow others to do so, for the United States Government purposes.

This report has been reviewed by the Public Affairs Office and is releasable to the National Technical Information Service (NTIS). At NTIS, it will be available to the general public, including foreign nations.

This technical report has been reviewed and is approved for publication.


JACK D. WILLIAMS
1st Lt, USAF
Project Officer

FOR THE DIRECTOR


RUDOLPH V. MATALUCCI
Lt Colonel, USAF
Chief, Simulation Branch


STEWART W. JOHNSON
Lt Colonel, USAF
Chief, Civil Engrg Rsch Division

DO NOT RETURN THIS COPY. RETAIN OR DESTROY.



UNCLASSIFIED

SECURITY CLASSIFICATION OF THIS PAGE (When Data Entered)

REPORT DOCUMENTATION PAGE		READ INSTRUCTIONS BEFORE COMPLETING FORM
1. REPORT NUMBER AFWL-TR-79-128	2. GOVT ACCESSION NO. AD-A089278	3. RECIPIENT'S CATALOG NUMBER
4. TITLE (and Subtitle) COMPUTATIONAL MODELING OF SIMULATION TESTS.	5. TYPE OF REPORT & PERIOD COVERED Final Report.	6. PERFORMING ORG. REPORT NUMBER UNM/CERF-AST-46
7. AUTHOR(s) G. Leigh W. Chown B. Harrison	8. CONTRACT OR GRANT NUMBER(s) F29601-76-C-0015	9. PROGRAM ELEMENT, PROJECT, TASK AREA & WORK UNIT NUMBERS 62704H/WDNS3520
10. PERFORMING ORGANIZATION NAME AND ADDRESS Eric H. Wang Civil Engineering Research Facility University of New Mexico Albuquerque, NM 87131	11. REPORT DATE June 1980	12. NUMBER OF PAGES 162
13. CONTROLLING OFFICE NAME AND ADDRESS Director Defense Nuclear Agency Washington, DC 20305	14. SECURITY CLASS. (of this report) UNCLASSIFIED	15. DECLASSIFICATION/DOWNGRADING SCHEDULE
14. MONITORING AGENCY NAME & ADDRESS (if different from Controlling Office) Air Force Weapons Laboratory (NTED) Kirtland Air Force Base, NM 87117	16. DISTRIBUTION STATEMENT (of this Report) Approved for public release; distribution unlimited.	
17. DISTRIBUTION STATEMENT (of the abstract entered in Block 20, if different from Report)		
18. SUPPLEMENTARY NOTES This research was sponsored by the Defense Nuclear Agency under Subtask H35KASXS355, Work Unit 18, Work Unit Title: "0703 Shelter Concept Development."		
19. KEY WORDS (Continue on reverse side if necessary and identify by block number) Nuclear Airblast Simulation HULL Computer Code High Explosive Simulation SAP Computer Code Dynamic Airblast Simulator Hydrodynamic Computer Codes Numerical Computation		
20. ABSTRACT (Continue on reverse side if necessary and identify by block number) This effort modeled two types of nuclear airblast simulators, the High Explosive Simulation Technique (HEST) and the Dynamic Airblast Simulator (DABS), with hydrodynamic Computer Codes. One dimensional similarity solutions, Modified 1-D, and 2-D calculations are described. High explosive burn routines and energy deposition schemes are described. For the HEST, explosive distribution and cavity configurations were studied. For the DABS, energy deposition, calculational cell size, and a preliminary look at shock-target interactions are presented.		

DD FORM 1 JAN 73 1473

UNCLASSIFIED 400976

SECURITY CLASSIFICATION OF THIS PAGE (When Data Entered)

CONTENTS

Accession For
 NTIS CLEAR
 DDC TAB
 Unannounced
 Justification

By _____

Dist _____

Availability _____

Dist _____

A

<u>Section</u>		<u>Page</u>
I	INTRODUCTION	5
II	CALCULATIONAL TOOLS	
	Similarity Solution	9
	APOD Hydrocode	9
	SAP Hydrocode	11
	HULL Hydrocode	13
III	HEST SIMULATOR CALCULATIONS	15
	One-Dimensional Similarity Solution-- HEST Single Explosive Plane	15
	HULL Hydrocode Calculation--HEST Single Explosive Plane	20
	One-Dimensional Hydrocode Calculations-- HEST Single Explosive Plane	27
	HULL Simulations of Detonating Cord Blast Effects in a HEST Cavity	39
	HULL Simulation of HEST Single Explosive Plane with Sweeping Wave	65
IV	DABS SIMULATOR CALCULATIONS	75
	Parametric Study of Blast Wave Characteristics as a Function of Cell Size and Explosive Charge Density (SAP Hydrocode)	75
	Simulation of 4.14-MPa Reflected Airblast Wave	85
	Parametric Study of SAP Lagrangian Hydrocode	95
	Evaluation of Diffusion Limitation in HULL Code	102
	HULL Numerical Simulation of Normal Reflection of 4.14-MPa Planar Shock Wave	110
	HULL Simulation of Typical DABS Experiment	117
V	CONCLUSIONS AND RECOMMENDATIONS	131
	REFERENCES	133
<u>Appendix</u>		
A	COMPUTER LISTING OF ONE-DIMENSIONAL SIMILARITY SOLUTION PROGRAM FOR PLANAR BLAST WAVE PROBLEM (BASIC LANGUAGE)	135
B	HYDROCODE CALCULATION DATA REPORTS PRODUCED DURING THIS TECHNICAL EFFORT	141
C	PROGRAM SHOK2B	145

ILLUSTRATIONS

<u>Figure</u>		<u>Page</u>
1	Typical HEST Airblast Pressure Trace	7
2	HORS I-3 HEST Experiment Configuration	16
3	One-Dimensional Approximation of HEST Explosion Cavity	16
4	Similarity Solution (Planar Blast Wave)	17
5	One-Dimensional Similarity Solution (Planar Blast Wave-- Multiple Explosive Planes)	19
6	HULL Calculation Mesh (One-Dimensional Planar Blast Wave)	21
7	HULL Calculation (One-Dimensional Planar Blast Wave at 2 and 12 μ s)	22
8	HULL Calculation (One-Dimensional Planar Blast Wave at 16 and 21 μ s)	23
9	HULL Calculation (One-Dimensional Planar Blast Wave-- Pressure Histories)	24
10	HULL Calculation (One-Dimensional Planar Blast Wave-- Pressure Histories--Real Air)	26
11	One-Dimensional Model of HEST Cavity	28
12	HULL Calculation 905.0020--Pressure versus Time	31
13	SAP Calculation 905.0021--Pressure versus Time	32
14	APOD Calculation 905.0022--Pressure versus Time	33
15	SAP Calculation 905.0031--Pressure versus Time	35
16	SAP Calculation 905.0041--Pressure versus Time	36
17	SAP Calculation 905.0051--Pressure versus Time	38
18	Basic Detonating Cord Pattern	40
19	Detonating Cord Patterns	42
20	Incident Wave Systems--Calculation 905.0030	43
21	Wave System at 4 μ s--Calculation 905.0040	45
22	Wave System at 7.5 μ s--Calculation 905.0040	46
23	Calculation 905.0040--HULL Simulation of HORS I-3 HEST Detonating Cord Array	47
24	Shock Wave Interactions--Calculation 905.0060	57
25	Calculation 905.0090--HULL Simulation of HORS I-3 HEST Detonating Cord Array	60
26	Peak Reflected Pressure at Cavity Floor	62
27	Station 7 Pressure	63
28	Station 10 Pressure	64

ILLUSTRATIONS (Continued)

<u>Figure</u>		<u>Page</u>
29	HEST Explosion Cavity with Sweeping Detonation	66
30	Calculation 905.1080--Pressure History at Station 28	68
31	HULL Calculation 905.1080--Sweeping Detonation Wave (48 μ s)	69
32	HULL Calculation 906.1010--Sweeping Detonation Wave (60 μ s)	71
33	HULL Calculaton 906.1020--Pressure History at Station 28	72
34	HULL Calculation 906.1020--Sweeping Detonation Wave (55 μ s)	73
35	HULL Calculations 905.1080 and 906.1020--Instabilities in Calculations	74
36	Calculational Matrix	77
37	Effective History Station Range	77
38	Comparison of Peak Pressures and Waveforms for Different Cell Sizes	78
39	Shock Arrival Time versus Cell Width at Various Ranges	79
40	Shock Rise Time versus Cell Width at Various Ranges	80
41	Peak Pressures versus Cell Width at Various Ranges	81
42	Peak Pressures versus Range at Various Widths	82
43	Impulse versus Cell Width at Various Ranges	83
44	Geometrical Descriptions for Calculations 906.1081 and 906.1091	86
45	Incident Wave History at 65 m	89
46	Incident Wave Profiles at 26 ms	90
47	Incident Wave Profiles at 46 ms	91
48	Reflected Wave Profiles at 36 ms	92
49	Reflected Wave Time History at 65.4 m	93
50	Reflected Wave Profiles at 44 ms	94
51	Unstable Oscillations Produced by SAP Calculations	97
52	Peak Pressure versus Length (Group I)	99
53	Peak Pressure versus Length (Group II)	100
54	Peak Pressure versus Length (Group III)	101
55	Shock Tube Geometry--Calculation 906.0040	103
56	Wave System Diagram--Calculation 906.0040	104

ILLUSTRATIONS (Concluded)

<u>Figure</u>		<u>Page</u>
57	Axial Density Profile--HULL Calculation 906.0040 at 3 ms	107
58	Axial Energy Profile--HULL Calculation 906.0040 at 3 ms	108
59	Axial Pressure Profile--Hull Calculation 906.0040 at 3 ms	109
60	Model Specifications--HULL Simulation 906.1090	111
61	Calculated Peak Pressure--Calculation 906.1090	112
62	Pressure History at 60 m--Calculation 906.1090	114
63	Pressure History at 65.4 m--Calculation 906.1090	115
64	Axial Pressure Profile at 20 ms--Calculation 906.1090	116
65	Axial Density Profile at 20 ms--Calculation 906.1090	118
66	Axial Energy Profile at 20 ms--Calculation 906.1090	119
67	Simulation Model--HULL Calculation 908.0010	120
68	Incident Pressure Versus Range	122
69	Reflected Pressure Ratio versus Angle of Incidence for Various Incident Pressure	123
70	Normal Reflections at Front Face of Target Structure	125
71	HULL Simulation--DABS Parameter Study (Calculation 908.0010)	126
72	Peak Pressures at Top of Target Structure	128

TABLES

<u>Table</u>		<u>Page</u>
1	Comparative Station Locations	29
2	Comparative Pressures and Arrival Times at Three Stations	34
3	Station Locations	67
4	Position of Detonation Products Boundary	88
5	Effects of Calculation Parameters on Peak Pressure	96
6	Driver Region Initial Conditions--HULL Calculation 906.0040	105
B-1	Hydrocode Calculation Data Reports Produced During This Technical Effort	142

SECTION I INTRODUCTION

The signing of the Limited Nuclear Test Ban Treaty in 1963 made necessary the development of methods for simulating nuclear airblast and groundshock effects. The High Explosive Simulation Technique (HEST) was developed during the mid-1960s to simulate airblast pressure and airblast-induced groundshock loadings on near-surface buried structures (Refs. 1 and 2). HEST, as originally devised, did not simulate the dynamic airblast effects (reflected pressures, etc.) which would be experienced by above-ground structural targets. The Dynamic Airblast Simulator (DABS) was developed during the mid-1970s to provide for the testing of above-ground missile shelter concepts (Ref. 3).

The development of these and other nuclear airblast and groundshock simulation methods over the past 15 years was accomplished by primarily experimental methods. Empirically derived expressions based on previous experimental data were used for the design and sizing of future tests (Ref. 4).

As the requirements for more accurate simulation of a wider range of nuclear blast environments continued to grow, these experimental and empirical design methods became less adequate. Certain problems continued to plague each of

1. Auld, H. E., D'Arcy, G. P., and Leigh, G. G., *Simulation of Airblast-Induced Ground Motions (Phase I)*, AFWL-TR-65-11, Air Force Weapons Laboratory, Kirtland Air Force Base, New Mexico, April 1965.
2. Auld, H. E., D'Arcy, G. P., and Leigh, G. G., *Simulation of Airblast-Induced Ground Motions (Phase II)*, AFWL-TR-65-26, Vol. I, Air Force Weapons Laboratory, Kirtland Air Force Base, New Mexico, April 1965.
3. Martens, Daniel P., and Bradshaw, Joel C., *Dynamic Airblast Simulator Parametric Test Series, Events I-A, I-B, I-C, I-D, and I-E Data Report*, AFWL-TR-76-018, Air Force Weapons Laboratory, Kirtland Air Force Base, New Mexico, November 1976.
4. Bratton, J. L., and Pratt, H. R., *Simulation of Airblast-Induced Ground Motions (Phase IIA)*, AFWL-TR-66-85, Air Force Weapons Laboratory, Kirtland Air Force Base, New Mexico, October 1967.

these simulators. Not only did variation of the experimentally derived design parameters fail to provide solutions, but certain phenomena observed in the data defied explanation by purely empirical means.

Over the past 15 years substantial progress has been made in the area of first-principle hydrodynamic calculations. Several large hydrodynamic computer codes (hydrocodes) have evolved with which the simulation methods can be examined in greater detail. A program of hydrocode calculations of the HEST and DABS simulators was undertaken to help understand the basic explosion mechanics of these simulators and to provide improved capabilities for design and prediction.

Some difficulties have been encountered with both the HEST and the DABS simulators which could not be resolved through experimental or empirical techniques. In HEST, high pressure spikes and severe oscillations were often encountered near the beginning of the pressure pulse (Fig. 1). Whether these were caused by positioning individual strands of detonating cord near the pressure gages or by larger shock oscillations within the HEST explosion cavity is not known. Tests conducted in which all explosives in the cavity were initiated nearly simultaneously resulted in greater peak pressures for a given charge density* than tests in which the detonation was caused to propagate through the explosion cavity at some specified rate (sweeping wave). Finally the relation between the charge density in the cavity and the resultant peak pressure was not well-defined for a wide range of pressures and for different explosive materials.

As in HEST the DABS technique must provide waveforms with the desired peak pressure and impulse. In addition DABS must generate blast waves with the appropriate dynamic pressure characteristics. These conditions alone place severe restrictions on the design of DABS. Coupled with the requirement for large-scale testing capability, these conditions make DABS a unique challenge for predictive numerical simulations.

* Charge density--the amount of explosive material per unit volume of explosion cavity.

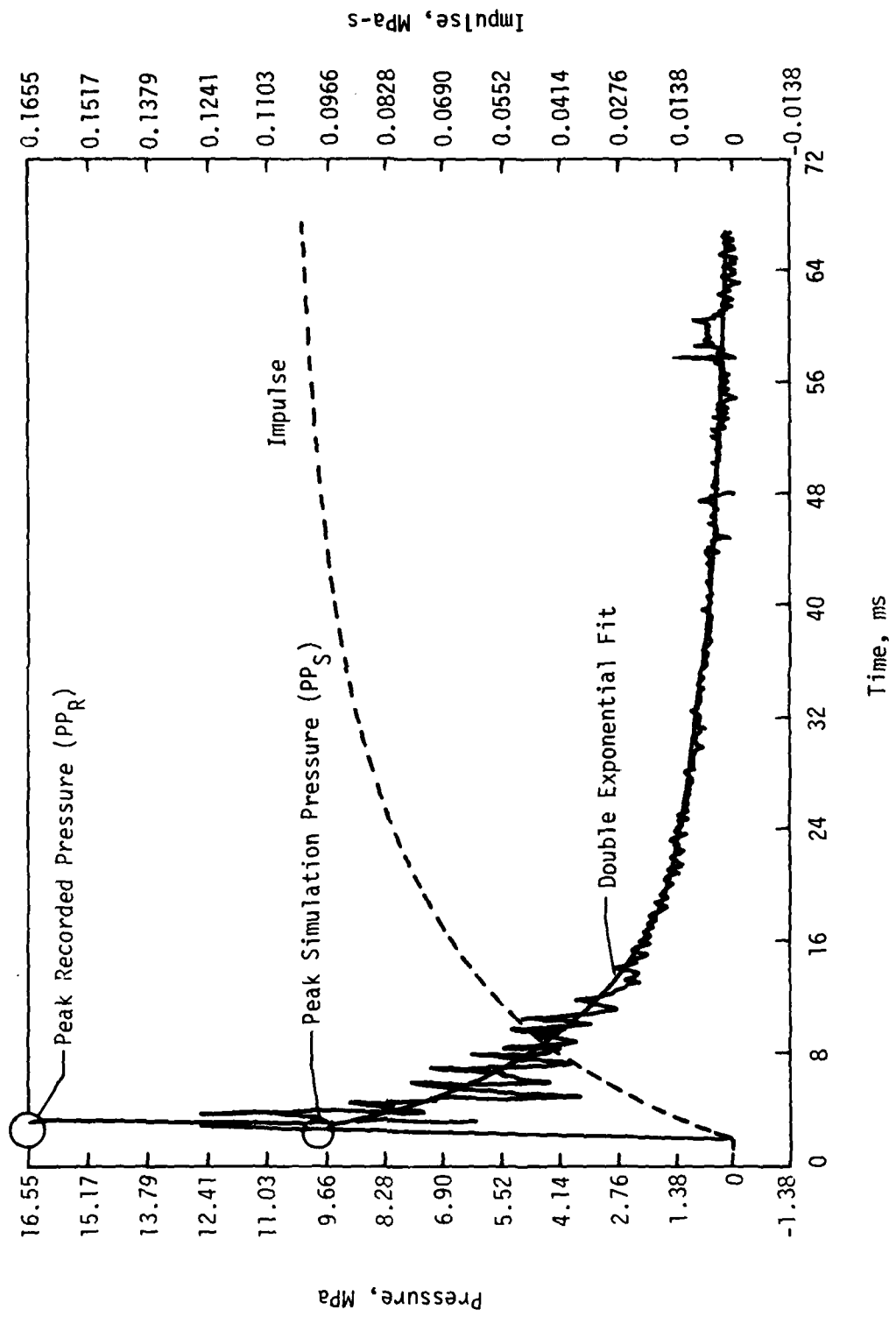


Figure 1. Typical HEST Airblast Pressure Trace

Difficulties encountered with DABS have included uncertainties about explosive charge density in the driver section versus peak pressures and impulse at locations down range, shock interaction from ribs in the trench sections, shock reflections and other interactions involving the contact surface,* and perturbation of the flow field by the test structure. These and other design considerations led to the need for hydrocode calculations to support the further development of these simulation methods. The extent to which the existing hydrocodes could model all aspects of these simulation experiments was not known nor were the costs of performing such calculations. Answers to both of these questions were to be obtained during this technical effort.

*Contact surface--the material interface between the detonation products and the shocked air.

SECTION II CALCULATIONAL TOOLS

The calculational tools used during this technical effort included the one-dimensional (1-D) similarity solution, the APOD 1 1/2-D hydrocode, the SAP 1-D hydrocode (both Eulerian and Lagrangian versions), and the HULL two-dimensional (2-D) hydrocode. Each is briefly described below.

SIMILARITY SOLUTION

The 1-D similarity solution followed the method of Sakurai (Ref. 5) which provides similarity solutions for blast waves in planar, cylindrical, and spherical geometries. A small code was written to computerize this method to ease the solution of a variety of problems. Idealized blast wave problems using a pure energy source in an ideal gas can be calculated out to the point of encounter with a reflecting surface. The similarity solution, however, will not handle shock reflections and thus can only be used to estimate the very early portion of most explosion problems. It also cannot be used to calculate the detonation of high explosive materials in a real gas medium. A listing (in BASIC) of this computer code is provided in Appendix A.

APOD HYDROCODE

APOD is a 1 1/2-D Lagrangian hydrodynamics computer code developed by Mr. Bob Port of Research and Development Associates (RDA), Marina Del Rey, California. The finite differencing scheme in APOD follows the method of S. K. Godunov (Ref. 6). The burn option is somewhat oversimplified but it does allow both left-to-right and right-to-left burn of the explosive driver material. No mixing of material is allowed by this code.

5. Sakurai, A., "On the Propagation and Structure of the Blast Wave, 1," *Journal of the Physical Society of Japan*, Vol. 8, No. 5, September-October 1953.
6. Richtmyer, Robert D. and Morton, K. W., *Difference Methods for Initial-Value Problems*, 2nd Edition, Interscience Publishers.

A real air equation of state (EOS) is used in the reaction portion of the mesh. However, the EOS for the driver section is a modified gamma-law scheme which approximates the driver EOS with a variable gamma dependent upon the ratio of change in cell thickness. Driver mass density and energy density are obtained from data card input on each run.

Cartesian coordinates are employed exclusively in APOD. Reflective and transmissive options for the right boundary condition are written into the code, but they still require internal code modification in order to be switched from one to the other. The left boundary condition, or backwall, was originally coded as an "energy sink," i.e., energy was allowed to pass into a mesh behind the driver section. Because thickness of the cell increased with distance behind the backwall boundary, pressure waves entering this region were never allowed to flow toward the backwall. In a recent modification of APOD* the backwall is now treated as a high-density soil whose behavior is governed by a soil lockup model.**

One of the primary advantages of APOD is the scheme for the expansion of the radial wall. This scheme leads to APOD's being referred to a 1 1/2-D code. In this scheme the main hydrocode is allowed to compute the flow parameters along the main axis. The pressure within a given cell is then used to compute a change in volume of that cell as the cross-sectional area expands due to the pressure. The code then calculates the corresponding change in mass density and loss of energy due to expansion of the cell walls. The same soil lockup model used in the backwall section is also the basis of the wall-expansion method.

APOD does not possess a restart capability. Fortunately, because it is a fast-running code, it can handle all but extremely long calculations. The plotting options for APOD are limited. There is no provision for any

*Chown, W., and Harrison, B. D., *Hydrocode for Calculating Interaction in Typical DABS Configurations*, Task Report, UNM/CERF AST-8, Eric H. Wang Civil Engineering Research Facility, University of New Mexico, Albuquerque, New Mexico, February 1978.

**Seusy, F., *Lock-up Impulse Code Description*, DED-A, Technical Memorandum, Air Force Weapons Laboratory, Kirtland Air Force Base, New Mexico, 5 November 1976.

data snapshots or profile plots. Histories of pressure and pressure-impulse times are overlaid on the same graph for a maximum of 10 stations.

Organization of the code is fixed with practically no flexibility to meet varying calculational demands. If the geometry of the problem changes, major code revisions are required. Another of the major drawbacks of the code is the reverse sense of the major axis. Originally designed for a specific purpose, the axis runs negative to the right, thus reversing the sense of most of the logic, a factor which leads to considerable confusion when internal code tracing is attempted.

SAP HYDROCODE

The SAP is a 1-D hydrocode developed at the Air Force Weapons Laboratory (AFWL) in 1966 by Whitaker et al. (Ref. 7). In 1975 SAP was integrated into the HULL system which used the SAIL updating management system (Ref. 8). The SAIL system provides numerous variations in coding by the appropriate selection of several options. This allows a high degree of versatility in specifying any given calculation.

Two finite differencing options are provided, and the code is adaptable with a minimum of effort to the differencing scheme desired. The first method is a Lagrangian method described in detail in AFWL-TR-66-141 (Ref. 7). The second method is an adaptation of the HULL differencing scheme which offers either Eulerian or Lagrangian methods and is described further in AFWL-TR-76-183 (Ref. 9).

7. Whitaker, W. A., et al., *Theoretical Calculations of the Phenomenology of HF Detonations*, AFWL-TR-66-141, Vol. 1, Air Force Weapons Laboratory, Kirtland Air Force Base, New Mexico, November 1966.
8. Graham, D. C., Gaby, L. P., II, and Rhodes, C. E., Jr., *SAIL, An automated Approach to Software Development and Management*, AFWL-TR-78-80, Air Force Weapons Laboratory, Kirtland Air Force Base, New Mexico, October 1976.
9. Fry, M. A., et al., *The HULL Hydrodynamics Computer Code*, AFWL-TR-76-183, Air Force Weapons Laboratory, Kirtland Air Force Base, New Mexico, September 1976.

Cartesian, cylindrical, or spherical coordinate systems may be elected. SAP may be run on smaller calculations with or without tapes. Because SAP offers a restart capability, a longer calculation may be continued should the calculation be interrupted before completion. The code will compute flows at any angle to the horizontal. The mesh may be rezoned periodically so that the shock is always located interior to the mesh.

SAP uses a real atmosphere that is stable under an R^{-2} gravity field and an air equation of state that is an empirical fit to Hilsenrath's data (Refs. 10 and 11). Six additional formulations provide EOSs for TNT, PBX, 9404, Pentolite, methane, and ammonium nitrate and fuel oil with provisions for including others if desired.

A continuous-burn routine based on Chapman-Jouget theory is present in the code. Any explosive material may be used if EOSs for both the burned and unburned material is known. This routine provides the conditions existing in the gaseous explosive products at the instant the detonation wave reaches the surface of the exploding charge. The routines work for forward burn only. In other words the process must be initiated by starting with at least one cell of burned material at the left-most perimeter of the section of the mesh containing the explosive material.

Some other features of SAP are as follows. First, boundary conditions may be specified by card input as transmissive, reflective, or a specified function of time. Second, one of the tapes used with SAP is a station tape which records the time histories of hydrodynamic variables at particular (fixed) locations. Next, plotting options for SAP allow graphs of pressure, density, and velocity versus radius to be generated at specified times during the calculation. After the calculation is completed a station plotter provides

10. Hilsenrath, J., Green, M. S., and Beckett, C. W., *Thermodynamic Properties of Highly-Ionized Air*, SWC-TR-56-35, National Bureau of Standards, Washington, DC, April 1957.
11. Doan, L. R., and Nickel, G. H., *A Subroutine for the Equation of State of Air*, RTD (WLR) TM-63-2, Air Force Weapons Laboratory, Kirtland Air Force Base, New Mexico, May 1963.

for plots of histories of pressure, pressure-impulse, density, velocity, dynamic pressure, and dynamic pressure-impulse.

Further, a provision for energy loss due to radiation is provided with three different techniques. And finally, to provide a sharply defined stable shock front, there are three viscosity options: 1) no artificial viscosity used, 2) addition of a constant viscosity term, and 3) the addition of a pseudoviscous pressure (Ref. 12).

HULL HYDROCODE

HULL is a 2-D hydrocode written for either Cartesian or cylindrical geometries (Ref. 9). It is an outgrowth of the SHELL-OIL code developed by Johnson in the early 1960s. Matuska and Durrett made the code second-order accurate in time and space in the Lagrangian phase and developed the SAIL software management system in 1971 (Ref. 8), thus providing accuracy and flexibility not previously possible. A 3-D Cartesian version is under development.

The HULL code was originally designed to model fluid behavior in a multi-dimensional Eulerian continuum. As a result of an extensive and on-going development program this code has evolved into a sophisticated and versatile computational tool. Among its capabilities are the simulation of high-explosive detonations, nuclear weapons effects (including airblast precursors), diffusion limitation for multimaterial environments, and so on. HULL is used in conjunction with the SAIL preprocessor program which efficiently tailors the calculational coding to the problem specifications.

The basic HULL code solves finite-difference analogs for a set of partial differential equations which govern the behavior of a compressible, nonconducting, inviscid fluid. The local state variables are updated in two phases.

-
12. Needham, C. E., *Development of an Artificial Viscosity Function*, AFWL-TR-77-53, Air Force Weapons Laboratory, Kirtland Air Force Base, New Mexico, August 1977.

First, the velocity and energy state of the fluid are advanced in time by a Lagrangian calculation. In the absence of mesh gradients this method is fully second-order accurate in the Lagrangian phase. Then, instead of reconfiguring the calculational mesh to complete the Lagrangian phase, final fluid properties are redefined in an Eulerian reference system by taking into account the flux of mass, momentum, and energy.

Two features of HULL are of particular importance when considering HEST and/or DABS simulation experiments. Detonation phenomena can be simulated by routines which both model the burning of an explosive and limit diffusion when treating several material species in the Eulerian framework. An algorithm controls the burning process so that the detonation propagates sequentially through the mesh at the local sound speed and in the direction of the local pressure gradient. Equations of state for both the unburned explosive and detonation products are used to update the relative masses and the internal energy as the detonation progresses. The HULL code diffusion limiter plays a significant role in such a multimaterial environment. It tends to restrict the mixing of species in the direction of flow and thereby preserves contact discontinuities which are characteristic of explosively generated blast waves. Diffusion is constrained by an algorithm which arbitrarily adjusts the flux of mass by giving preference to those species already downstream.

Options available for use with HULL include multimaterial modeling, high-explosive burn, immovable islands, stations, and special input-boundary conditions. The islands permit calculation of shock interactions with structures. The boundary conditions permit input from previous SAP or HULL calculations. The stations allow description of all the hydrodynamic variables as a function of time at any designated point in the calculational space.

SECTION III HEST SIMULATOR CALCULATIONS

The pressures and shock oscillations produced during the explosion of a HEST cavity are of substantial interest to the community of research in simulation development. A number of complex hydrocode calculations have been performed to further understand and define these HEST characteristics. To achieve a crude approximation of HEST cavity pressures, a 1-D similarity solution was generated for comparison with a recently performed HEST experiment. The HEST Over Rectangular Slab (HORS) I-3 experiment (Ref. 13) produced good pressure data and was selected for calculational modeling using a 1-D similarity approximation. The HORS I-3 HEST configuration, depicted in Figure 2, contains five planes of explosive materials in a 355.6-mm explosion cavity. A first approximation for this experiment is achieved by considering the five explosive planes in the experiment to be consolidated into a single plane located along the midplane of the cavity (Fig. 3). The charge density of 2×10^{-5} g/mm³ used in the experiment is equivalent to a planar charge density of 4.297×10^8 ergs/mm². The foam-filled cavity used in HORS I-3 is considered to be filled with an ideal gas ($\gamma = 1.4$). Upon initiation, shock waves propagate from either side of the explosive plane and eventually impinge on the cavity boundaries. Since the cavity is symmetrical about the explosive plane, only a half-space need be calculated.

ONE-DIMENSIONAL SIMILARITY SOLUTION--HEST SINGLE EXPLOSIVE PLANE

The results from the similarity solution are shown in Figure 4. To carry the solution beyond the point of arrival of shock at the boundary is not valid because the similarity solution does not hold for reflected shocks.

-
13. Gagnon, L. W., *HEST Over Rectangular Slab (HORS)--Phase I*, AFWL-TR-78-238, Air Force Weapons Laboratory, Kirtland Air Force Base, New Mexico, March 1979.

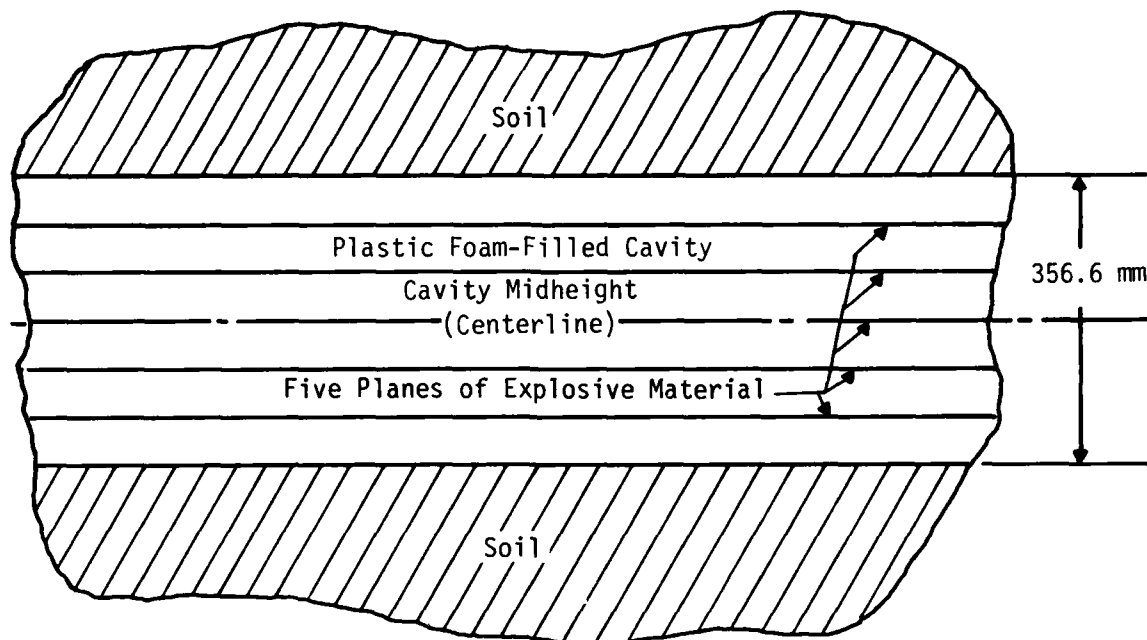


Figure 2. HORS I-3 HEST Experiment Configuration

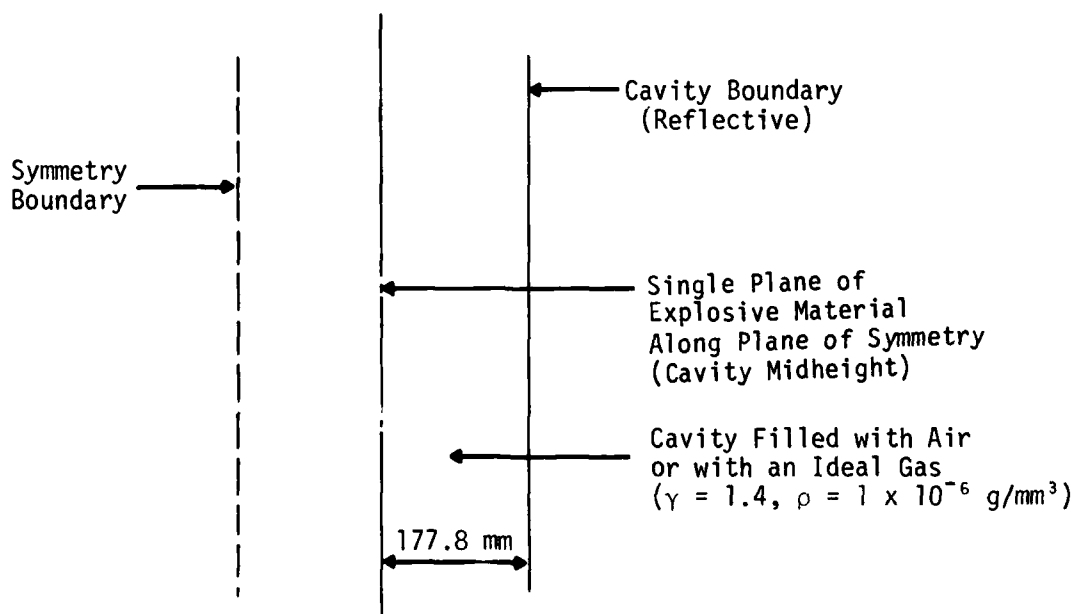


Figure 3. One-Dimensional Approximation of HEST Explosion Cavity

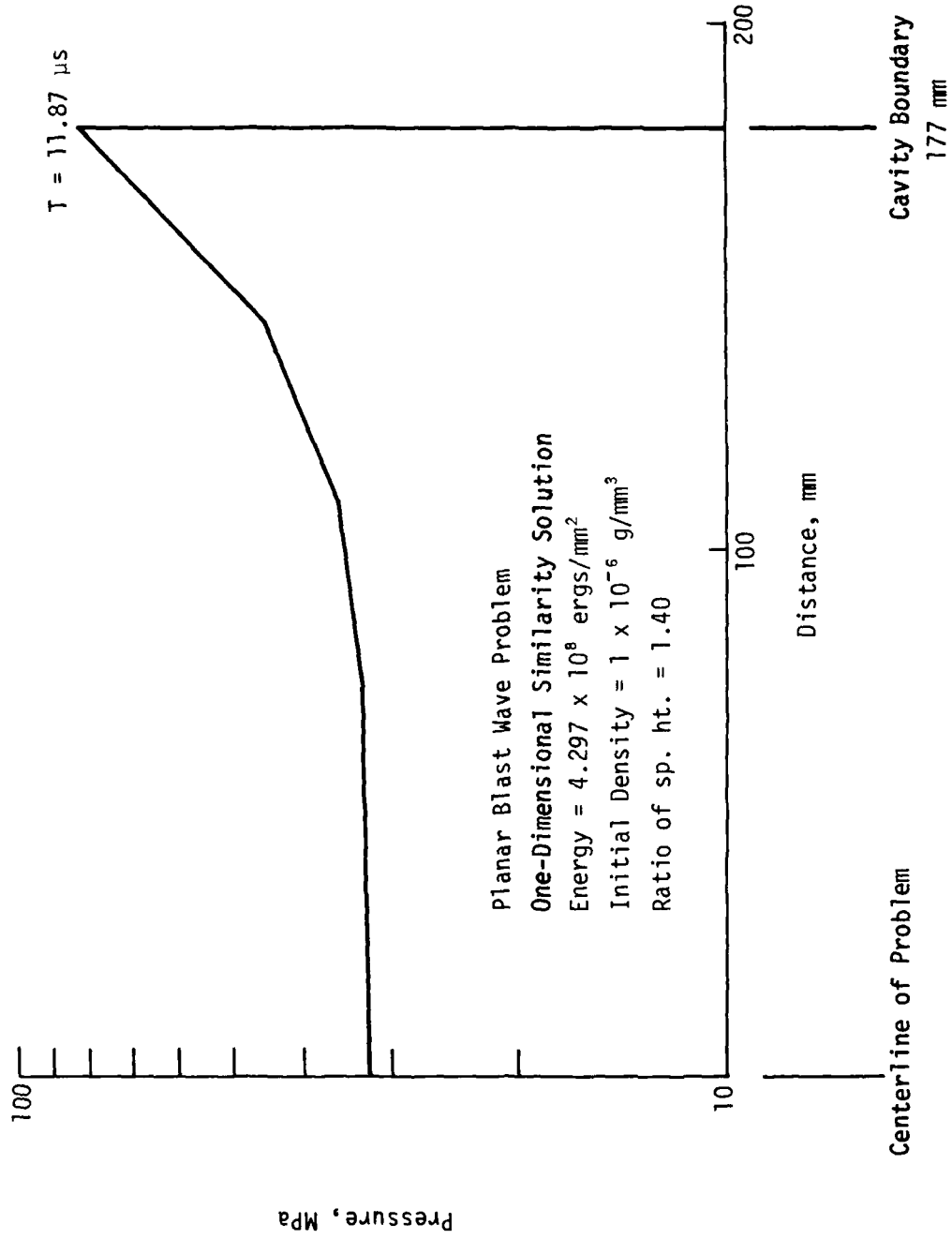


Figure 4. Similarity Solution--Planar Blast Wave

The solution shows the shock arrival at the cavity edge (177.8 mm) at 11.87 μ s with a peak pressure of 83.5 MPa which would cause reflected shocks in the neighborhood of 665 MPa (Ref. 14). The cavity equilibrium pressure near the center of the cavity at this time is approximately 32 MPa. The data from the experiment showed the cavity equilibrium pressure (peak simulation pressure) to be approximately 34.65 MPa and the peak recorded pressure spikes to be in excess of 207 MPa. There is some question as to whether the instrumentation system was able to respond to higher frequency transient pressure spikes. Hence reflected shocks with magnitudes in the range of 665 MPa may have occurred but were not recorded.

A second 1-D model of the HEST cavity contained five explosive planes as shown in Figure 2. The same amount of explosive energy as in the previous problem (single midheight plane-- 4.297×10^8 ergs/mm²) was considered to be distributed uniformly among the five planes of explosive material, i.e., 8.594×10^7 ergs/mm² at each plane. The explosion from the plane nearest the cavity boundary was calculated out to the time of arrival at the cavity boundary using the 1-D similarity solution. The results, plotted in Figure 5, show the shock arriving at the cavity boundary at 5.12 μ s with a peak incident pressure of 49.728 MPa which is substantially less than the 83.5 MPa obtained with the single midheight plane of explosives. Hence it appears that a greater dispersion of the explosives in the HEST cavity leads to a reduction in the peak incident pressure arriving at the cavity boundary (and a reduction in resulting reflected pressures) along with an earlier arrival of the first shock.

The 1-D similarity solution has provided a first-order approximation for the initial blast wave produced in HEST experiments which can serve as a basis for comparison for the hydrocode calculations.

14. Kinney, G.F., *Explosive Shocks in Air*, McMillan, p. 57., 1962

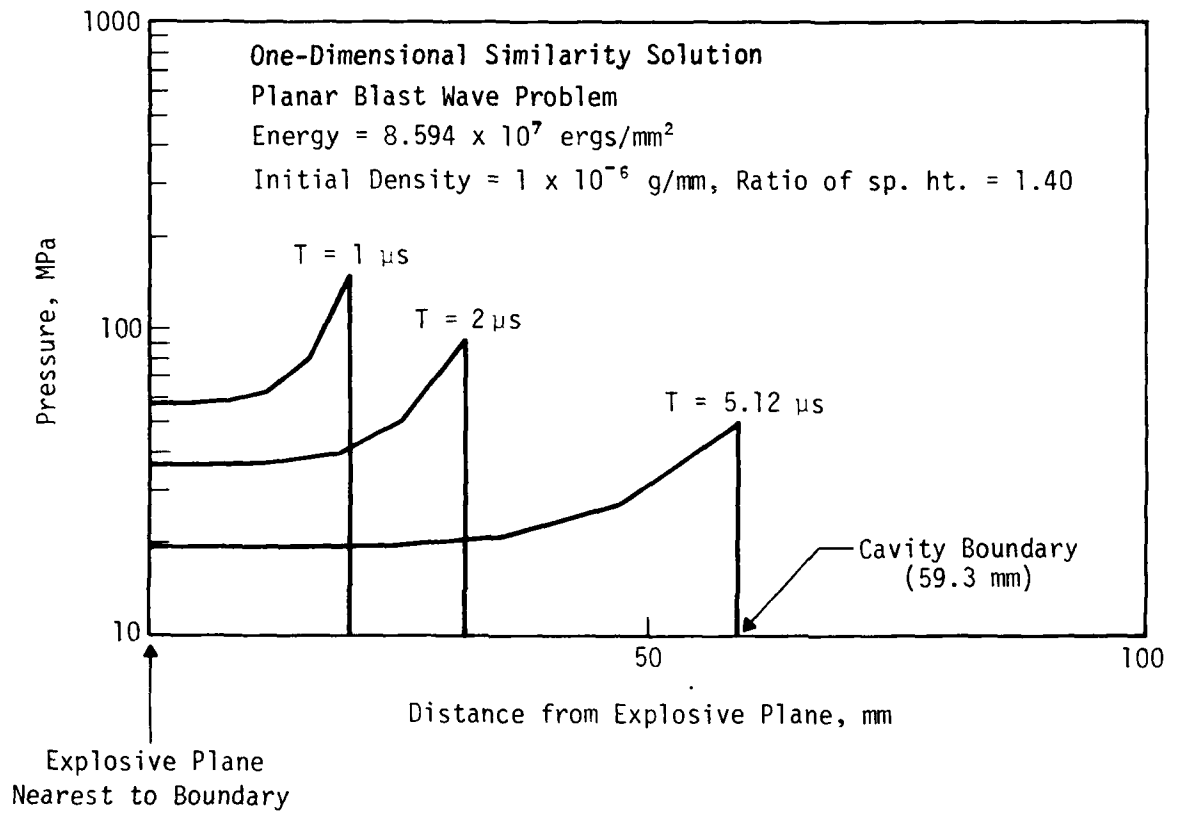


Figure 5. One-Dimensional Similarity Solution (Planar Blast Wave--
Multiple Explosive Planes)

HULL HYDROCODE CALCULATION--HEST SINGLE EXPLOSIVE PLANE*

A HULL calculation (No. 905.0020)** was performed for comparison with the 1-D similarity solution discussed previously (Fig. 3). A 6- by 72-cell Cartesian mesh was used with the left boundary considered to be the midheight of the HEST cavity (Fig. 6). The right boundary was set to be reflective in order to simulate the floor of the HEST explosion cavity. Top and bottom boundaries were also set to be reflective. The mesh was loaded initially with an ideal gas having a gamma of 1.4 and a density of 1.225×10^{-6} g/mm³. A quantity of energy (5.4567×10^8 ergs) was introduced into each of the cells along the left boundary at time zero to initiate the explosion process. This deposition resulted in a planar energy density along the midplane of 4.358×10^8 ergs/mm² (half being introduced on each side of the midplane). The value of 4.358×10^8 differs slightly from the 4.297×10^8 value used in the 1-D similarity solution because of an adjustment in the mesh cell size which was made while setting up the problem.

The results of this HULL calculation are shown in Figures 7 through 9. Figure 7a shows the calculated shock wave at 2 μ s moving from the plane of symmetry (left boundary) toward the right boundary (located at 177.8 mm). Figure 7b shows the shock immediately before arrival at the reflecting boundary. The time is 12 μ s and the peak overpressure is 81.31 MPa, which agrees well with the 11.87 μ s and 83.87 MPa obtained from the similarity solution.

Shock reflections from rigid surfaces can be calculated with the HULL code. Figure 8a shows the calculated wave profile at 16 μ s, a short time after reflecting at the right boundary. It is shown to be moving back toward the plane of symmetry and has a peak pressure of 389 MPa. Figure 8b shows the profile of the reflected wave at 21 μ s as it continues to move toward the left with the peak pressure now down to 114 MPa.

*A table listing all of the hydrocode calculation data reports produced during this technical effort is provided in Appendix B.

**Hydrocode Calculation 905.0020, Data Report, UNM/CERF AST-35, December 1978.

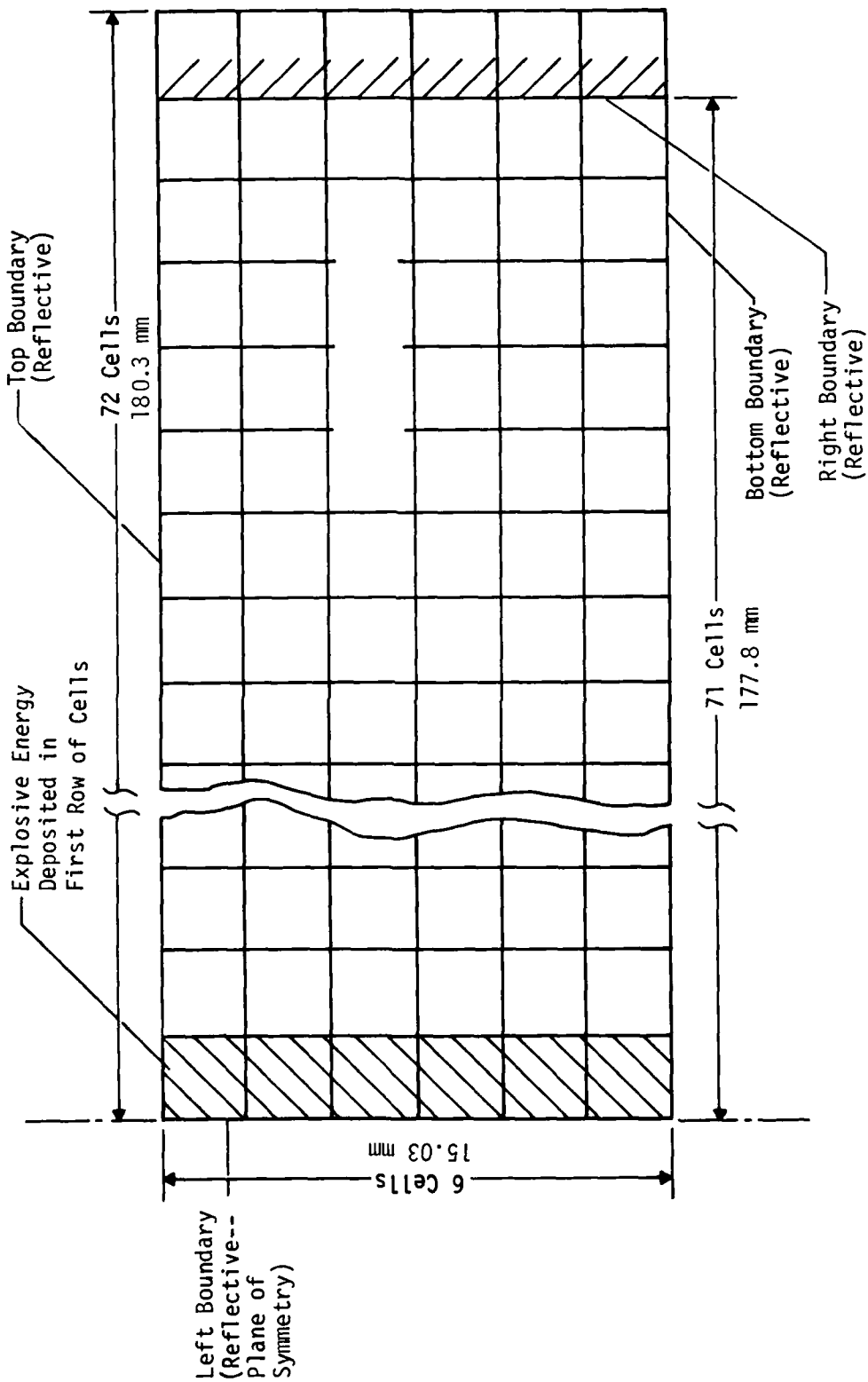


Figure 6. HULL Computational Mesh (One-Dimensional Planar Blast Wave)

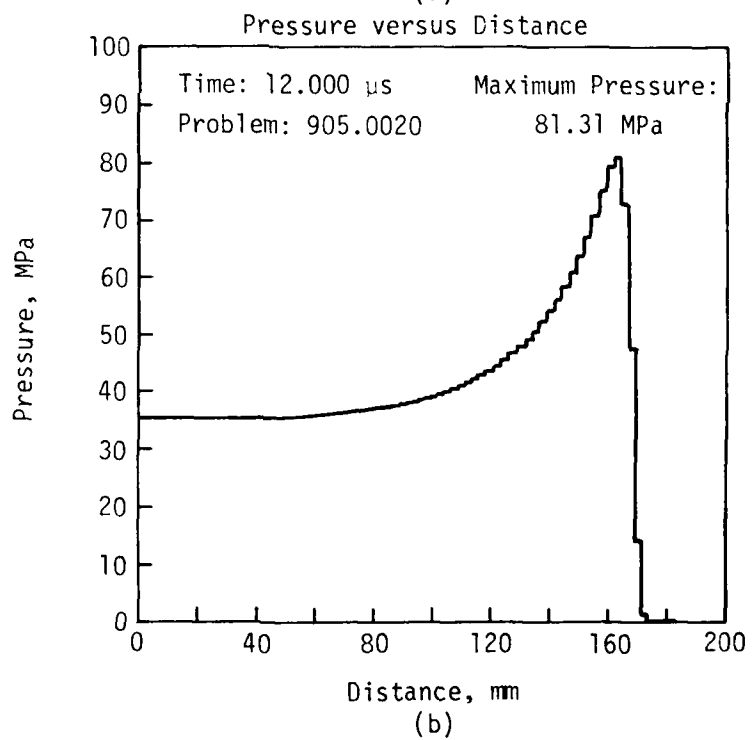
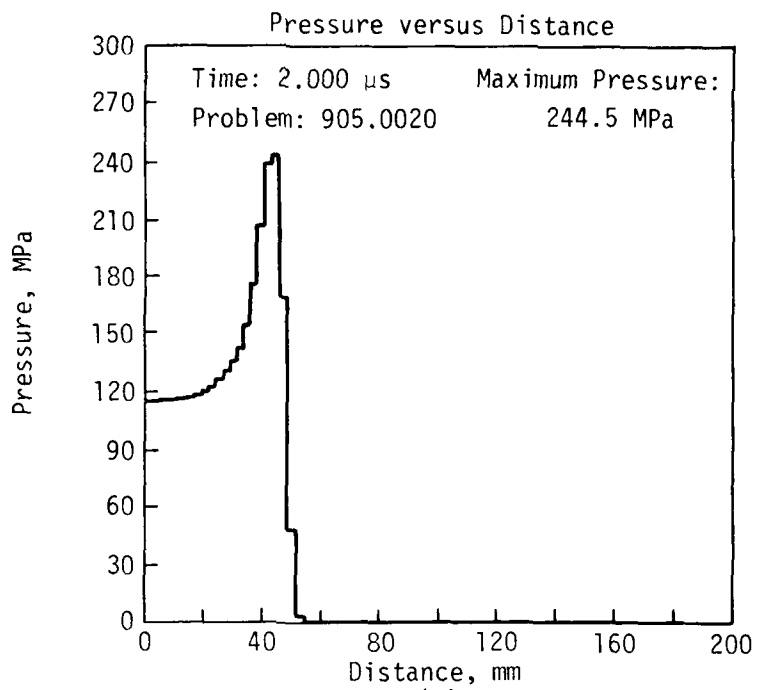


Figure 7. HULL Calculation (One-Dimensional Planar Blast Wave at 2 and 12 μ s)

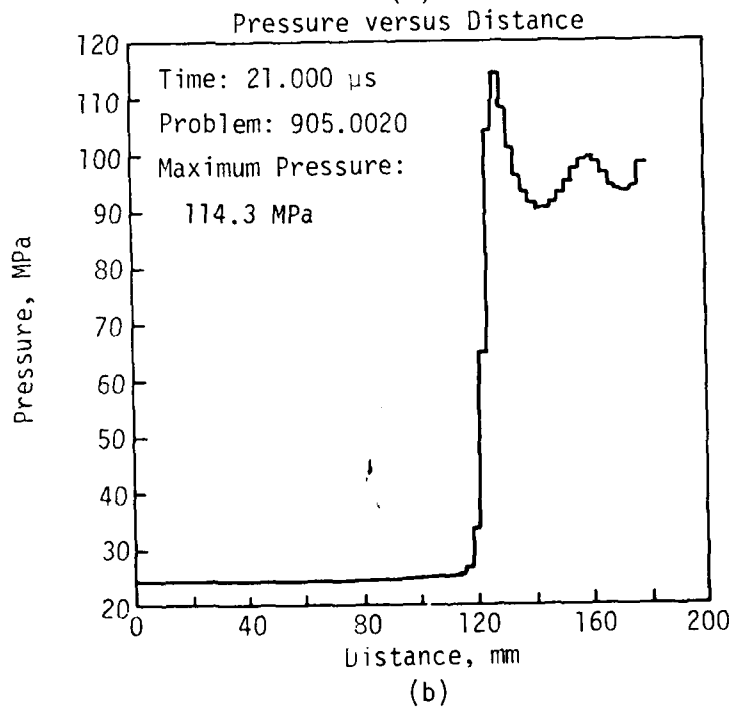
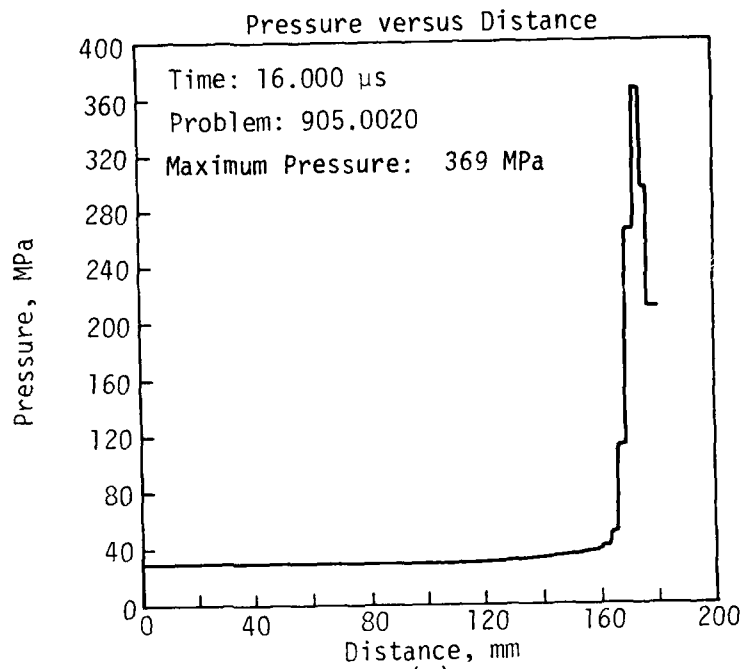


Figure 8. HULL Calculation (One-Dimensional Planar Blast Wave at 16 and 21 μ s)

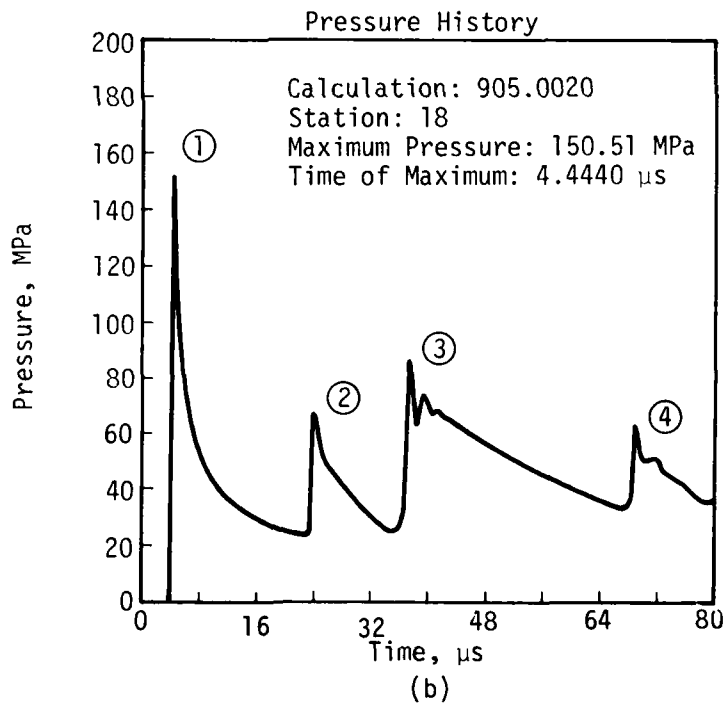
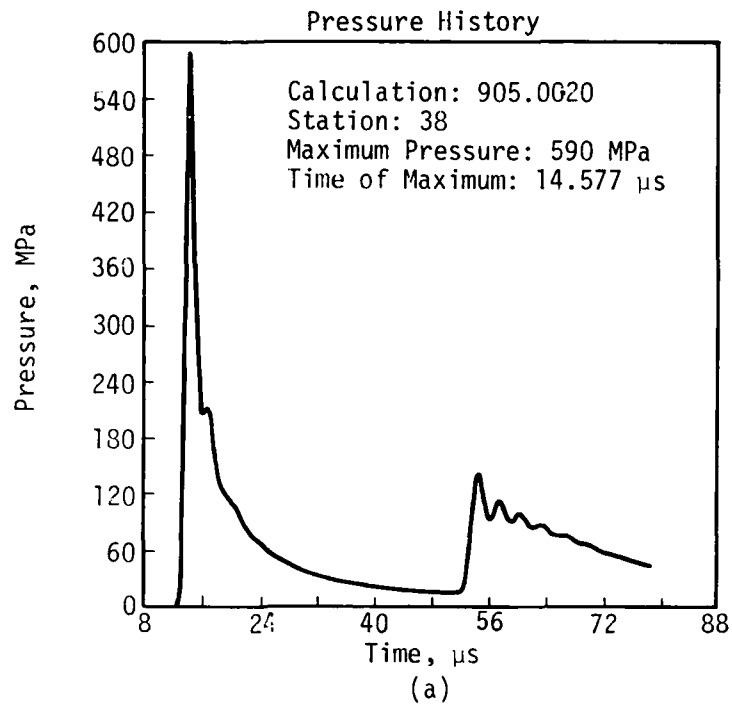


Figure 9. HULL Calculation (One-Dimensional Planar Blast Wave-- Pressure Histories)

Figures 9a and 9b are history plots of calculated pressures for two gage stations. Station 38 is at the right reflecting boundary (177.8 mm) and Station 18 is midway between the plane of symmetry and the right boundary. The peak reflected pressure at the right boundary is 589 MPa, occurring at 14.57 μ s. The readings are in reasonable agreement with the estimate of 665 MPa based on the similarity solution. The arrival and reflection of the shock from the right boundary a second time can also be seen in Figure 9a. The peak reflected pressure is substantially lower the second time (140 MPa) due to the second shock traveling through previously shocked ideal gas and to pseudoviscous effects inherent in the HULL code. Figure 9b shows four distinct shock arrivals which are identified as 1) the first arrival of the incident wave traveling from the plane of symmetry toward the right boundary, 2) the arrival of the reflected wave from the right boundary, 3) the arrival of the reflected wave from the plane of symmetry, and 4) the arrival of the second reflection from the right boundary. The small oscillations in the waveform following the third and fourth peaks are caused by instabilities in the calculation.

From these results it can be seen that in a HEST experiment where a single plane of explosive is placed at the midheight of the explosion cavity, a large pressure spike, many times the magnitude of the cavity equilibrium pressure, is to be expected at the floor of the cavity. Numerous shock oscillations can be expected throughout the cavity during the first few milliseconds of the experiment.

Calculation 905.0020 was repeated in calculation 905.0050* except that the equation of state [$P = f(\rho, E)$] described the explosion cavity gases as real air instead of an ideal gas. The resulting pressure history plots for Stations 38 and 18 (which are the same stations shown in Figure 9) are shown in Figure 10. Although the wave shapes are similar a significant reduction in peak pressures (approximately one-half) and a delay in arrival times can be observed when compared with Figure 9. This would tend to

*Hydrocode Calculation 905.0050, Data Report, UNM/CERF AST-33, December 1978.

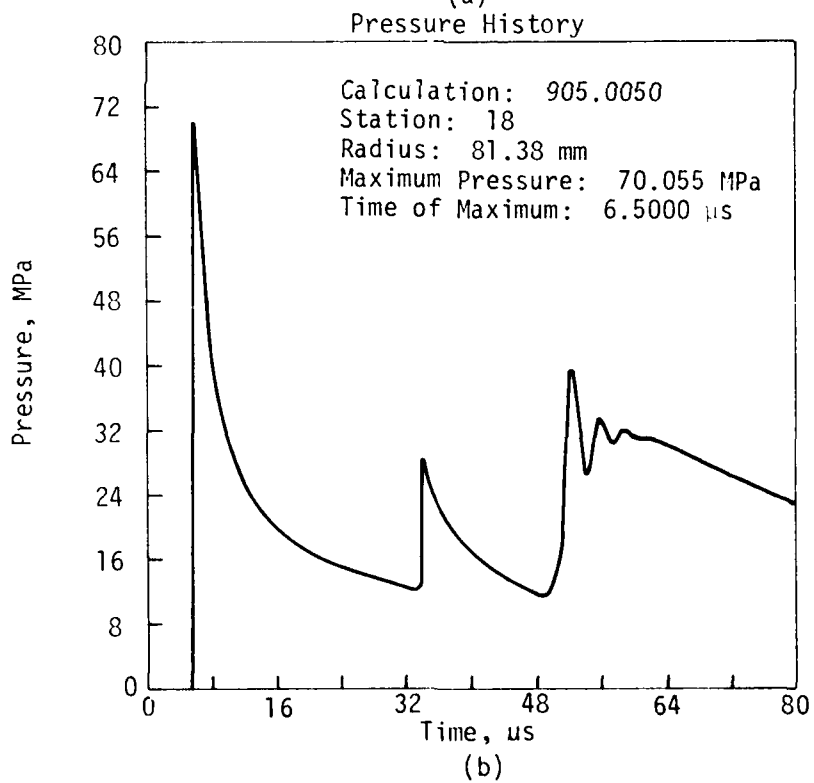
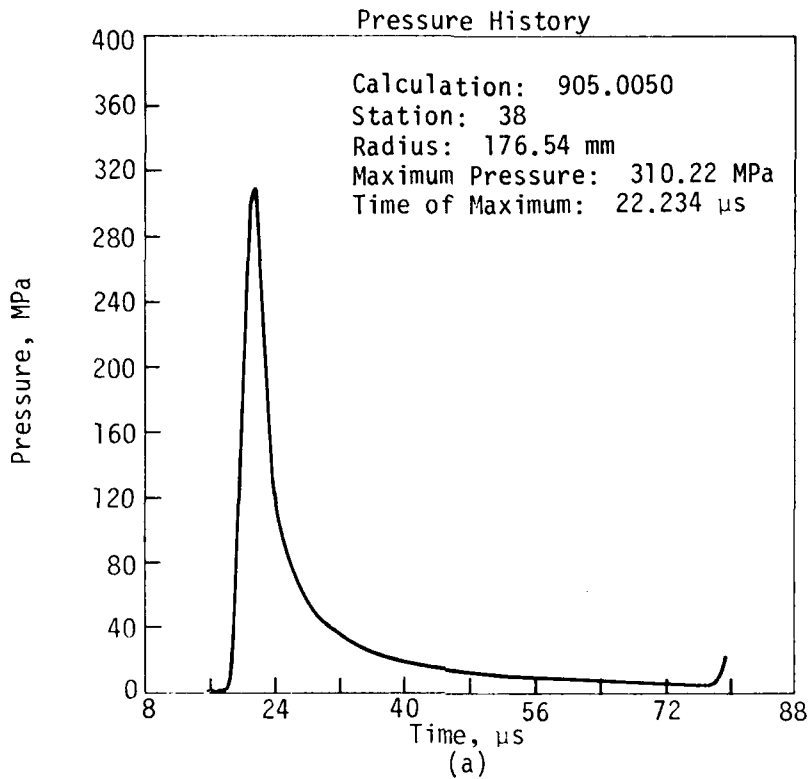


Figure 10. HULL Calculation (One-Dimensional Planar Blast Wave--Pressure Histories--Real Air)

discredit the previously mentioned reasonable agreement between the 1-D similarity solution and the HORS I-3 experiment. Such may not be the case. Recalling that the explosion cavity in the HORS I-3 experiment was filled with a polystyrene plastic foam material, it is quite possible that the departure from real air behavior caused by the plastic foam would cause similar results to those caused by the use of an ideal gas EOS (e.g., higher peak pressures and more rapid shock propagation). This issue is not fully resolved and more study is required to completely answer the question.

ONE-DIMENSIONAL HYDROCODE CALCULATIONS--HEST SINGLE EXPLOSIVE PLANE

The objective of this calculational study was to evaluate various other methods for computer simulation of the test environment existing in a HEST explosion cavity. Calculations were performed using the SAP and APOD hydrocodes. The configuration selected as a baseline for comparison was an air-filled cavity as shown in Figure 3. The plane of symmetry represents the cavity midheight as well as the location of the explosive plane. The specifications for the HORS I-3 experiment (355.6 mm cavity height and 4.297×10^8 ergs/mm² planar explosive charge density) were used to model the calculations within a Cartesian mesh. Detonation of the explosive plane was modeled to occur instantaneously along this midplane.

Five calculations (905.0021, 905.0022, 905.0031, 905.0041, and 905.0051)* were made simulating the one-dimensional flow between the plane of symmetry and the reflecting soil boundary. The APOD hydrocode was used for 905.0022 and the SAP hydrocode was used for the rest. The plane of symmetry was also treated as a reflecting boundary. Four of the calculations modeled the material within the main cavity as an ideal gas with a constant value for gamma (1.4). The fifth calculation modeled this region with a real

*Hydrocode Calculation 905.0021, Data Report, UNM/CERF AST-34, December 1978.
Hydrocode Calculation 905.0022, Data Report, UNM/CERF AST-22, December 1978.
Hydrocode Calculation 905.0031, Data Report, UNM/CERF AST-21, December 1978.
Hydrocode Calculation 905.0041, Data Report, UNM/CERF AST-23, December 1978.
Hydrocode Calculation 905.0051, Data Report, UNM/CERF AST-24, December 1978.

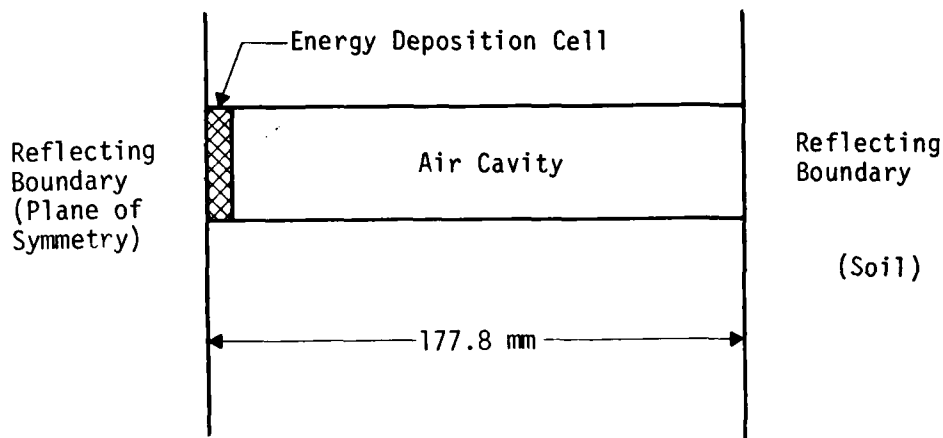


Figure 11. One-Dimensional Model of HEST Cavity

air EOS. The mesh was initialized with a mass density of $1.225 \times 10^{-6} \text{g/mm}^3$ and an energy density of $2.067484 \times 10^9 \text{ ergs/g}$ which yielded an ambient pressure of 0.102366 MPa within the reaction cavity. Energy, corresponding to one-half the charge density, was deposited in the cell next to the plane of symmetry as shown in Figure 11.

Data history stations were placed as shown in Table 1 for the three hydrocodes used (the HULL calculation 905.0020 has been included). Station radius is the distance of the station from the plane of symmetry. The reflecting boundary was located at 177.8 mm (between SAP Stations 38 and 39). Stations beyond 177.8 mm were used in SAP calculations 905.0031 and 905.0041 which treated the reflecting boundary as the surface of a very dense gas rather than a rigid wall.

Calculations 905.0020, 905.0021, and 905.0022 were run to formulate a direct comparison of the results of the HULL, SAP, and APOD hydrocodes respectively. Input parameters were specified to make the initial conditions in the three calculations agree as closely as possible. APOD is a purely Lagrangian code

TABLE 1. COMPARATIVE STATION LOCATIONS

Station Radius, mm	HULL Station No.	SAP Station No.	APOD Station No.
1.25	1	1	1
3.75	2	2	2
6.26	3	3	3
11.26	4	4	--
16.27	5	5	--
21.28	6	6	--
26.29	7	7	--
31.30	8	8	--
36.31	9	9	4
41.31	10	10	--
46.32	11	11	--
51.33	12	12	--
56.34	13	13	--
61.35	14	14	--
66.36	15	15	--
71.37	16	16	5
76.37	17	17	--
81.38	18	18	--
86.39	19	19	--
91.40	20	20	--
96.41	21	21	--
101.41	22	22	--
106.42	23	23	6
111.43	24	24	--
116.44	25	25	--
121.45	26	26	--
126.46	27	27	--
131.46	28	28	--
136.47	29	29	--
141.48	30	30	7
146.49	31	31	--
151.50	32	32	--
156.51	33	33	--
161.51	34	34	--
166.52	35	35	--
171.53	36	36	8
174.03	37	37	9
176.54	38	38	10
179.04	--	39	--
181.55	--	40	--
184.05	--	41	--
191.57	--	42	--

while both HULL and SAP contain both Eulerian and Lagrangian features. Figures 12, 13, and 14 show comparable pressure history plots at two stations for each of the three calculations.

Table 2 presents a comparison of the peak values at these stations. The lower curve of Figure 12 represents the HULL solution for the station immediately in front of the reflecting boundary (Station 38). The peak reflected pressure at the right boundary is 589.84 MPa occurring at 14.577 μ s. The reflection of the shock from the right boundary a second time can also be noted. This second peak is substantially lower (140 MPa) due to the change in properties of the ideal gas after the passage of the first shock and to pseudoviscous effects within the HULL hydrocode. The upper curve of Figure 12 is for Station 30 which is 141.48 mm from the plane of symmetry and shows four distinct shock arrivals which are identified from left to right as 1) the initial arrival of the incident wave traveling from left to right, 2) the arrival of the reflected wave from the right boundary, 3) the arrival of a wave reflected from the plane of symmetry, and 4) the arrival of the second reflection from the right boundary. The HULL and SAP curves (Figs. 12 and 13) are almost identical in shape and arrival time. The APOD curves (Fig. 14) have the same general form but the peak values are somewhat lower and the shock waveforms are definitely smeared, taking on an overdamped appearance rather than the sharp definition of the other two solutions.

In calculations 905.0031 and 905.0041 the reflecting wall of the HEST cavity was simulated with a nonrigid, partially reflecting heavy gas (the rigid wall of 905.0021 was replaced with additional cells of ideal gas which had a mass density of 1.602×10^{-3} g/mm³). A gamma coefficient of 1.05 and an energy density of 1.279×10^7 ergs/g were selected for 905.0031, while 905.0041 used the same gamma (1.4) used in the main cavity and an energy density of 1.581×10^6 ergs/g. In both calculations the energy density was computed as a function of the specified mass density and gamma so that the ambient pressure would match that of the main cavity. Figures 15 and 16 show the pressure histories for these two calculations at the same two stations as shown previously (Figs. 12, 13, and 14). Note in Table 2 and Figure 15 that calculation 905.0041 produces the first reflections with reduced peaks and slightly delayed arrival times, but that all of the secondary reflections

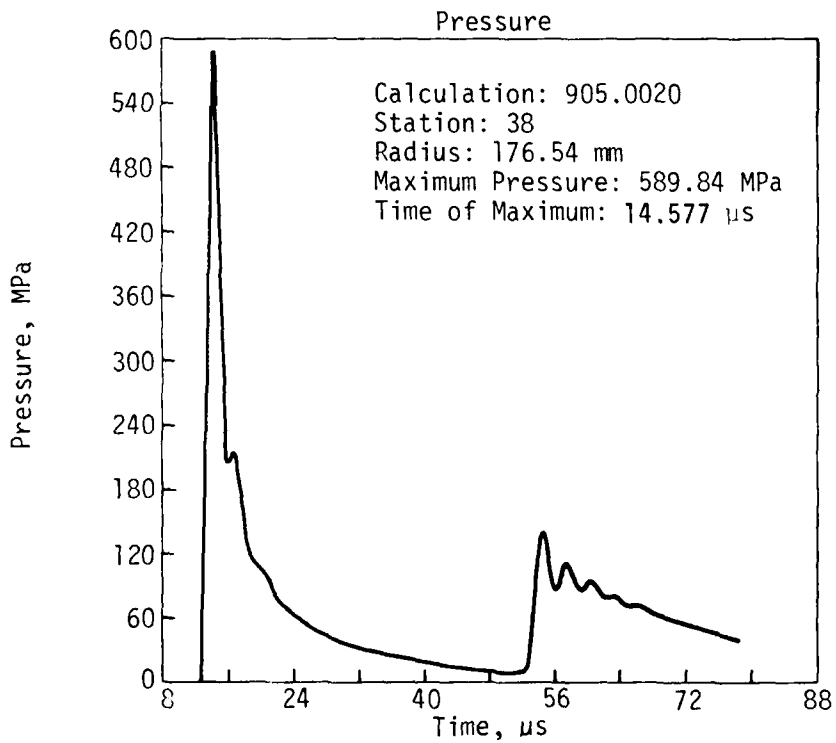
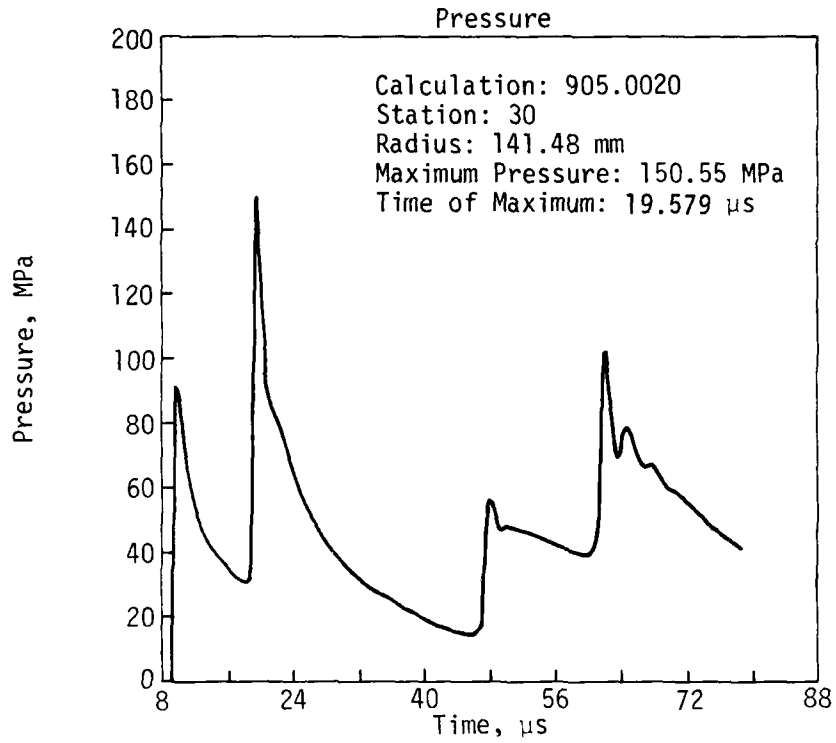


Figure 12. HULL Calculation 905.0020--Pressure versus Time

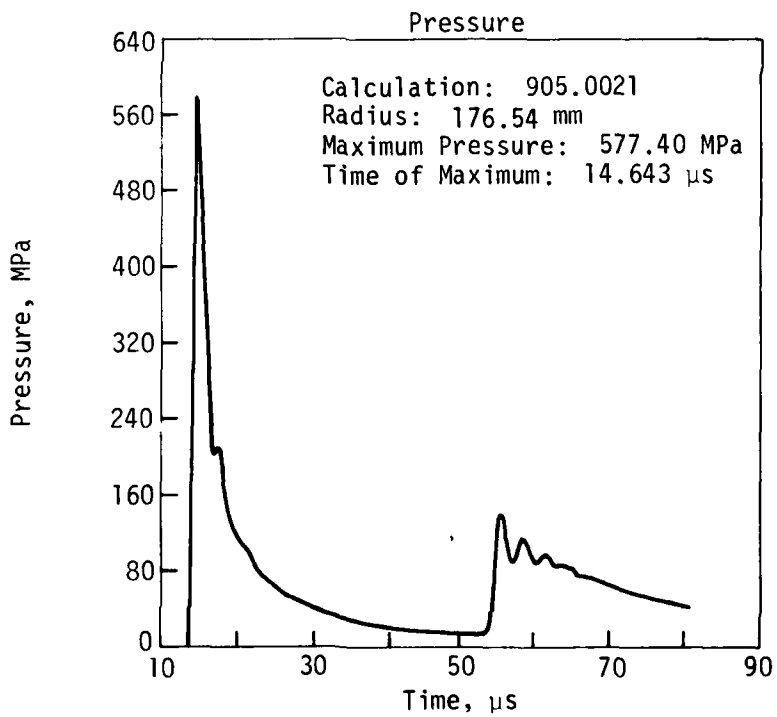
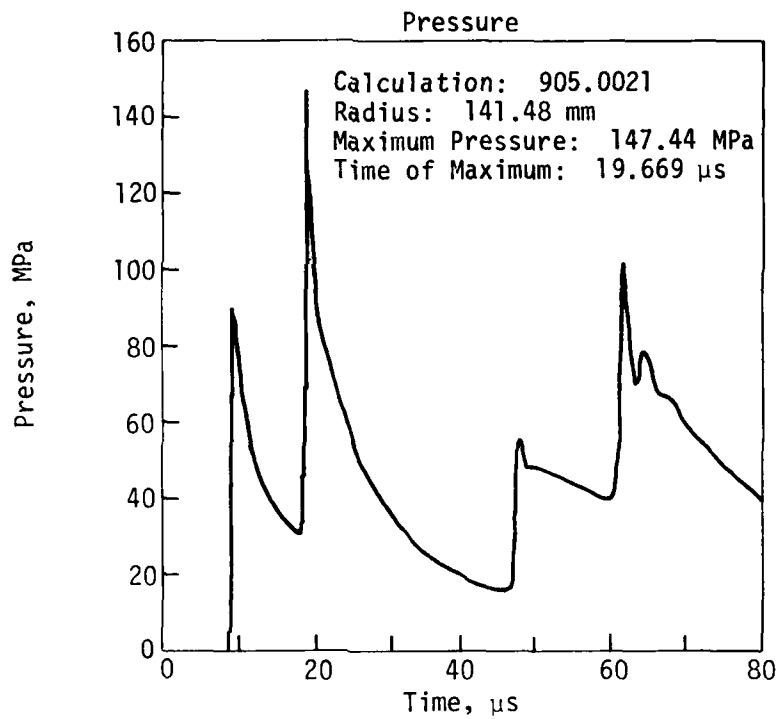


Figure 13. SAP Calculation 905.0021--Pressure versus Time

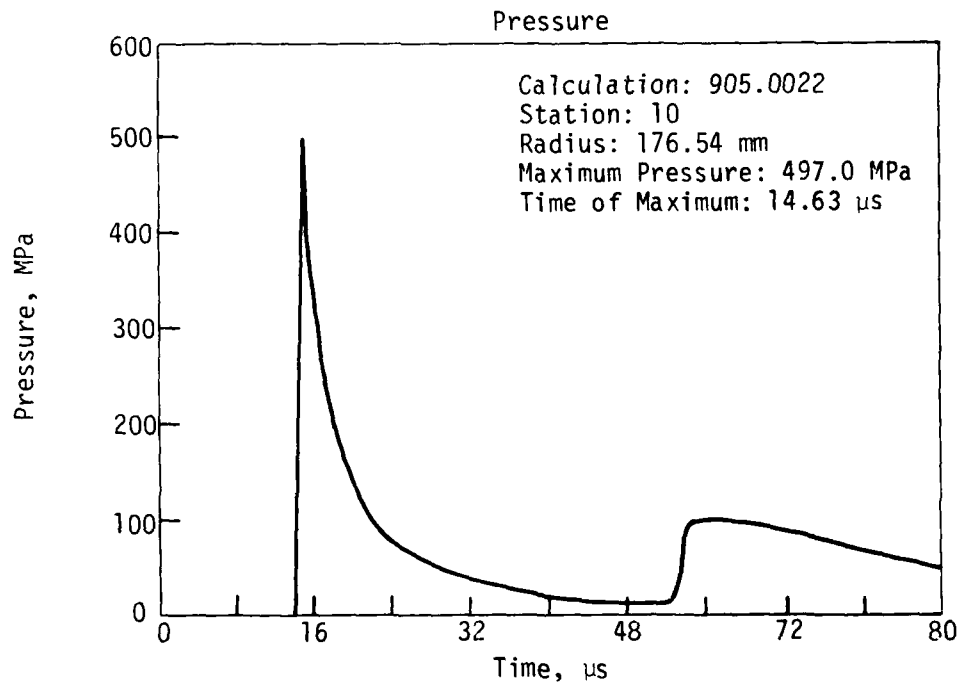
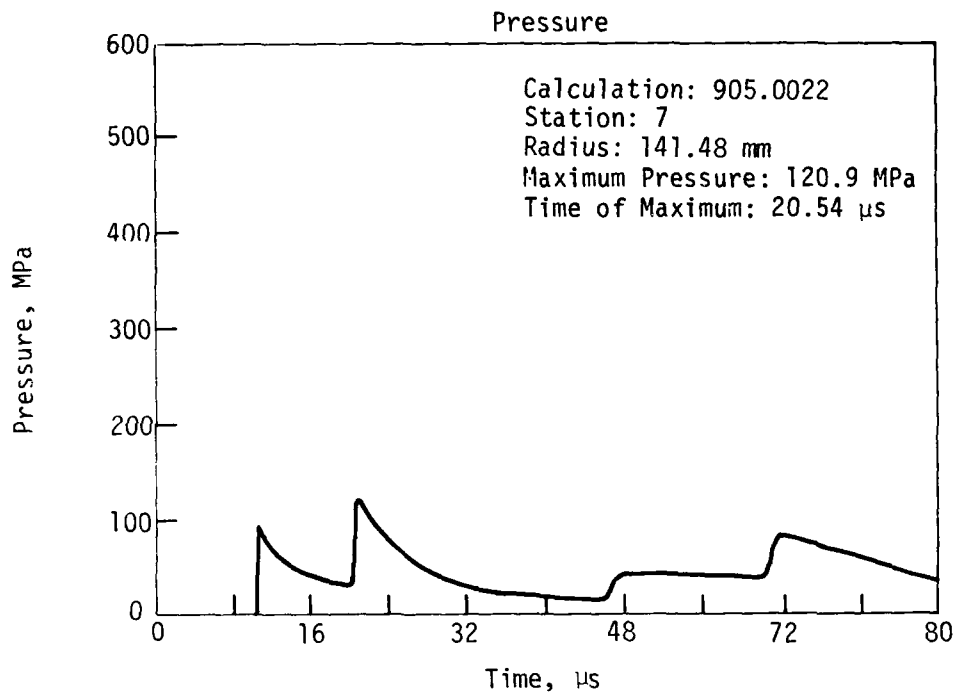


Figure 14. APOD Calculation 905.0022--Pressure versus Time

TABLE 2. COMPARATIVE PRESSURES AND ARRIVAL TIMES AT THREE STATIONS

Peak Pressure at Arrival Time,
MPa at μ s

Calculation Number/Code	Type	Station Radius = 1.25 mm	Station Radius = 141.48 mm	Station Radius = 176.54 mm	Reaction Cavity EOS
905.0020 HULL	Eulerian	3520.9 at 0.001	150.5 at 19.58	589.8 at 14.56	Constant- γ
905.0021 SAP	Eulerian	3473.6 at 0.003	147.7 at 19.67	577.0 at 14.64	Constant- γ
905.0022 APOD	Lagrangian	3469.4 at 0.001	120.9 at 20.54	497.0 at 14.63	Constant- γ
905.0031 SAP	Eulerian	3473.6 at 0.003	89.9 at 9.90	145.9 at 17.12	Constant- γ
905.0041 SAP	Eulerian	3473.6 at 0.003	116.3 at 21.05	315.4 at 15.66	Constant- γ
905.0051 SAP	Eulerian	1807.1 at 0.003	57.3 at 29.58	304.6 at 22.34	Real Air

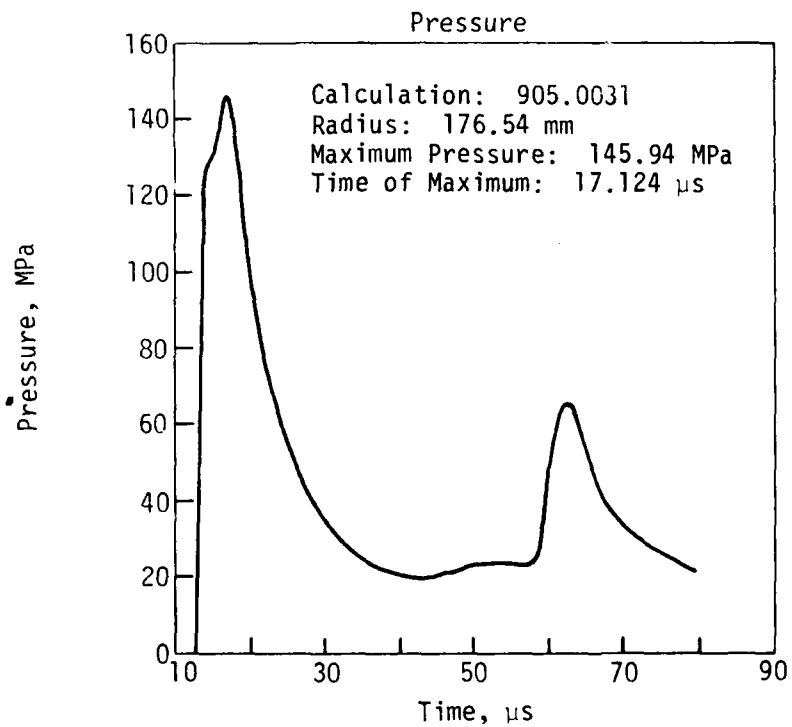
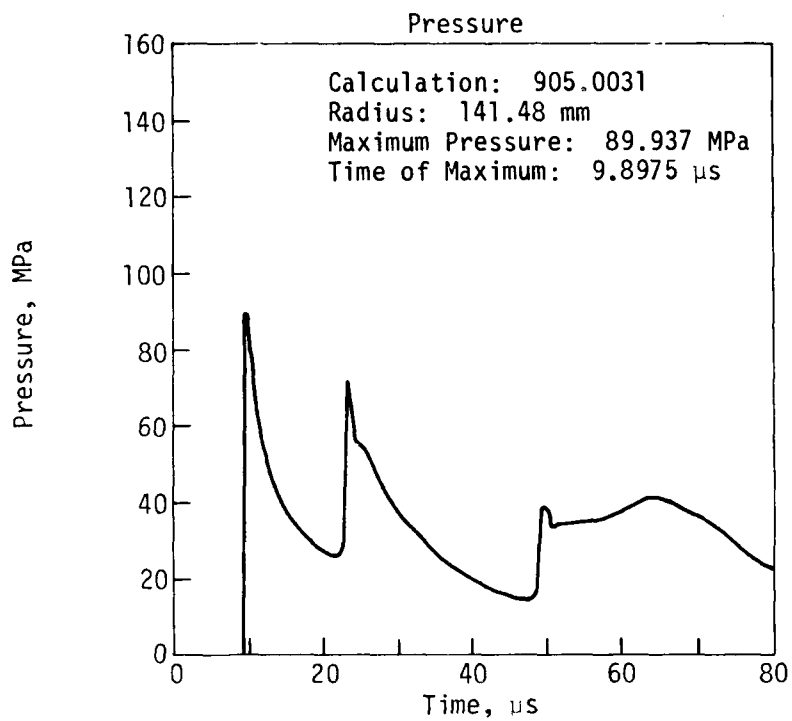


Figure 15. SAP Calculation 905.0031--Pressure versus Time

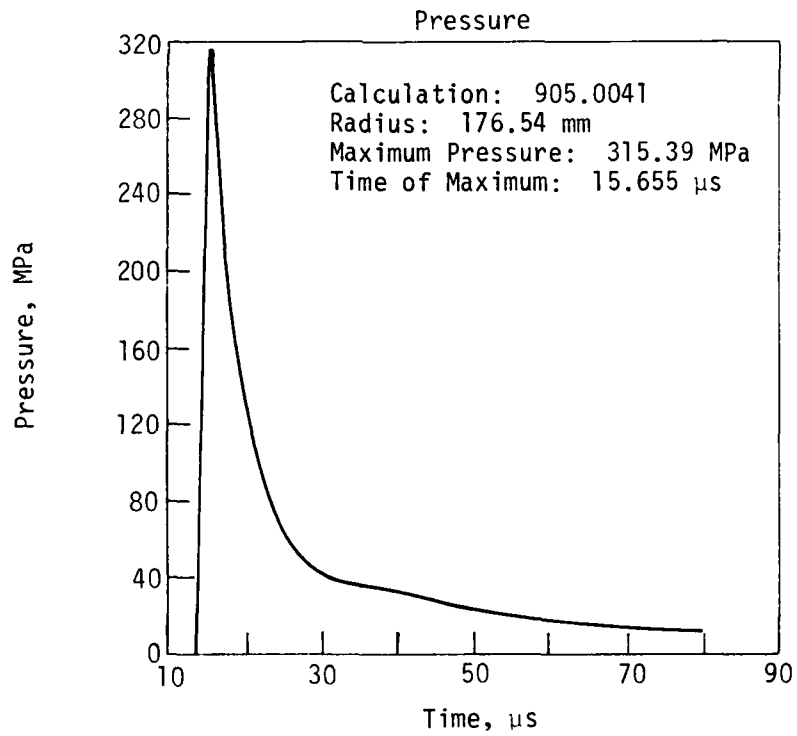
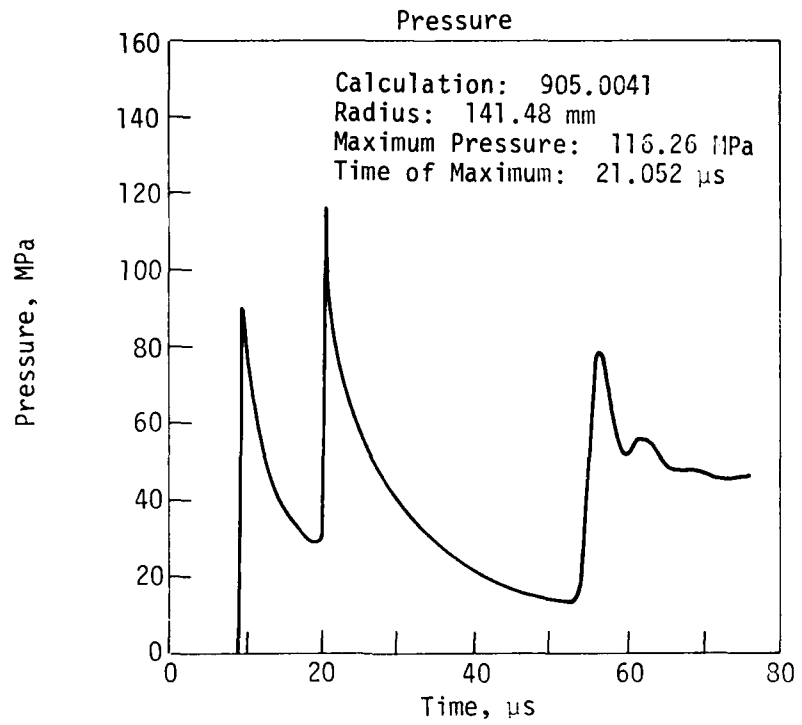


Figure 16. SAP Calculation 905.0041--Pressure versus Time

are quite different with much later arrival times. However, calculation 905.0031 is an entirely different story; here the first reflection is extremely weak. Note also in Table 2 and Figure 15 at 141.48 mm the reflected peak is lower than the incident peak, contrary to all of the other calculations. This method of modeling a nonrigid reflecting boundary does not appear to be satisfactory.

Calculation 905.0051 is a modification of 905.0021 with the ideal gas replaced with real air employing a variable gamma. The reflecting surface represents rigid, fully reflecting wall. Even with the same initial mass and energy deposition, the equation of state employed in 905.0051 produces an initial peak pressure of 1807.1 MPa which is approximately one-half the comparable peak of 3473.6 MPa for calculation 905.0021. This trend is evident at the other stations (Table 2 and Fig. 17). The arrival times in the real air case were considerably later than those for the ideal gas. These results are consistent with the earlier findings in calculations 905.0020 and 905.0050.

Computer costs for performing SAP, APOD, and HULL calculations were obtained during this study. The SAP and APOD calculation costs were approximately the same, \$10.50 for APOD and \$8.00 for SAP. The HULL calculation cost \$95.00. All calculations were run to 80 μ s.

The APOD hydrocode was dropped from any further utilization during this technical effort. The versatility of SAP, having both a Lagrangian and Eulerian capability, as well as an excellent supporting executive program and a strong plot program at the same cost level as APOD, makes SAP far more attractive for one-dimensional problems. Additionally SAP provided results almost identical to HULL results. The one advantage held by APOD is that of having a 1 1/2-D capability which will be overcome with the proposed SAP 1 1/2-D modification. SAP will then be used for one-dimensional problems and certain 1 1/2-D problems while HULL will be used in 2-D applications.

The work described above has clearly shown the capability of the SAP and HULL codes to qualitatively model a number of 1-D shock reflection and multiple

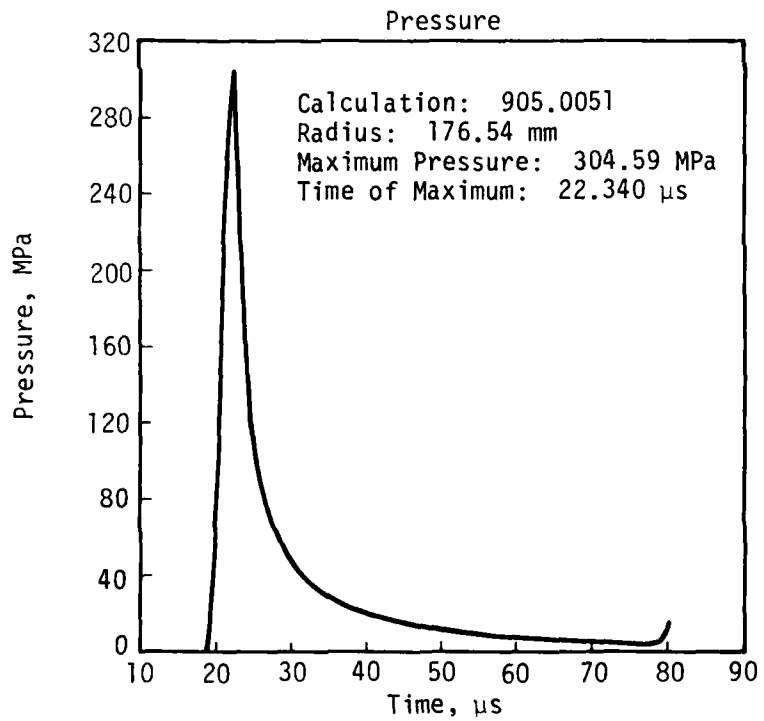
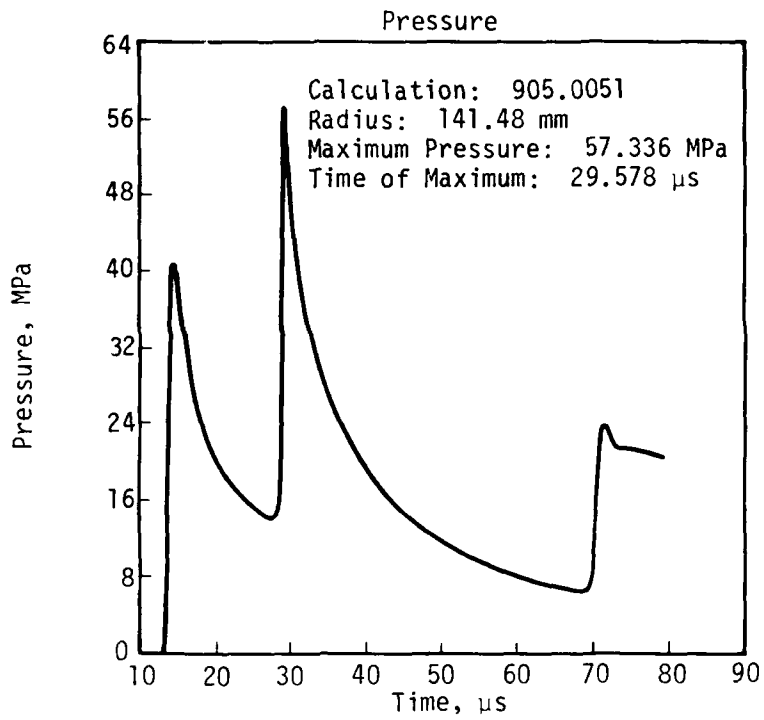


Figure 17. SAP Calculation 905.0051--Pressure versus Time

shock problems encountered in HEST simulation experiments. Additional work is now required to validate these hydrocodes quantitatively using high quality experimental data.

HULL SIMULATIONS OF DETONATING CORD BLAST EFFECTS IN A HEST CAVITY

The explosive charge used with the HEST simulator has generally been fabricated using individual strands of detonating cord. A matter of concern to HEST designers has been the severity of the blast environment to which pressure gages are exposed. The validity of data obtained from gages in the vicinity of detonating cords is frequently questioned. To better understand and help resolve this issue a series of four HULL calculations was performed. Individual strands of detonating cord were coarsely modeled in layered planes within a typical HEST explosion cavity. Of particular interest were the reflected peak pressures experienced at the cavity floor where gages are often installed.

The HEST explosion cavity was assumed to be initially filled with an ideal gas ($\gamma = 1.4$) having properties approximating a standard sea level atmosphere. All boundaries of the calculational mesh were specified as reflective to represent the cavity walls as fixed surfaces. For the purposes of these calculations the cavity was assumed to contain five equally spaced horizontal explosive planes composed of equally spaced strands of detonating cord (Fig. 18). The lateral distance between strands was taken to be equal to the distance between planes.

Variations of the basic detonating cord pattern were simulated in a 2-D Cartesian geometry where the plane of symmetry represented the cavity midheight. Individual strands were represented with rectangular blocks of 20 cells so that the cross-sectional area corresponded to a cord diameter of 13 mm.

Detonations were assumed to be instantaneous as well as simultaneous and were simulated by depositing energy into the designated cells between the second and third calculational cycles. In all cases this deposition was apportioned

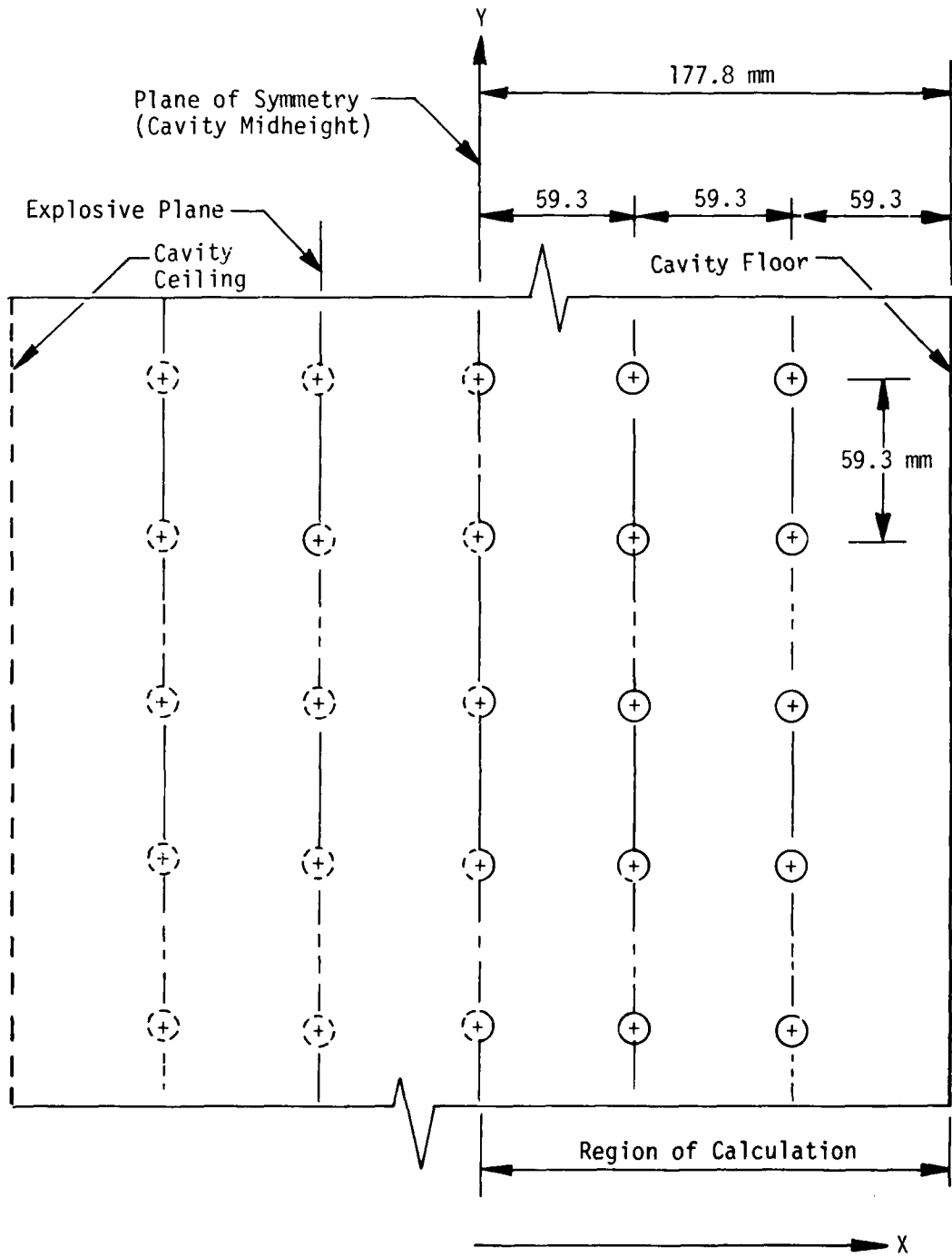


Figure 18. Basic Detonating Cord Pattern

equally among the explosive planes to achieve an overall horizontal planar density similar to that of the HORS I-3 experiment (4.297×10^8 ergs/mm²).

This calculational study must be considered qualitative since several physical phenomena were not modeled in the calculations. Not considered were the mass of the explosive material, the detonation process, and the products of combustion. Consequently detonations are simulated by the rapid expansion of a very hot ideal gas. A baseline calculation (905.0030) simulated the blast environment produced by the basic detonating cord pattern. In succeeding calculations (905.0040, 905.0060, and 905.0090) this basic pattern was variously modified (Fig. 19) in attempts to locally attenuate the peak reflected pressure at the right-hand boundary which represents the cavity floor where pressure measuring gages would be located.

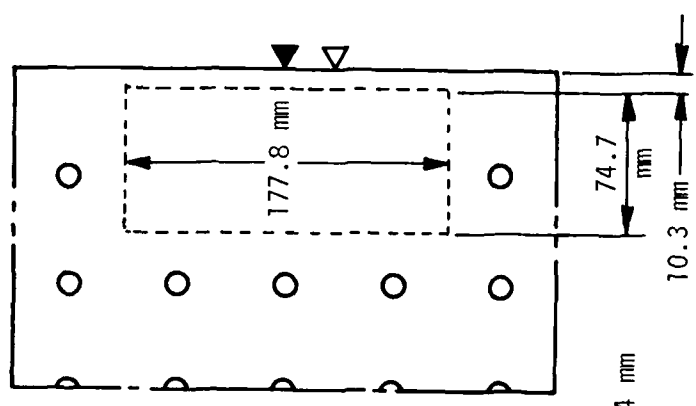
Calculation 905.0030*

Fluid properties were monitored at two locations on the right-hand reflective boundary. At locations immediately opposite a detonating cord (e.g., Station 10) the calculated peak reflected pressure of 158 MPa was caused by the regular reflection of the shock front impinging at near normal incidence. The maximum reflected peak (227 MPa) was observed at the floor location approximately midway between two adjacent detonating cords (Station 7). In this instance it is believed that the incident wave system (Fig. 20) is a Mach configuration generated by the simultaneous explosion of two equal charges (Ref. 15). The plane of symmetry midway between these detonations is essentially a reflective surface. Since at early times the shocks are very strong, nonregular (i.e., Mach) reflections occur and give rise to a Mach shock front which is perpendicular to this plane and which is generated by the interaction of the two cylindrically expanding shock waves from the individual detonating cords. The reflection at Station 7 is most likely the result of the normal incidence of this Mach shock front.

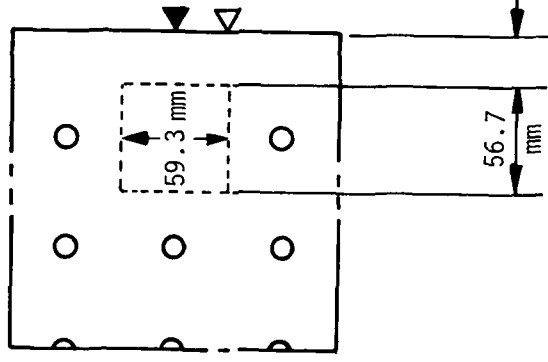
15. Courant and Friedrichs, *Supersonic Flow and Shock Waves*, pp. 334-5
Interscience Publishers, New York, 1948.

*Hydrocode Calculations No. 905.0030 and 905.0070, Data Report, UNM/CERF
AST-43, December 1978.

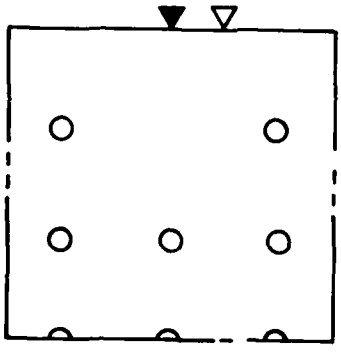
Buffer Zone (Region of Uniform Energy Density)



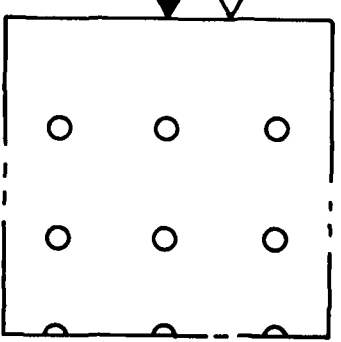
905.0090



905.0060



905.0040



905.0030

- Symmetry Plane ————
- Cavity Floor ————
- Reflective Boundary - - - -
- Detonating Cord Location ○
- Station 7 Location ▽
- Station 10 Location ▼

Figure 19. Detonating Cord Patterns

- S Primary Shock Fronts
- R Reflected Shock Fronts
- M Mach Shock Front
- D Contact Discontinuities
- E Detonating Cord Location

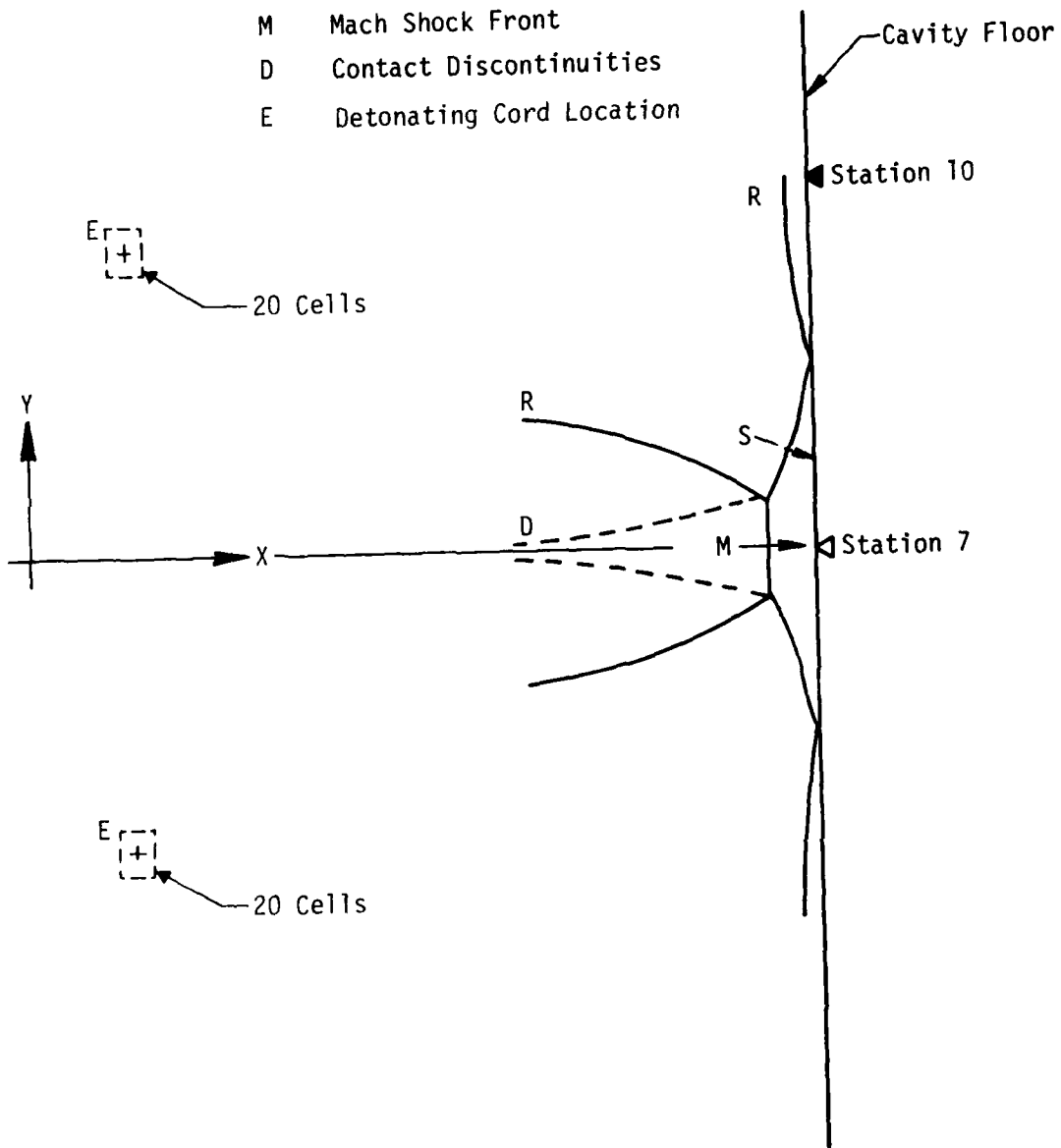


Figure 20. Incident Wave System--Calculation 905.0030

Calculation 905.0040*

In this model the basic pattern is interrupted by omitting the detonating cord directly above Station 10. Otherwise the model specifications are identical to those for calculation 905.0030. An illustration of the wave system produced by this pattern is depicted in Figure 21. As this wave system evolves it is symmetrical with respect to the X-Z plane containing Station 10. The reflected peak pressure of 91 MPa at Station 7 was the result of the oblique incidence of the shock front generated by the detonation of the cord at E_1 . The 634 MPa reflected peak pressure observed at Station 10 involves the staging of several Mach interactions and then the nearly simultaneous convergence of the resulting *Mach Jet* and the reflections of the two oblique shocks at the cavity floor (Fig. 22).

The first shock interactions occur midway between cords E_1 and E_2 , and E_2 and E_3 . The M_1 shock fronts produced here converge at F_1 and act to reinforce the M_2 shock in the direction of F_2 . The convergence of the M_2 and M_2' fronts at F_2 eventually leads to the formation of a Mach jet since the flow is locally constrained by the primary shock fronts propagating inward from E_3 and E_3' . The evolution of this wave system and eventual convergence of shocks at F_3 is clearly discernible in the sequential display of the contoured pressure fields (Fig. 23).

Calculation 905.0060**

This calculation simulated a proposed technique for suppressing the shock focusing experienced in calculation 905.0040. The region of energy deposition for the cord immediately above Station 10 was expanded so that the energy previously deposited in a few cells was now uniformly distributed among 506 cells (called a buffer zone). Otherwise the model specifications remained unchanged. Since the initial pressure in this region is approximately 60 MPa, it acts as a local buffer zone and the wave system seen in the 905.0040

*Hydrocode Calculaton No. 905.0040, Data Report, UNM/CERF AST-39, December 1978.

**Hydrocode Calculation No. 905.0060, Data Report, UNM/CERF AST-40, December 1978.

- S Primary Shock Fronts
- R Reflected Shock Fronts
- D Contact Discontinuities
- M Mach Shock Fronts
- E Detonating Cord Locations
- F Confluence of Fronts or Front Systems

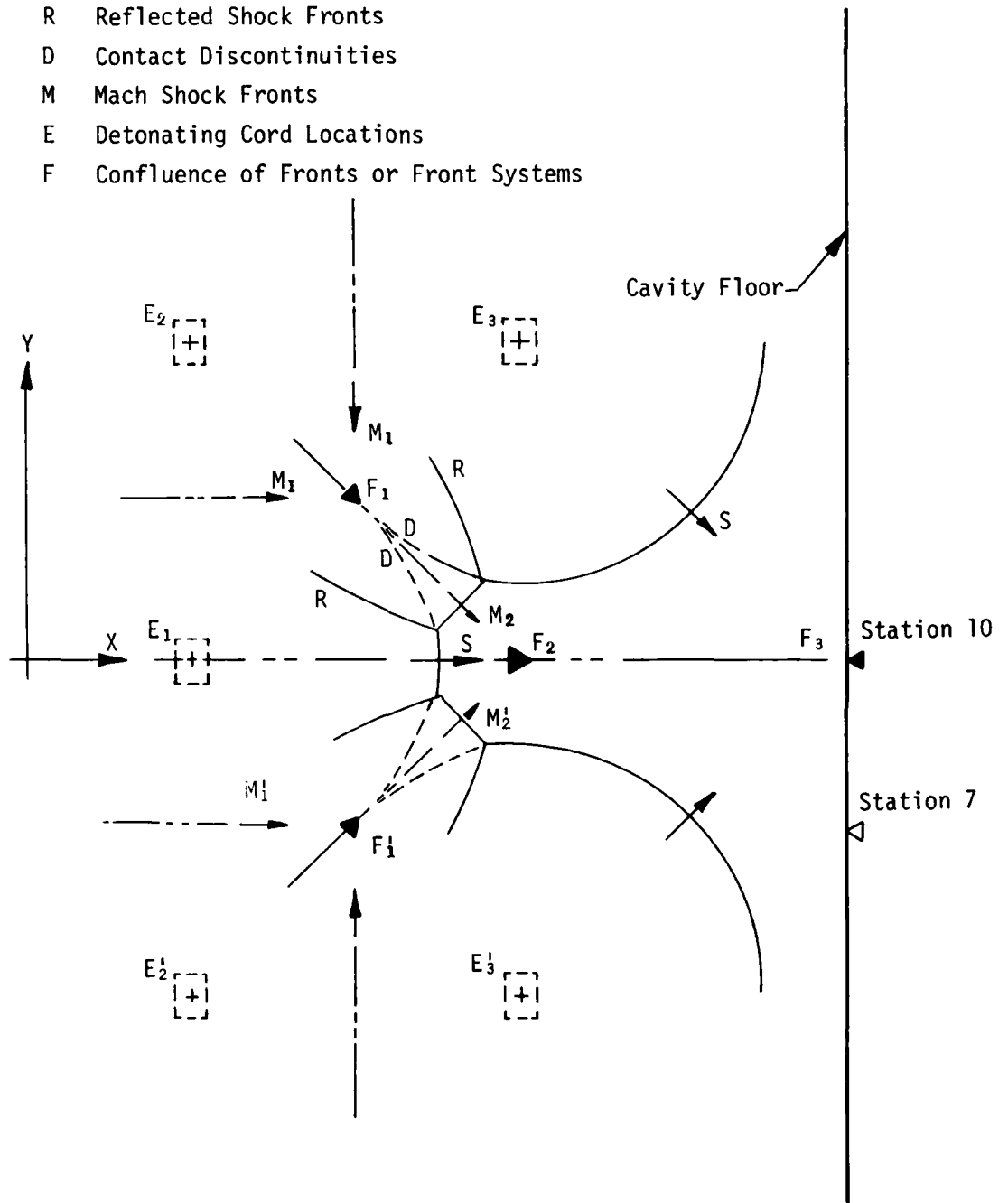


Figure 21. Wave System at 4 μ s--Calculation 905.0040

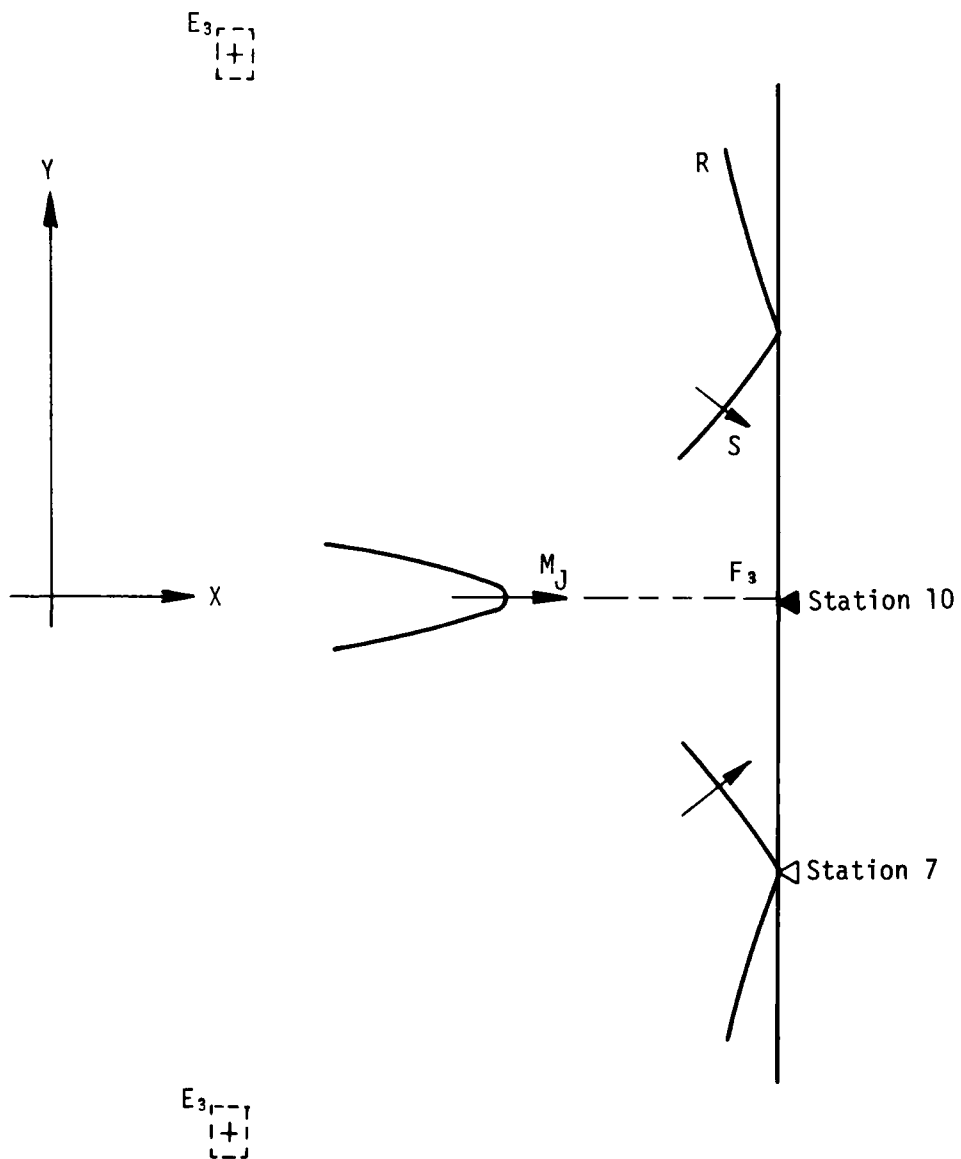


Figure 22. Wave System at $7.5 \mu\text{s}$ --Calculation 905.0040

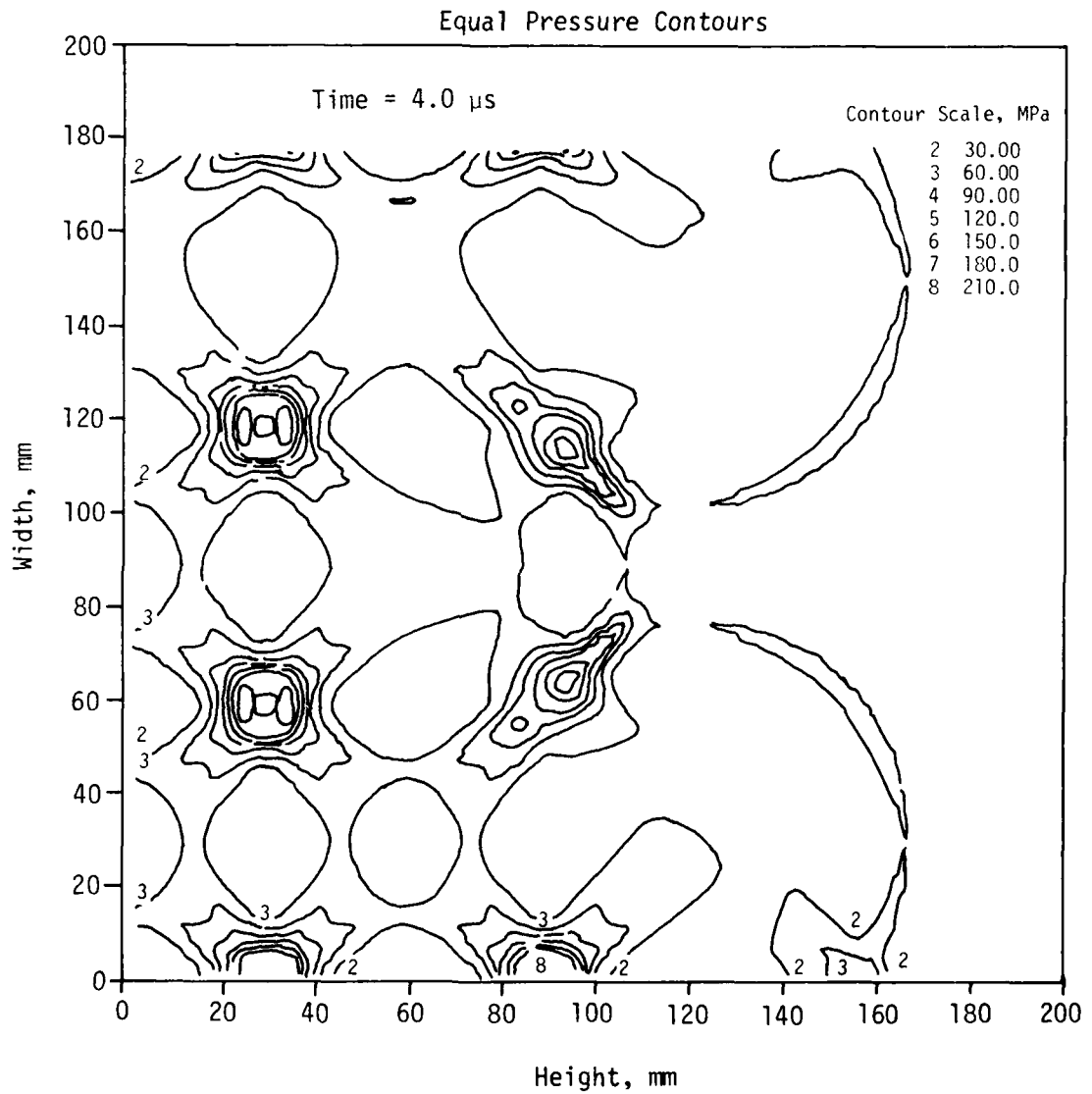


Figure 23. Calculation 905.0040--HULL Simulation of HORS I-3 HEST Detonating Cord Array (1 of 10)

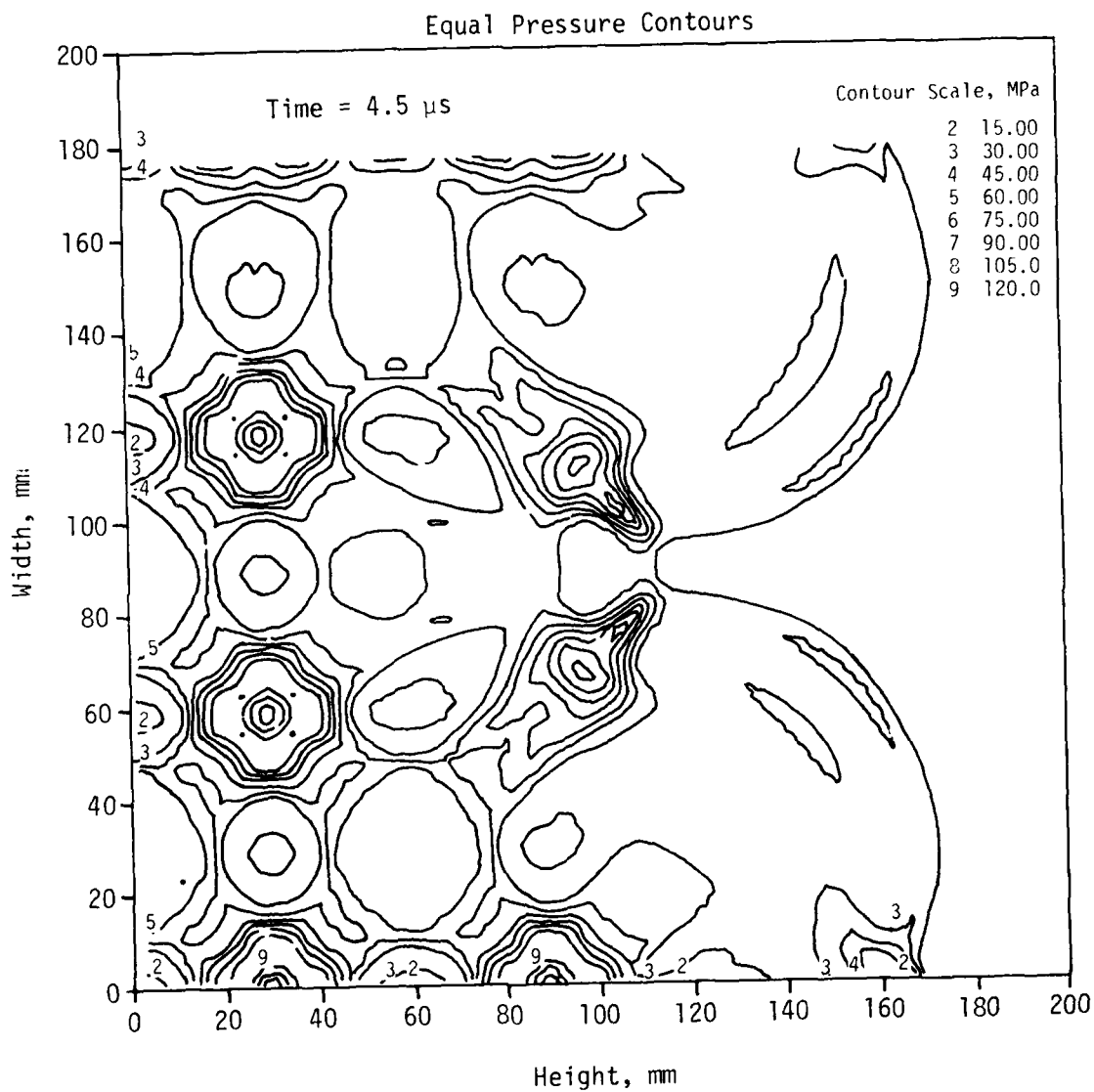


Figure 23. Calculation 905.0040--HULL Simulation of HORS I-3 HEST Detonating Cord Array (2 of 10)

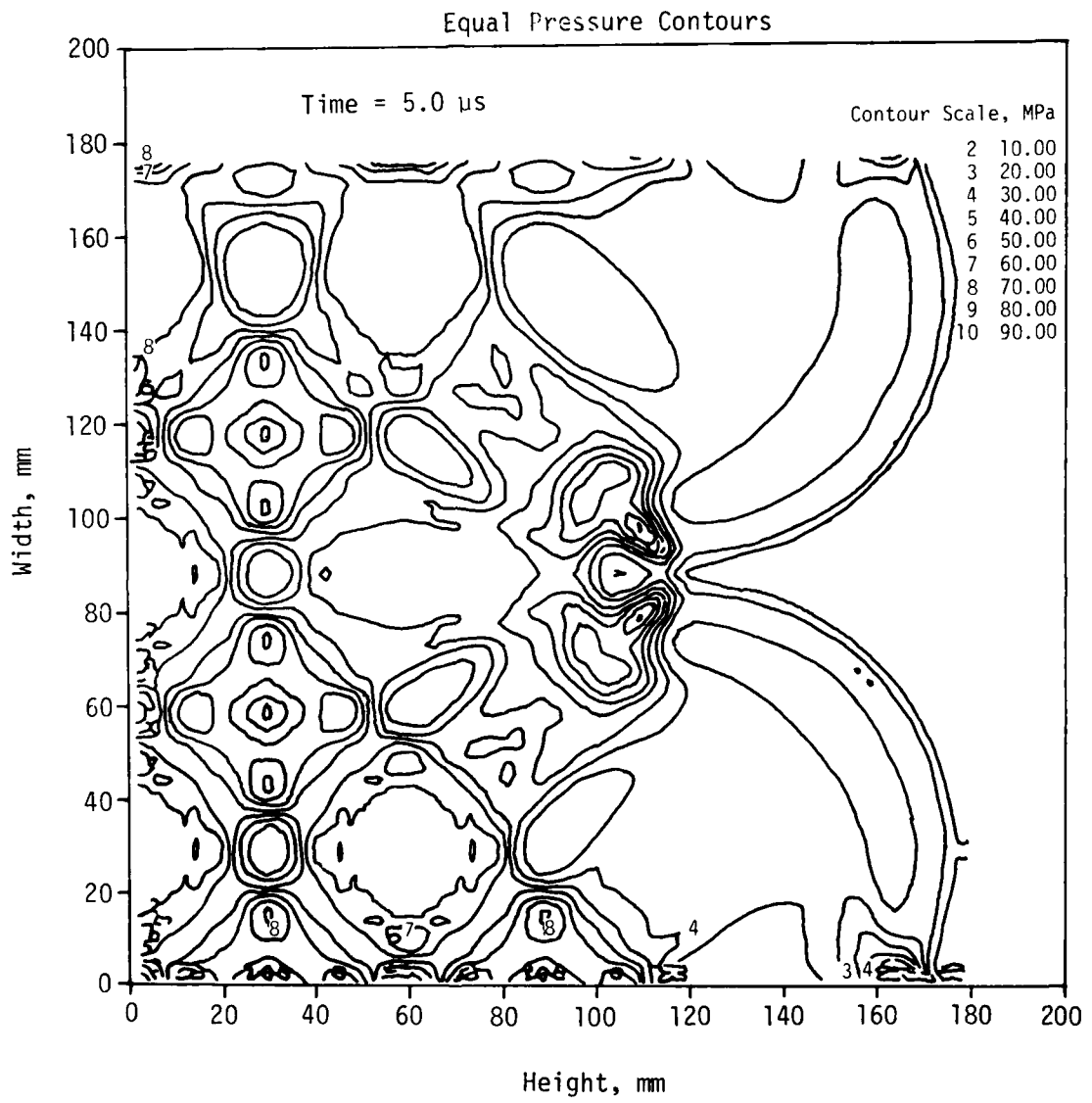


Figure 23. Calculation 905.0040--HULL Simulation of HORS I-3 HEST Detonating Cord Array (3 of 10)

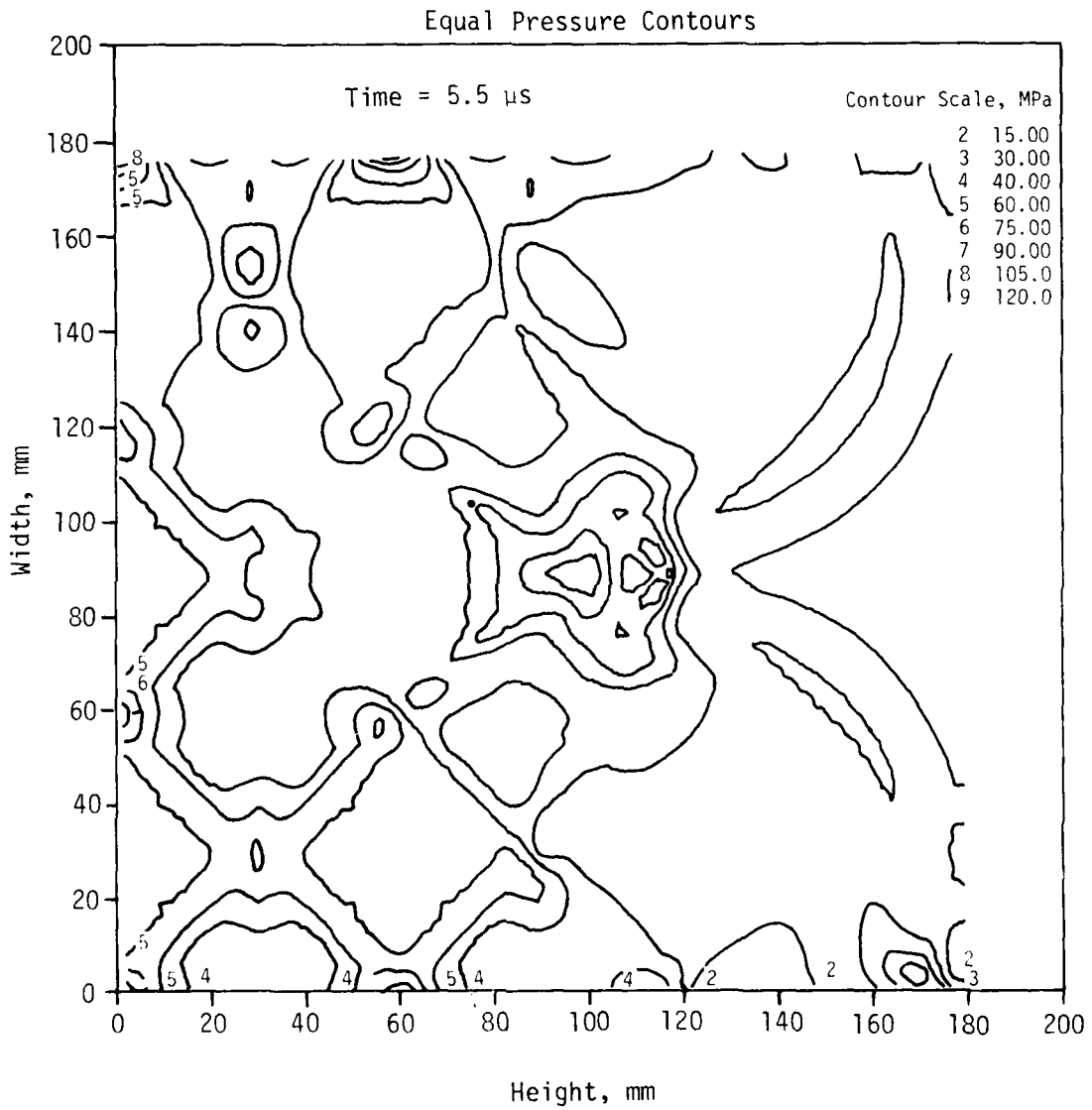


Figure 23. Calculation 905.0040--HULL Simulation of HORS I-3 HEST Detonating Cord Array (4 of 10)

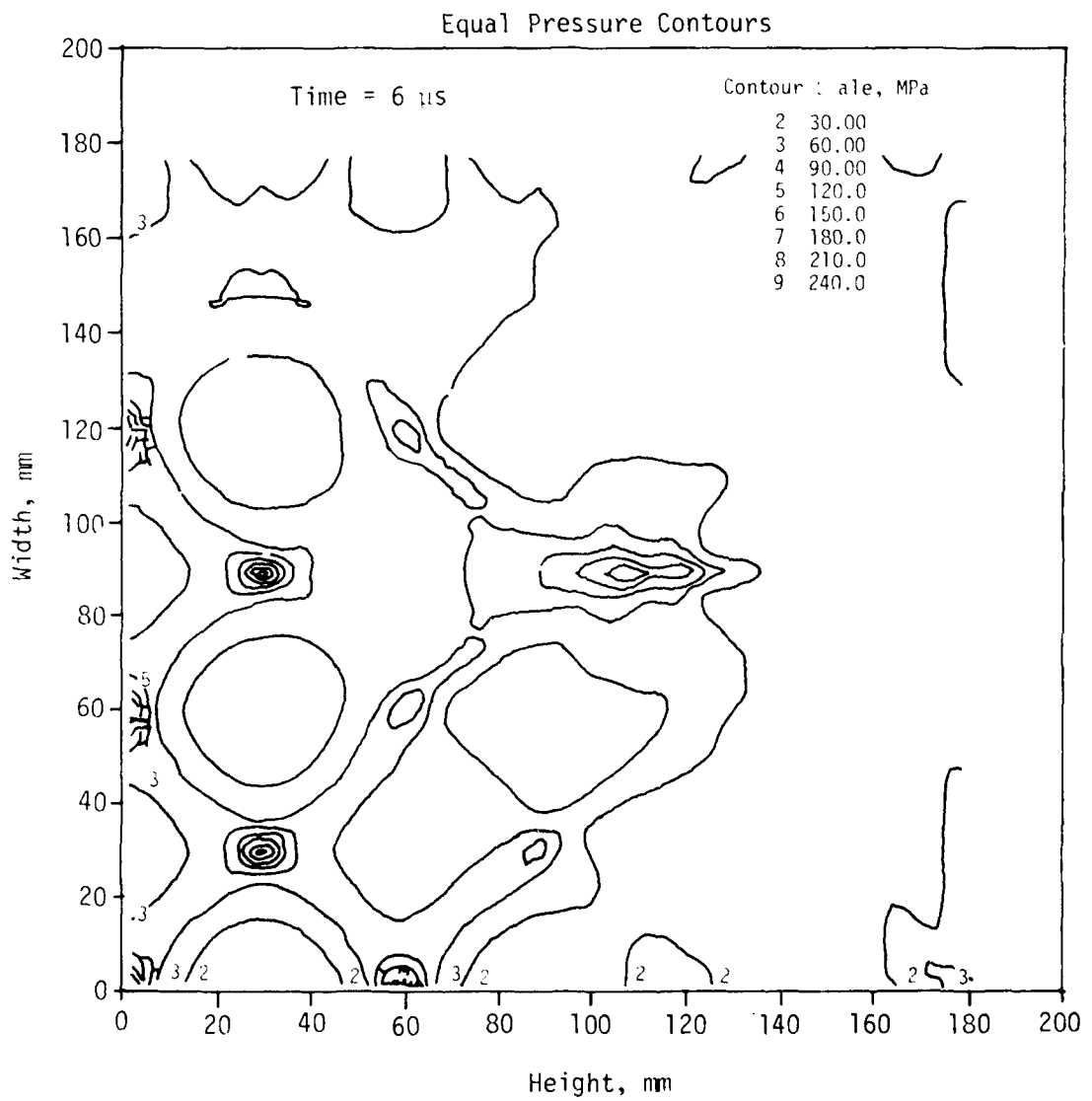


Figure 23. Calculation 905.0040--HULL Simulation of HORS I-3 HEST Detonating Cord Array (5 of 10)

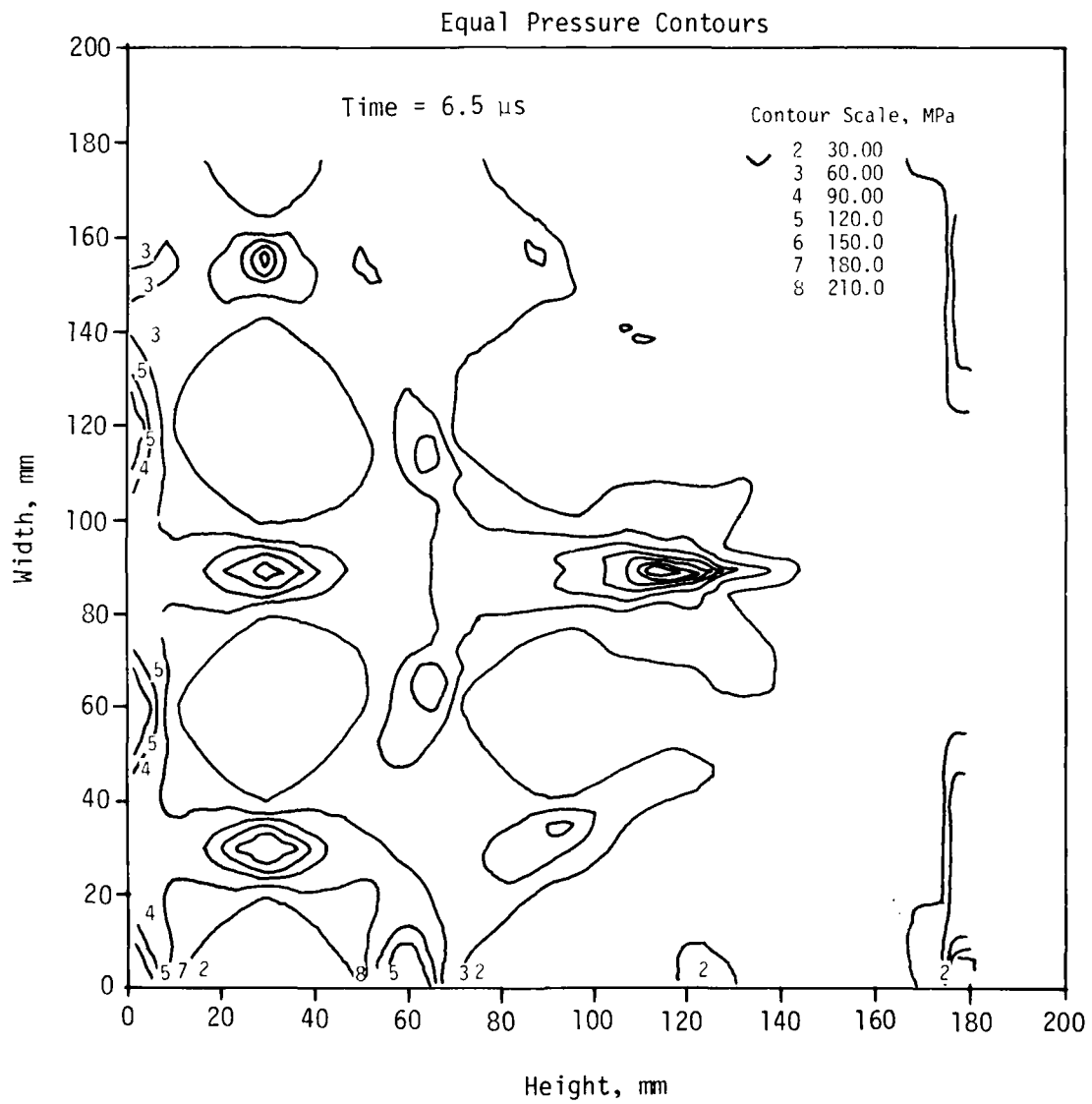


Figure 23. Calculation 905.0040--HEST Simulation of HORS I-3 HEST Detonating Cord Array (6 of 10)

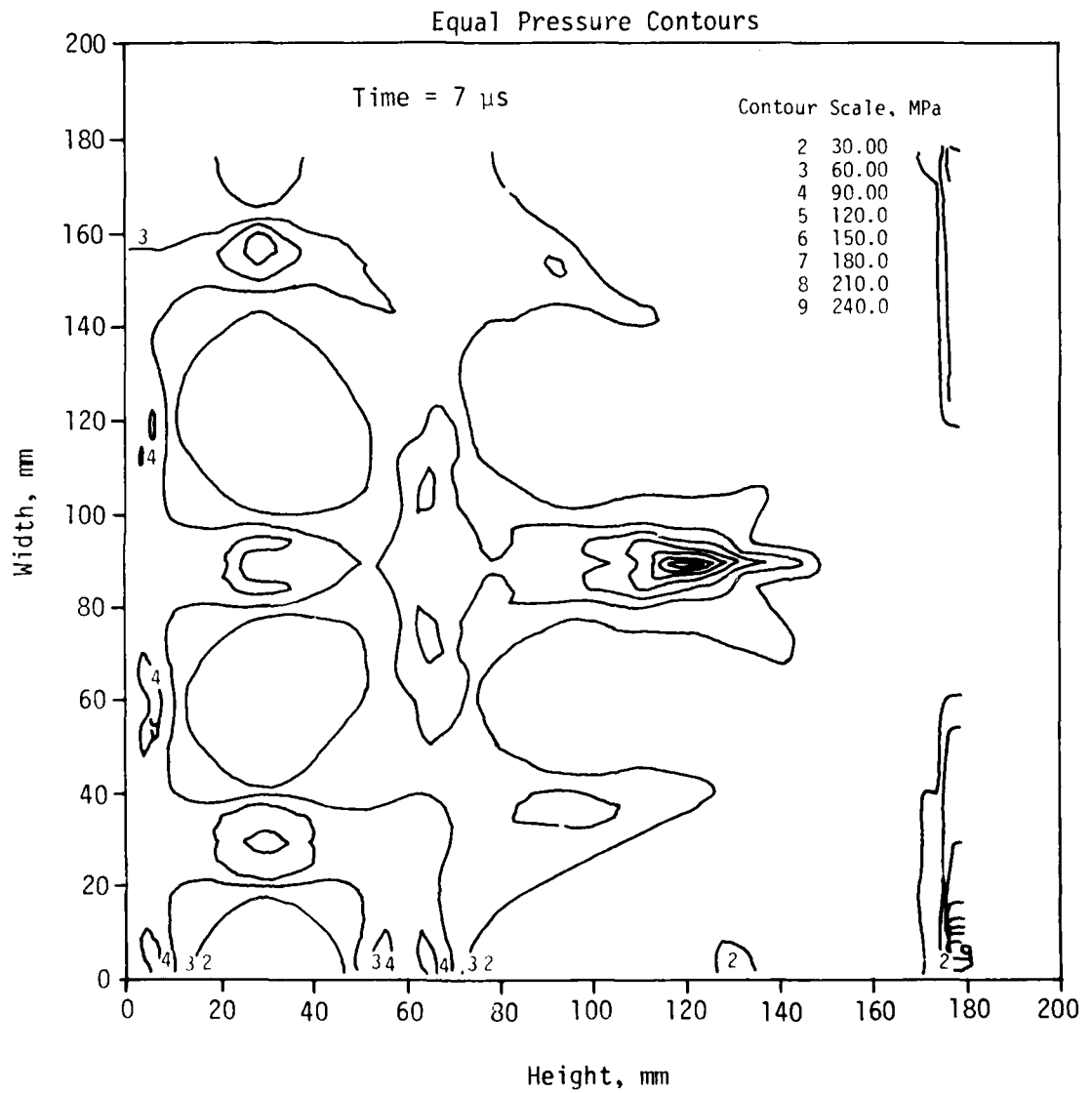


Figure 23. Calculation 905.0040--HULL Simulation of HORS I-3 HEST Detonating Cord Array (7 of 10)

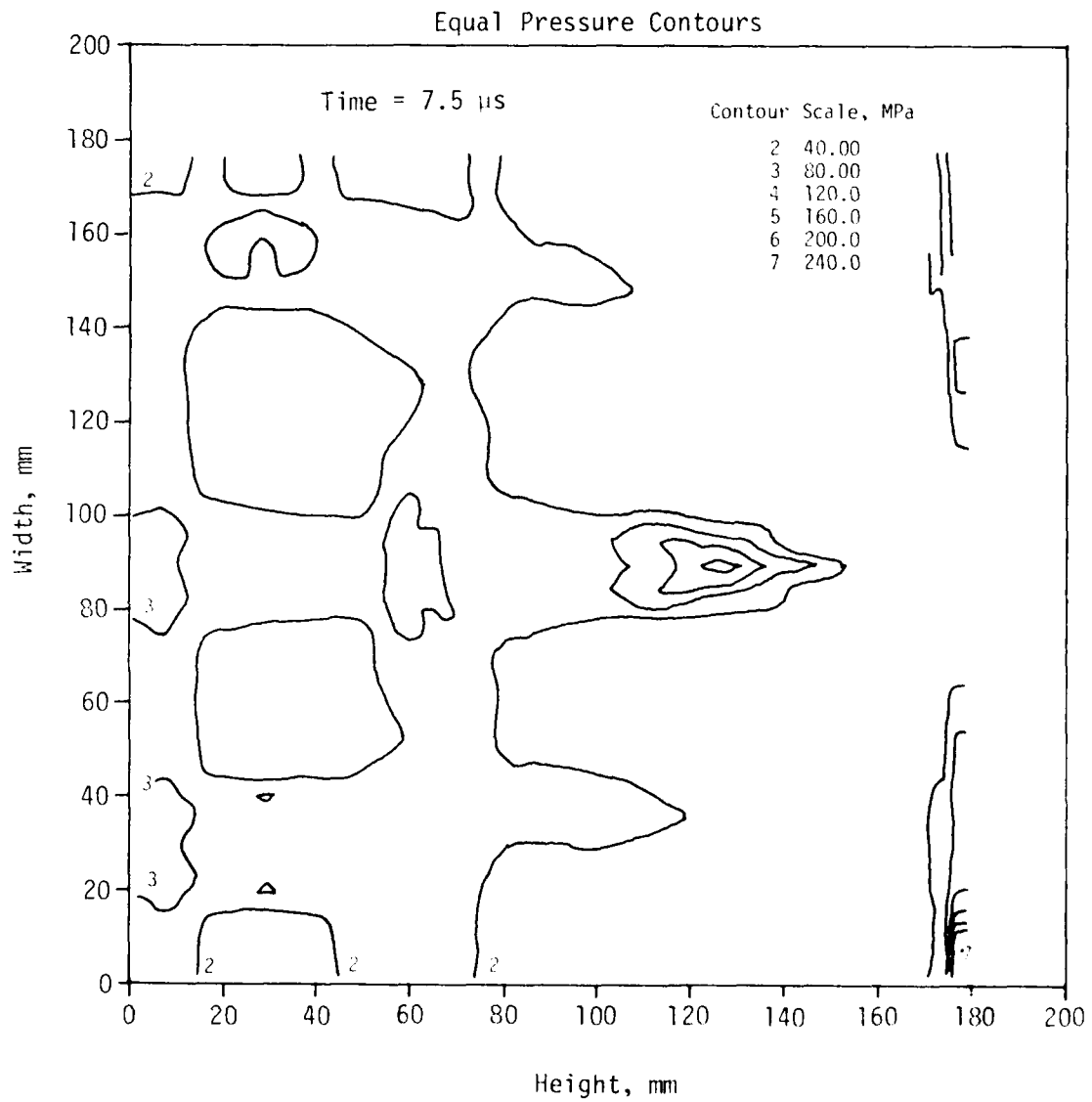


Figure 23. Calculation 905.0040--HULL Simulation of HORS I-3 HEST Detonating Cord Array (8 of 10)

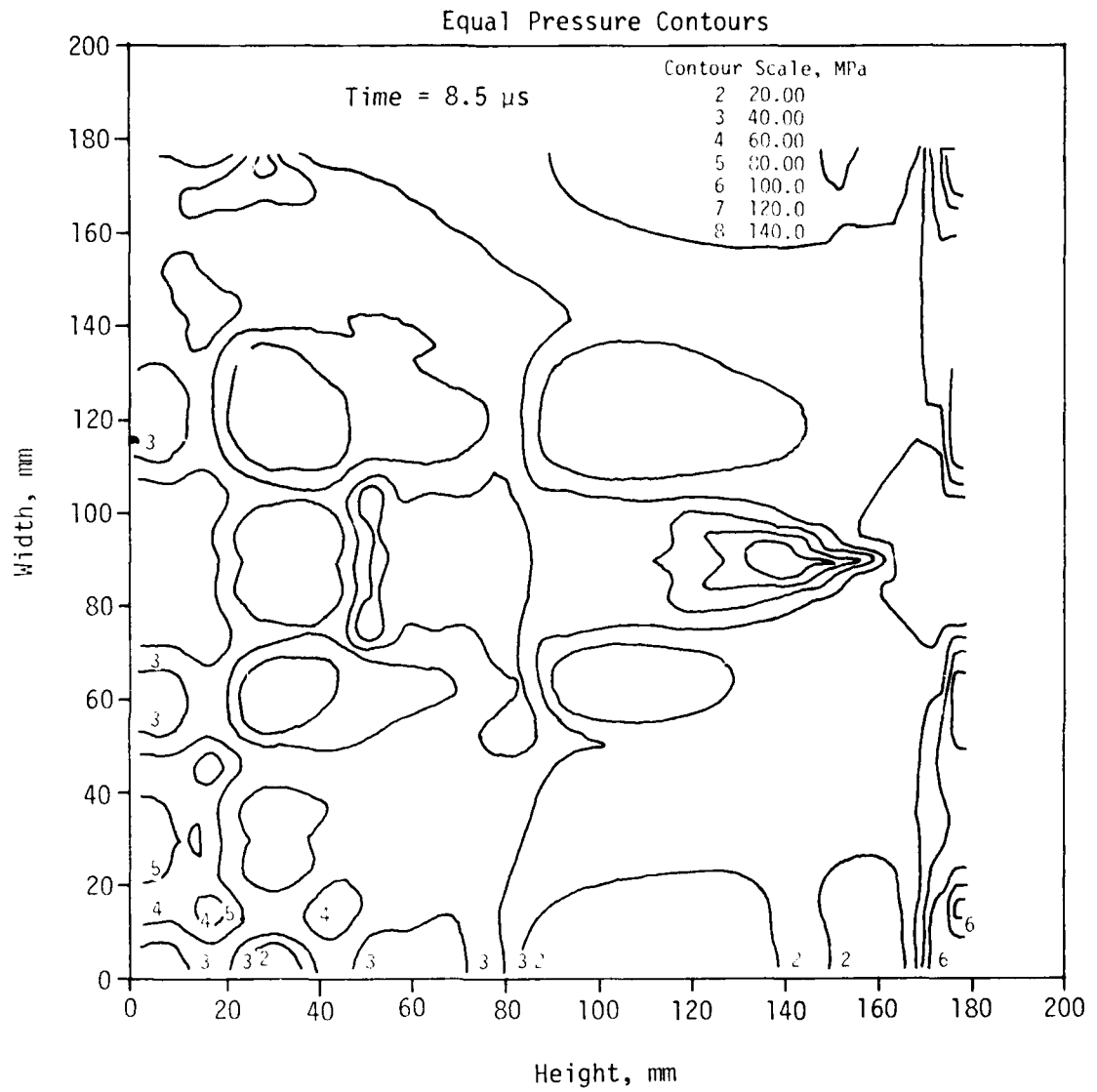


Figure 23. Calculation 905.0040--HULL Simulation of HORS I-3 HEST Detonating Cord Array (9 of 10)

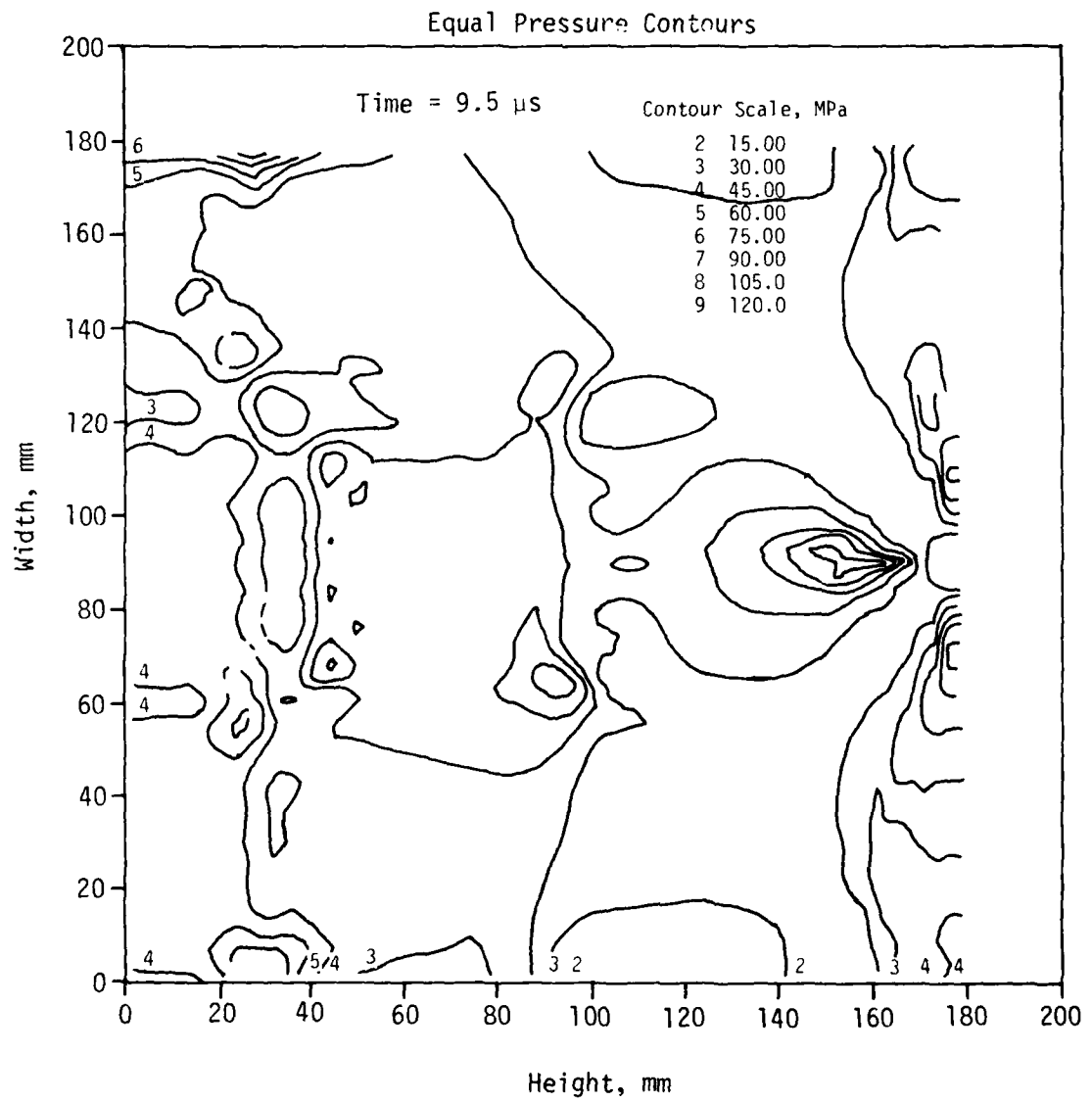


Figure 23. Calculation 905.0040--HULL Simulation of HORS I-3 HEST Detonating Cord Array (10 of 10)

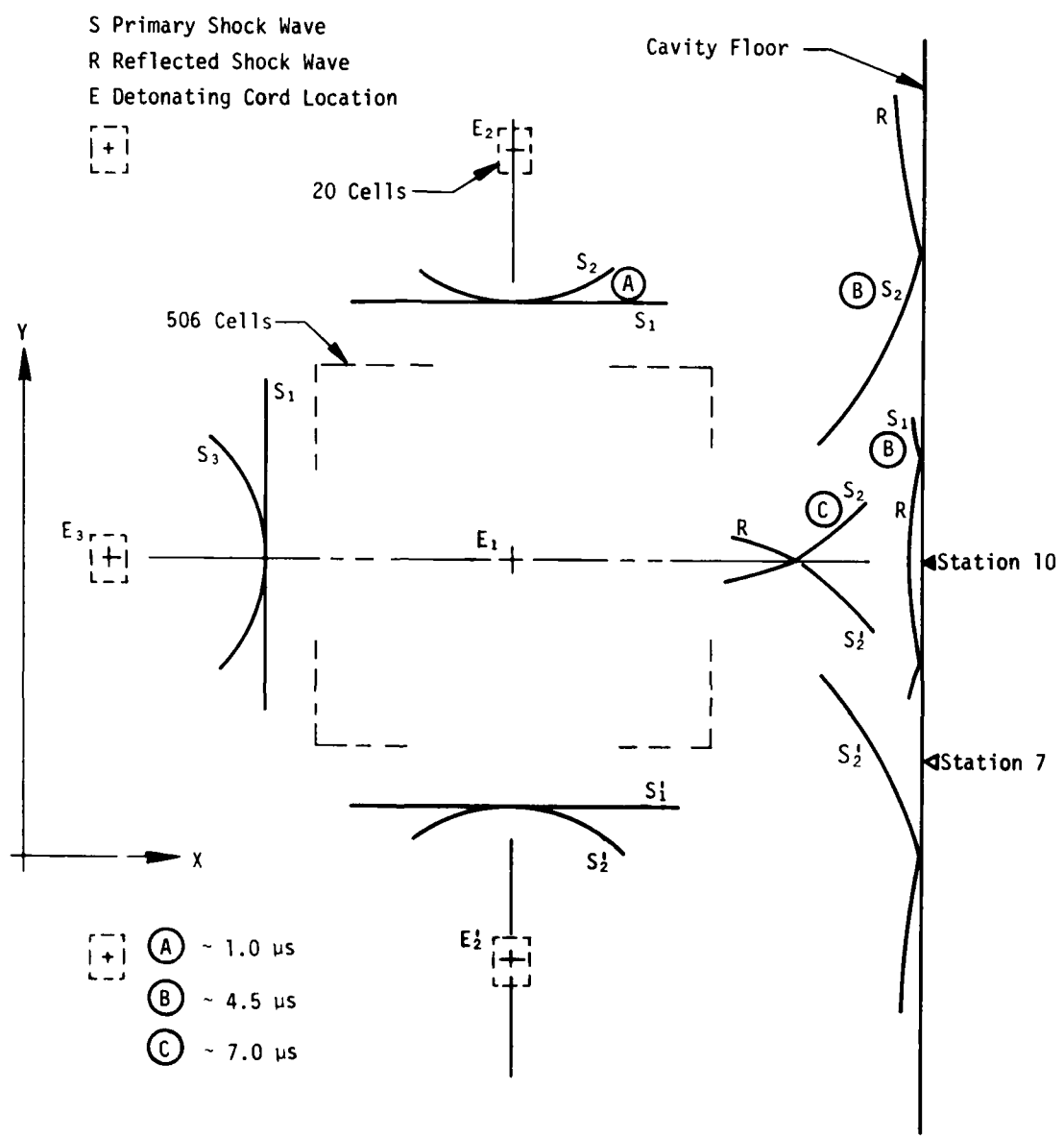


Figure 24. Shock Wave Interactions--Calculation 905.0060

solution did not fully develop. Instead a secondary wave system developed within this expanding zone (Fig. 24) and the reflected peak pressure at Station 10 was reduced to 195 MPa. The initial front interaction with this configuration would be the head-on collisions of the nearly planar S_1 fronts with the much stronger S_2 , S_2^* , and S_3 shocks. These shock waves penetrate each other and in the process both are attenuated. At approximately 4 μ s the S_1 shock wave impinges on the cavity floor at Station 10. Meanwhile the weakened S_2 and S_2^* shocks propagate into the buffer zone and interact at the X-Z plane containing Station 10. This plane functions as a reflecting surface, and the regular reflections of S_2 and S_2^* eventually act to retard the S_1 reflection advancing upward from Station 10. The constraint of this converging wave system may be responsible for the pressurization at this location. Finally the reflected peak pressure observed at Station 7 (221 MPa) is believed to be caused by the convergence of the regular reflections of the primary S_1 and S_2^* waves. Although these results do not compare too favorably with those produced by the original basic pattern (905.0030), they do demonstrate the feasibility of the protective buffering technique.

Calculation 905.0090*

This calculation is actually a sequel to calculation 905.0060. To evaluate its attenuating capability the buffer zone was expanded to include 2001 cells among which energy equivalent to the deposition for 3 detonating cords was evenly distributed. As a result the initial pressure in this zone was reduced to 46.5 MPa. Since, in this case, the lower boundary of the zone is approximately 10 mm from the cavity floor, the initial reflected peak pressure at both Stations 10 and 7 (80 MPa at 3.5 μ s) is simply due to the early time expansion of this buffer zone. However, late-time reflections are substantially greater. Peaks of 99 MPa at 12.5 μ s and 108 MPa at 13.5 μ s are experienced at Stations 7 and 10 respectively.

The evolution of the pressure field leading up to these secondary reflections is not clear, but some general observations can be made. The complex wave system spawned by the shock interactions within the cavity interior undergoes

* Hydrocode Calculation No. 905.0090, Data Report, UNM/CERFAST-41, December 1978.

a two-stage attenuation. At approximately 1.5 μ s the upper plane wave from the buffer zone collides with the convex shock fronts produced by detonating cords immediately above. As these weakened and retarded fronts descend through the buffer zone the center portion of the wave system eventually develops into a shallow concave front followed by a local high-pressure wedge. Meanwhile the reflected planar shock front has been propagating upward from the cavity floor (the pressure histories for Stations 6 and 9* would indicate an arrival at approximately 7 μ s). As these opposing fronts meet, the shocks approaching the cavity floor are once again slowed and diminished. The second collision apparently occurs at 9 μ s and may be correlated with the high-pressure ridge which is observed in the contoured pressure field (Fig. 25). Once these attenuated shocks impinge on the floor the subsequent interaction of the reflections is quite similar to that observed during calculation 905.0060.

A final consideration in this study was to evaluate the case where the buffer zone represents the entire cavity (representing cavity equilibrium pressure). Assuming the cavity is perfectly insulated and maintains its original size and shape, a solution of the EOS would yield the *equilibrium* pressure (i.e., the uniform pressure within the cavity after an infinite time).** Given that for an ideal polytropic gas

$$P = k\rho\varepsilon (\gamma - 1) \quad (1)$$

where

- P = pressure (MPa)
- ρ = mass density = 1.225×10^{-6} g/mm³
- ε = specific internal energy (ergs/g)
- γ = adiabatic exponent = 1.40457725
- k = conversion factor = 10^{-4}

it is first necessary to solve for the cavity uniform energy density. Given the cavity horizontal planar energy density (4.297×10^6 ergs/mm²), it then follows that

*Located 30 mm above the cavity floor.

**The equilibrium pressure corresponds most closely to the peak simulation pressure (PP_5) defined in Figure 1.

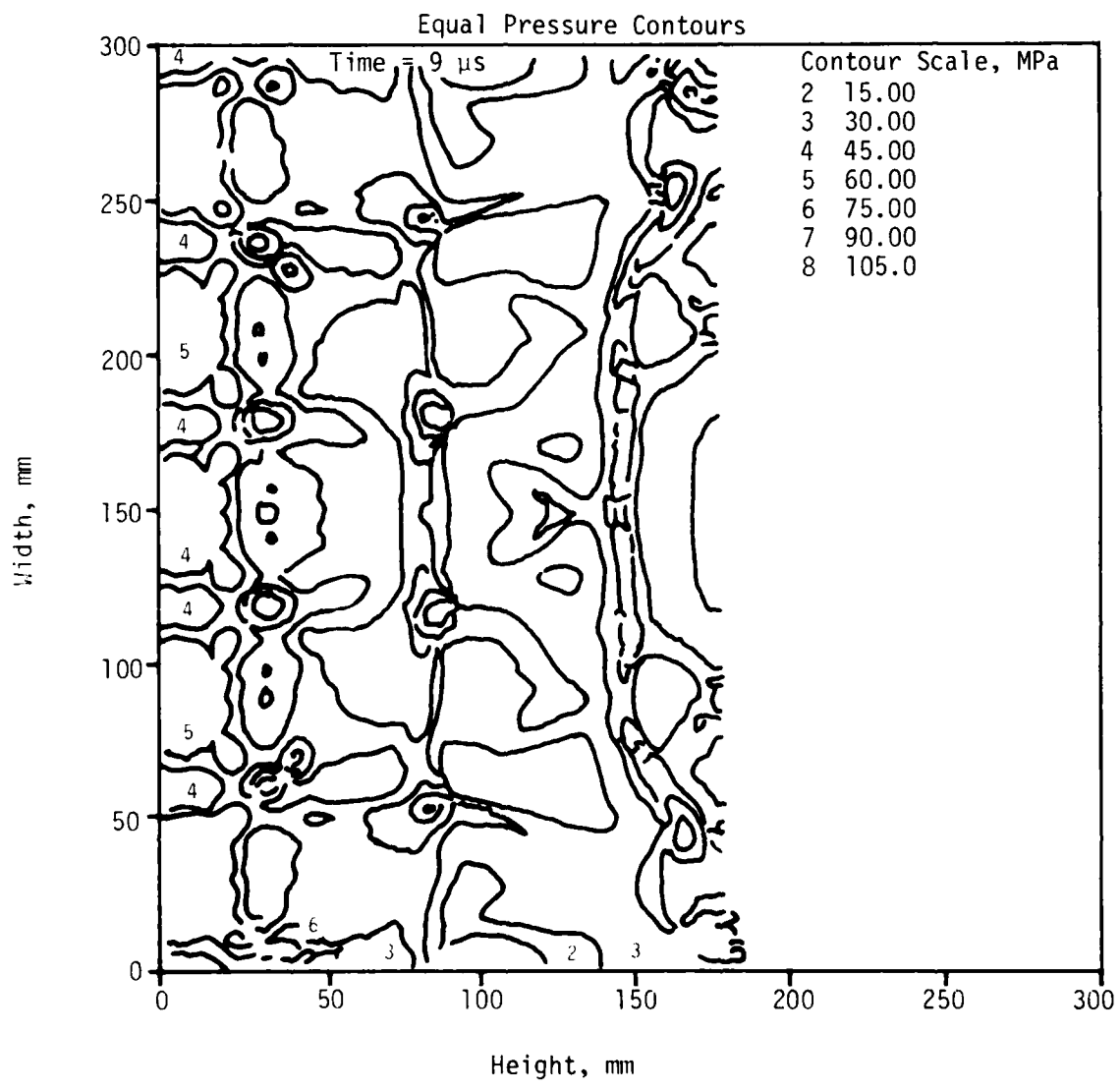


Figure 25. Calculation 905.0090--HULL Simulation of HORS I-3 HEST Detonating Cord Array

$$\epsilon = \frac{4.297 \times 10^8 / (14 \times 25.4)}{1.225 \times 10^{-6}} \quad (2)$$

and therefore that

$$P = [4.297 \times 10^8 / (14 \times 25.4)] (\gamma - 1) (10^{-4}) \quad (3)$$

$$= 48.9 \text{ MPa}$$

HULL calculation 905.0080 was run with the explosive energy uniformly introduced in each of the cells in the calculational mesh to obtain a computed cavity equilibrium pressure. The calculation was run twice, once with an ideal gas and once with a real air EOS, resulting in equilibrium pressures of 48.99 MPa and 20.48 MPa respectively. Since the calculation was run for only a few cycles, no data reports were produced.

A comparison of the calculation results and the equilibrium pressure is shown in Figures 26 through 28. Calculation 905.0020 was included in Figure 26 to provide a comparison with the case where all the explosive energy was deposited in the column of cells adjacent to the plane of symmetry at cavity midheight.

These calculations clearly demonstrate that complex shock interactions which take place within an explosively driven test cavity can result in severe local pressure concentrations. This is particularly true for the typical HEST field experiment where the desired pressure environment is generated by techniques using concentrated explosive charges. It is also evident that it may be possible to distribute the explosive energy more evenly to locally attenuate the pressure field at gage locations.

However, when one considers applying the protective buffering technique used in calculations 905.0060 and 905.0090, some practical constraints must be borne in mind. An absolutely uniform energy distribution throughout such a buffer zone cannot be achieved experimentally. There are, for instance, obvious limitations if one elects to refine the detonating cord pattern in order to produce the buffer. Even with the use of the smallest cord available, reflected peak pressures could be appreciable. Other seemingly more appropriate techniques such as the use of an explosive gaseous mixture have proven unsatisfactory because of safety and engineering considerations.

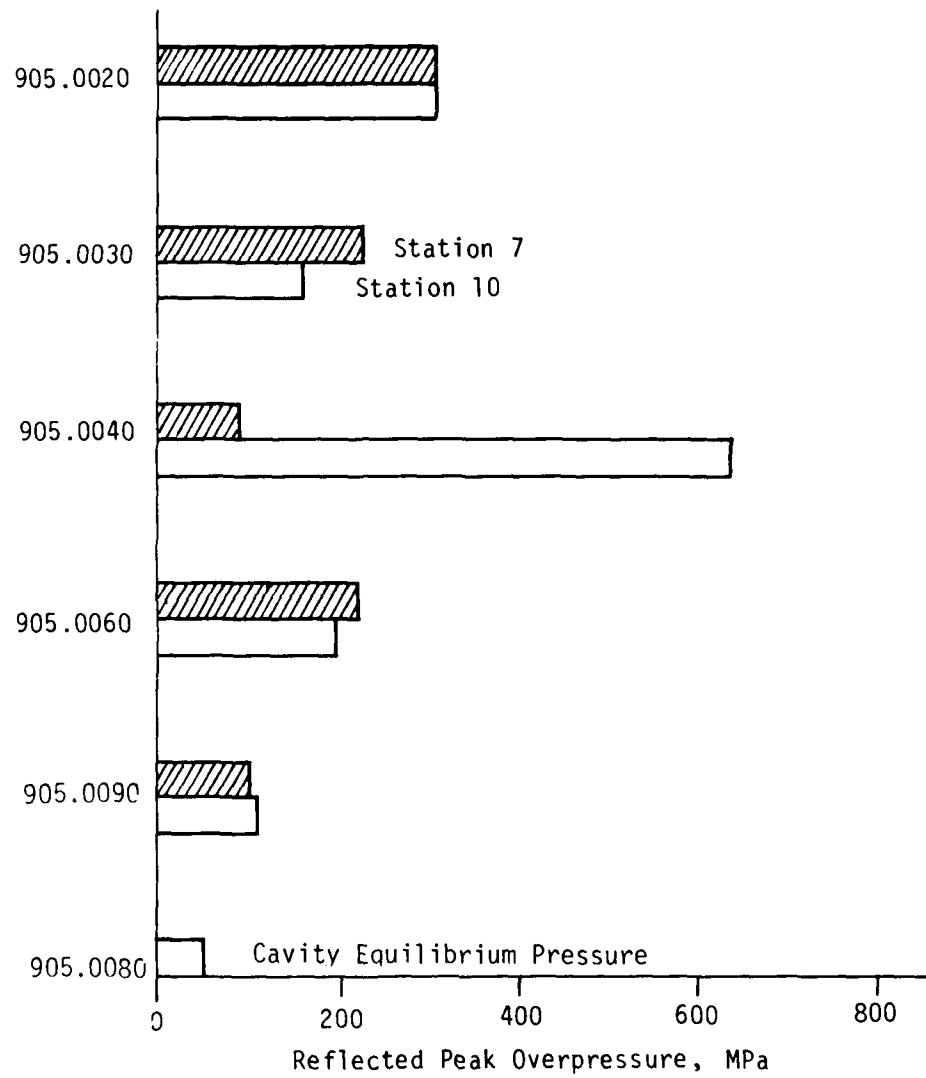


Figure 26. Peak Reflected Pressure at Cavity Floor

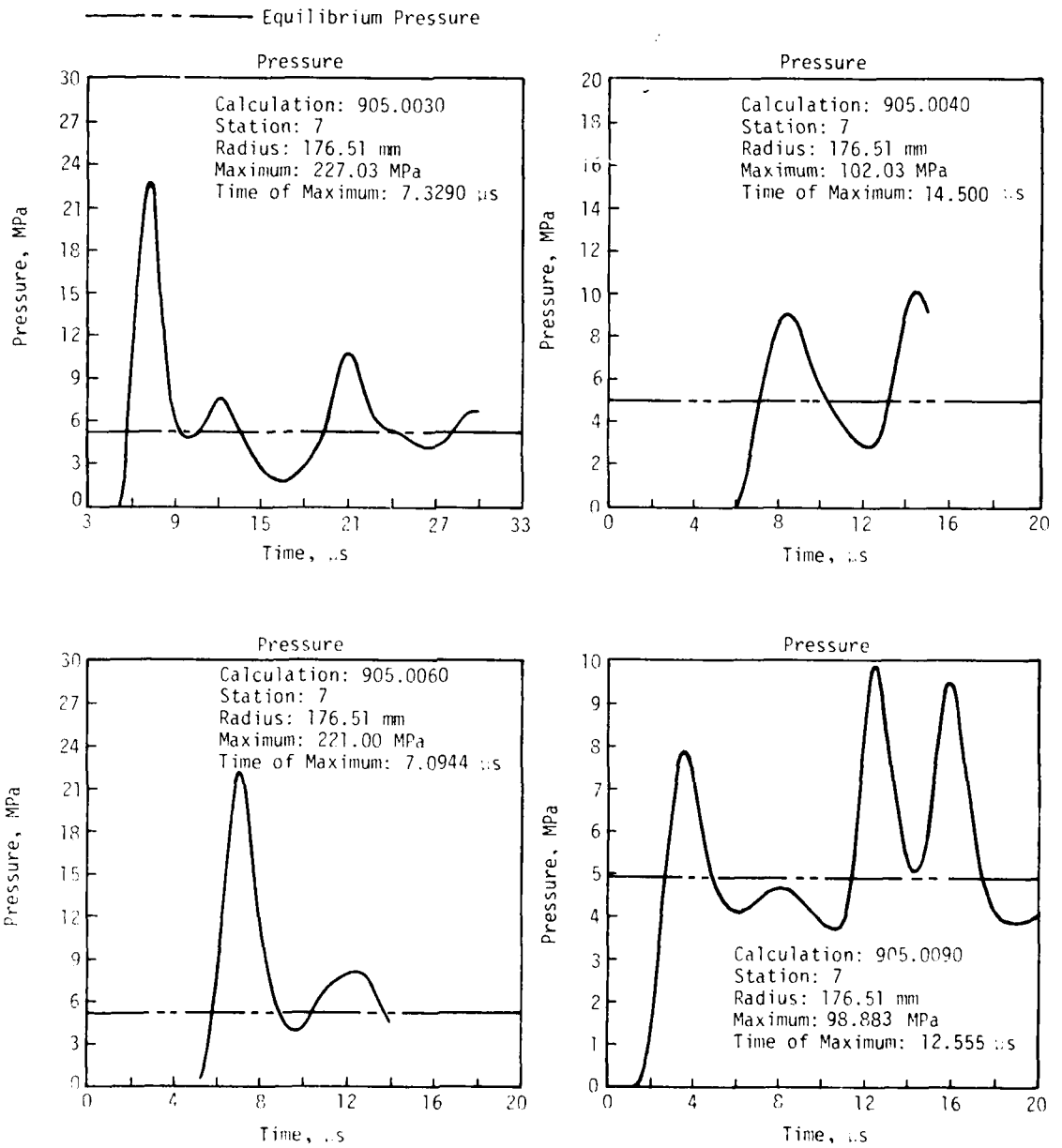


Figure 27. Station 7 Pressure

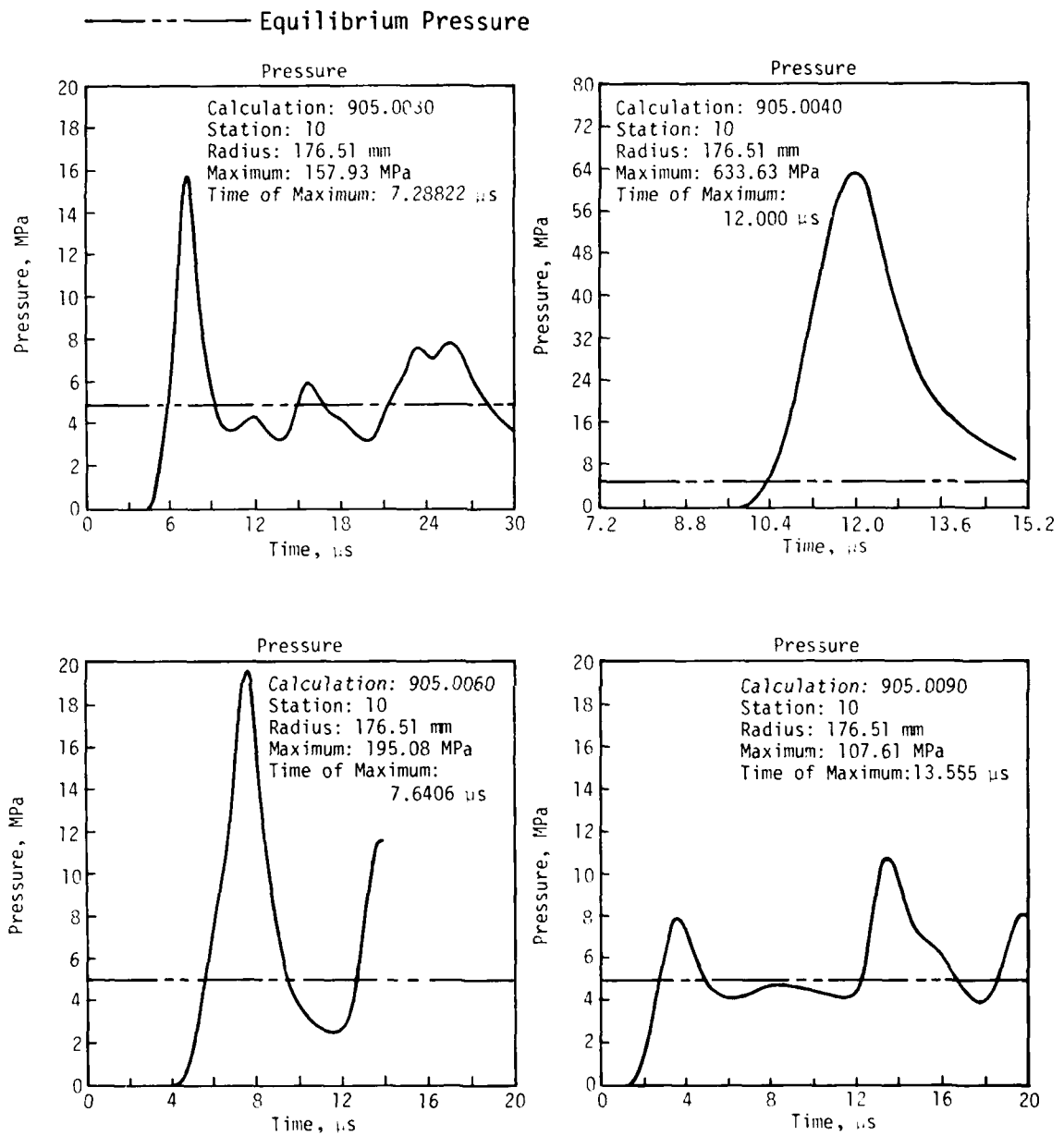


Figure 28. Station 10 Pressure

In summary the results of these calculations are not quantitatively conclusive. For example, the aforementioned inadequacies in the simulation of detonation phenomena may have had a marked effect on these solutions. To relate such numerical simulations more meaningfully to the HEST environment the calculational model must be refined in several respects.

1. The material model for the detonating cord explosive must realistically represent:
 - a. the mass of the explosive and its surrounding plastic case,
 - b. the detonation process, and
 - c. the products of detonation.
2. The high temperatures encountered in blast environments require that air be treated as a real gas with variable specific heats.
3. Protective buffer zones should be simulated as the result of multiple detonations rather than as a uniform pressure field.

Some qualitative conclusions can be made. The practice of removing strands of detonating cord from the region immediately above the pressure-measuring location should be discouraged. Instead the gages should be placed directly in line beneath the detonating cord strand, or even better, placed in the space midway between the strands and the line between the strand (midway between Station 10 and Station 7 in the preceding calculations). The greatest disbursement of explosive materials in the explosion cavity should be used, consistent with cost and practical construction considerations. The range of the pressure-measuring gage should be specified, based on calculated estimates of the incident and reflected peak pressures at that boundary (much higher than the anticipated peak simulation pressure for the experiment).

HULL SIMULATION OF HEST SINGLE EXPLOSIVE PLANE WITH SWEEPING WAVE

Calculations 905.0020, 905.0021, and 905.0051 simulated the HORS I-3 HEST air cavity with the simple technique of a one-time energy dump into a 1-D mesh. Another approach to modeling this experiment was attempted utilizing a timed sequence of energy dumps along the plane of symmetry of a 2-D mesh, thus producing a sweeping explosion wave. This sweeping wave of energy dumps more realistically represents the exploding edge of a woven layer of detonating cord used in more conventional HEST experiments.

In Figure 29 the Y-axis represents the plane of symmetry (centerline) of a HEST explosion cavity. In the calculations this is modeled as a reflecting boundary due to the symmetry of the cavity. The right boundary of Figure 29 is also a reflecting boundary representing the soil overburden. Energy is introduced into the mesh in the cells adjacent to the Y-axis, starting at the origin and proceeding in the positive Y-direction in proportion to the computed distance traveled at a specific problem time. A constant detonation velocity is used. The position of the sweeping detonation point at some arbitrary time is represented in Figure 29.

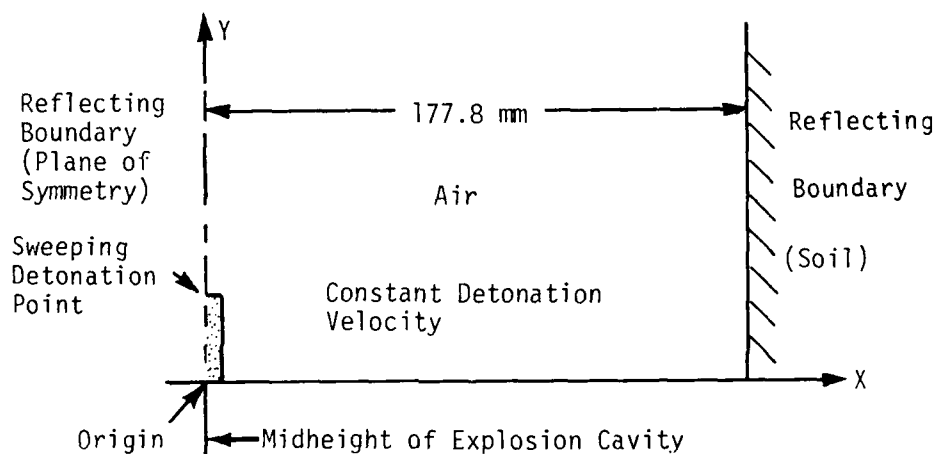


Figure 29. HEST Explosion Cavity with Sweeping Detonation

Three HULL calculations were accomplished using the sweeping wave simulation. In each of these calculations a cell width and height of 10.459 mm was used. The right reflecting edge was located at 177.8 mm. The mesh was considered to be air having a mass density of 1.225×10^{-6} g/mm³ and an energy density of 2.067×10^9 ergs/g. These conditions yielded an initial cell mass of 1.34×10^{-3} g, an initial cell energy of 2.77×10^6 ergs, and an ambient cavity pressure of 0.1025 MPa. The constant velocity of detonation was 6.4008×10^5 mm/s. A real air EOS was used with a variable gamma coefficient. Data history stations were placed as shown in Table 3 for all three calculations.

In calculations 905.1080 and 906.1010* the energy added to the mesh was 5.459×10^9 ergs per cell which amounted to a planar charge density of 9.98×10^7 ergs/mm². This value is substantially lower than the desired planar charge density of 4.297×10^8 ergs/mm² due to an oversight. In both calculations the top (sweep exit) boundary was transmissive.

TABLE 3. STATION LOCATIONS

Station No.	Co-ordinates		Station No.	Co-ordinates	
	X	Y		X	Y
	mm			mm	
1	170	30	29	20	180
17	170	60	30	30	180
2	170	90	31	40	180
18	20	120	32	60	180
19	30	120	33	80	180
20	40	120	34	90	180
21	60	120	35	110	180
22	80	120	36	130	180
23	90	120	37	150	180
24	110	120	38	170	180
25	130	120	39	170	180
26	150	120	4	170	210
27	160	120	50	170	250
28	170	120	5	170	280
3	170	150	61	170	310

Calculation 905.1080 utilized a transmissive lower (sweep entry) boundary while calculation 906.1010 had the same parameters except for a reflective lower boundary. Figure 30 shows a pressure history at a station next to the right reflecting boundary while Figure 31 shows a plot of equal pressure contours and a plot of velocity vectors corresponding approximately to the time of maximum reflected pressure in Figure 30. It appeared that the transmissive lower boundary may be allowing mass and/or energy to escape from the problem mesh. The bottom row of velocity vectors in Figure 31 shows several vectors directed outside the mesh which leads to this interpretation. Calculation 906.1010 was then accomplished with the lower boundary changed to

*Hydrocode Calculation No. 905.1080, Data Report, UNM/CERF AST-25, December 1978.

Hydrocode Calculation No. 906.1010. Data Report, UNM/CERF AST-29, December 1978.

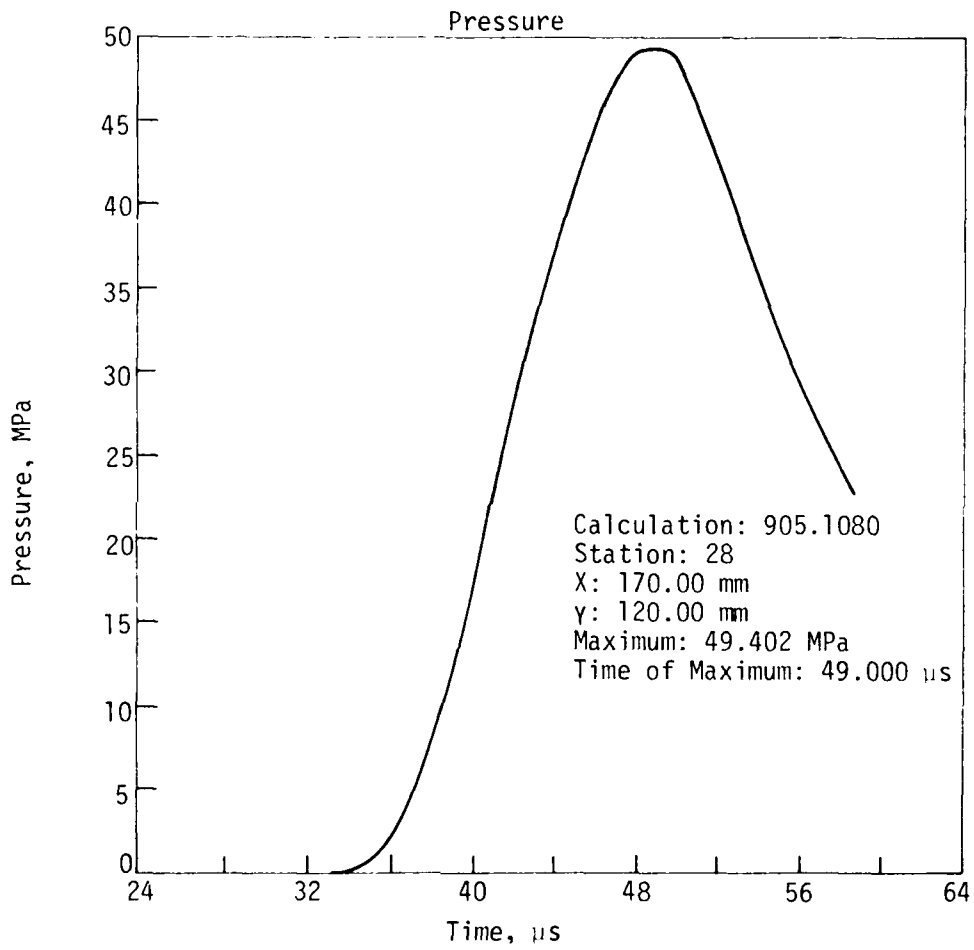


Figure 30. Calculation 905.1080--Pressure History at Station 28

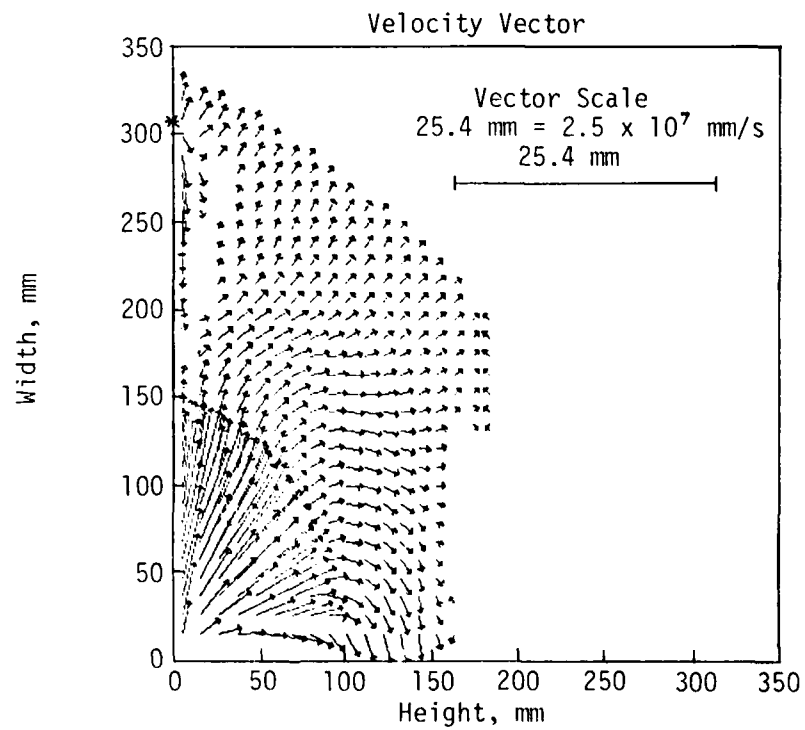
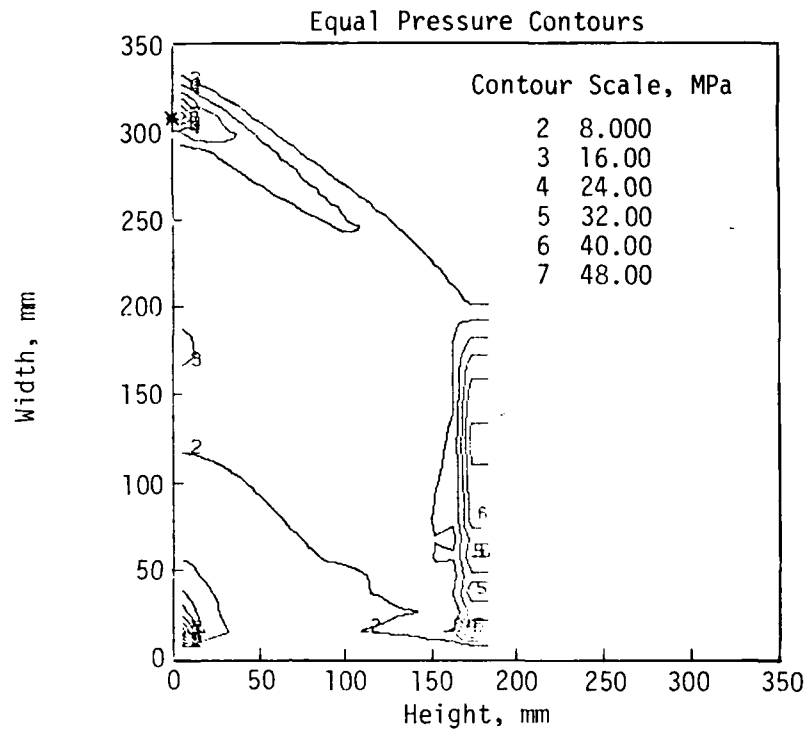


Figure 31. HULL Calculation 905.1030--Sweeping Detonation Wave (48 μ s)

be reflective rather than transmissive. The reflective lower boundary had a very significant effect on the total results. The pressure at the stations next to the right boundary had only begun to show a pressure increase for calculation 906.1010 when the problem was stopped at 60 μ s. Note that in Figure 32 there is a row of vectors originating from a lower position than the lowest row of Figure 31. This observation leads to the implication that the transmissive boundary of calculation 905.1080 earlier thought to be allowing mass and energy loss may only be transmitting from the second row back into the first row.

In calculation 906.1020* the deposited energy was increased to 2.364×10^{10} ergs per cell. The transmissive lower boundary was again specified. The individual cell dimensions were retained; therefore the effective charge density was 2.1611×10^7 ergs/mm³, which is still lower than the desired charge density. In Figure 33 the maximum reflected pressure of the station next to the right boundary was 25.5 MPa. This fact indicates an unexplained reversal in magnitude compared to the peak value of 49.4 MPa for calculation 905.1080 (Fig. 28) which was run with the smaller deposited energy. Pressure contours and the velocity field for the approximate time of peak pressure are shown in Figure 34. The pressure histories in Figure 35 shed some light in explaining this reversal. The grid used in all three calculations was too coarse. Instabilities are present in the pressure histories for calculation 905.1080 at Stations 18 and 29 adjacent to the plane of symmetry. They are even more evident at the same stations for calculation 906.1020. It is conceivable that the increased energy in calculation 906.1020 was enough to generate the observed oscillations which may in turn have caused excessive attenuation of the wave.

The computer costs for each of these problems were \$10 to define and initialize the mesh, \$50 to perform the actual calculation, and \$20 to plot the output. If the mesh is refined the cost would increase accordingly, perhaps as much as an order of magnitude.

The results of these calculations were not fully conclusive in that they do not yet provide a basis for comparison with the calculation of the 1-D simultaneous detonation.

*Hydrocode Calculation No. 906.1020, Data Report, UNM/CERF AST-38, December 1978.

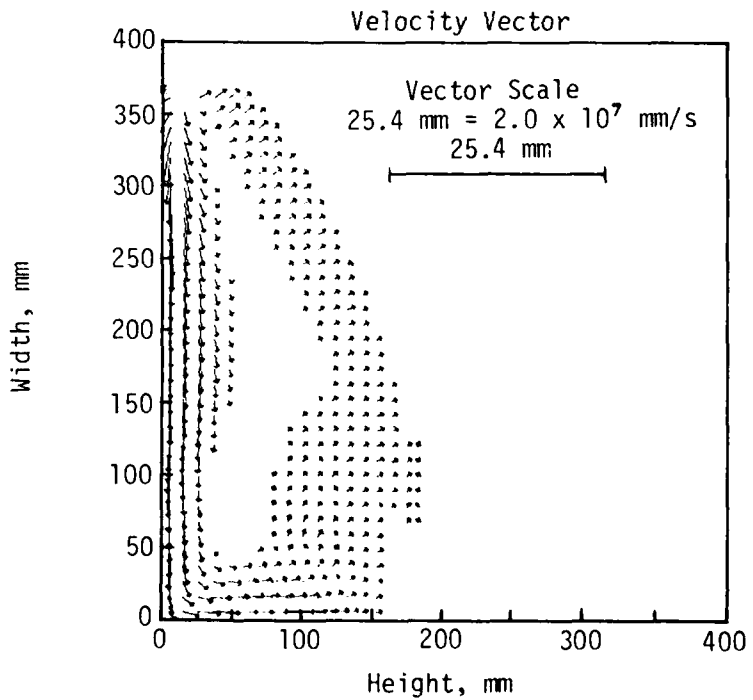
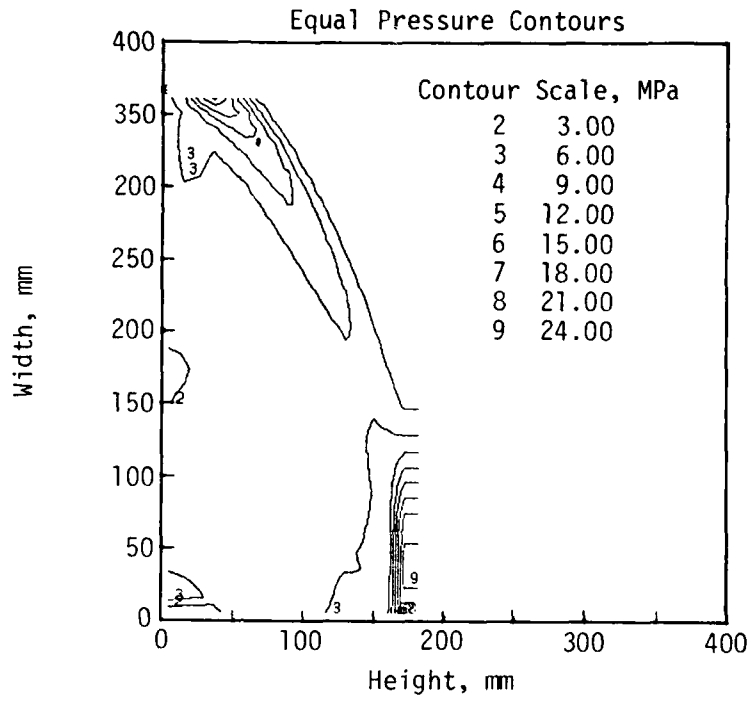


Figure 32. HULL Calculation 906.1010--Sweeping Detonation Wave (60 μ s)

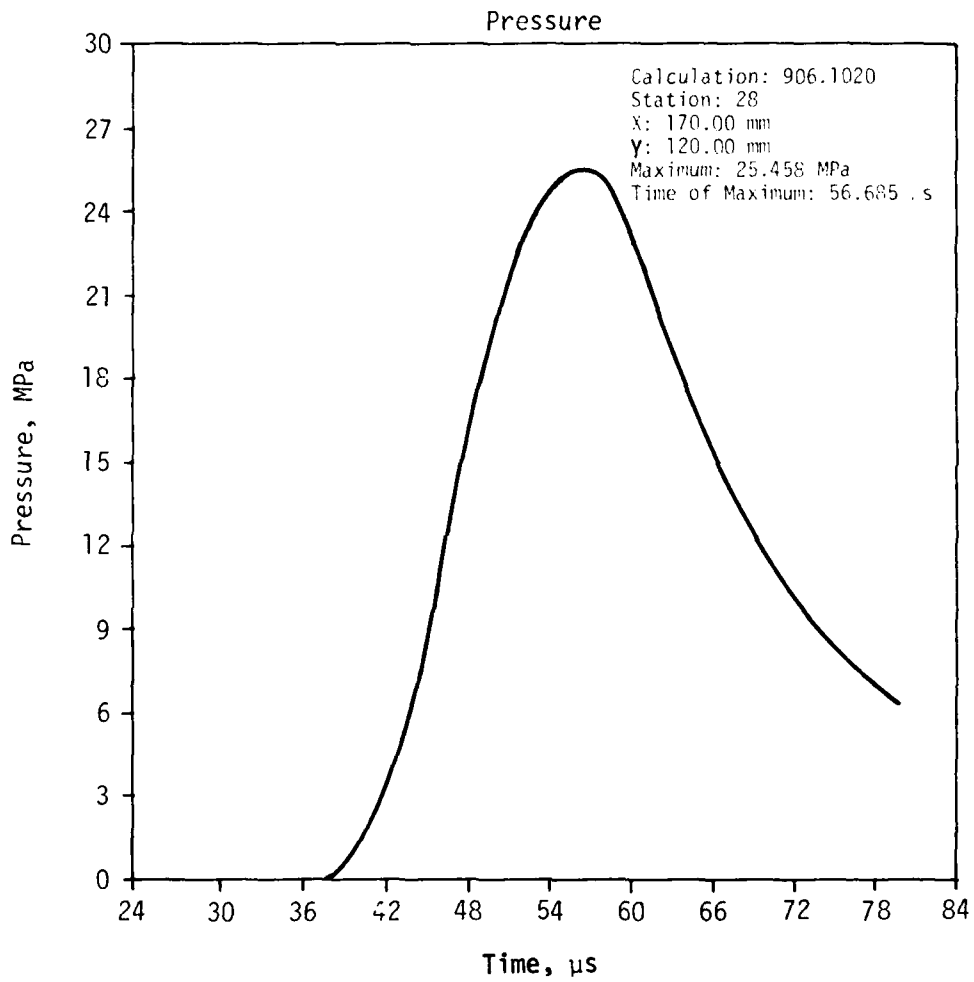


Figure 33. Calculation 906.1020--Pressure History at Station 28

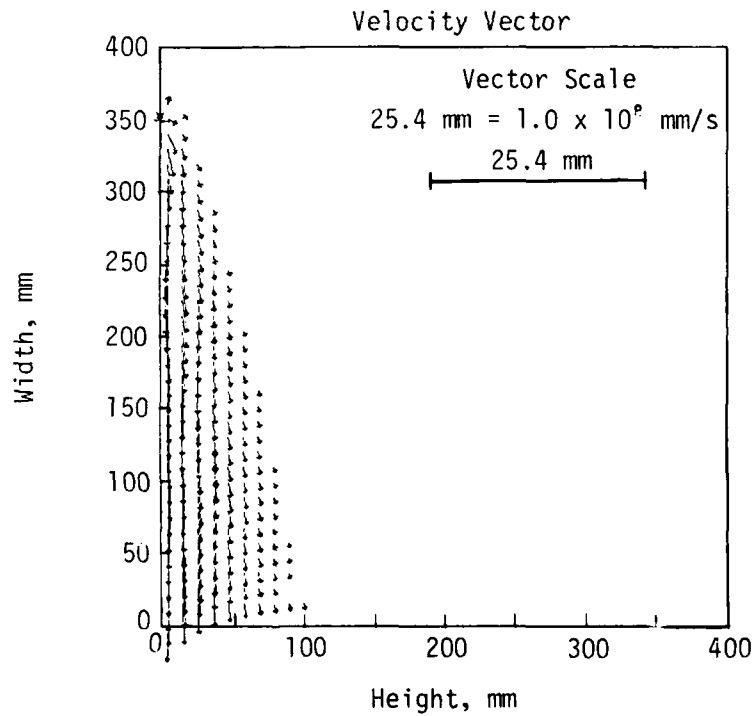
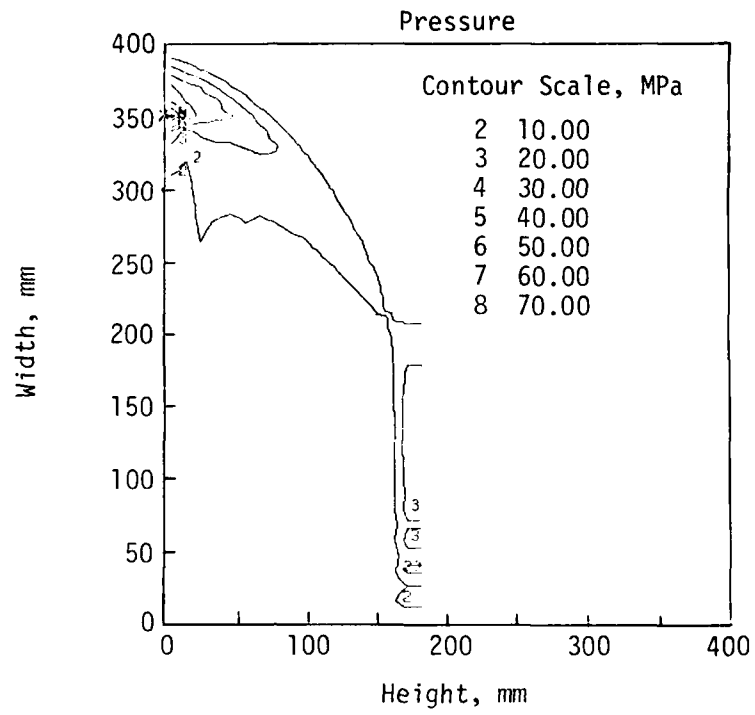


Figure 34. HULL Calculation 906.1020--Sweeping Detonation Wave (55 μ s)

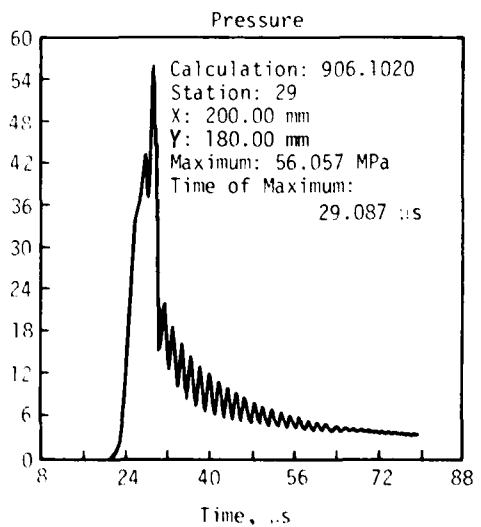
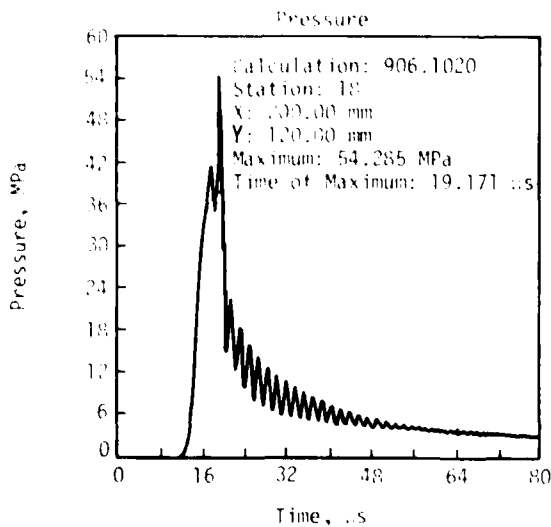
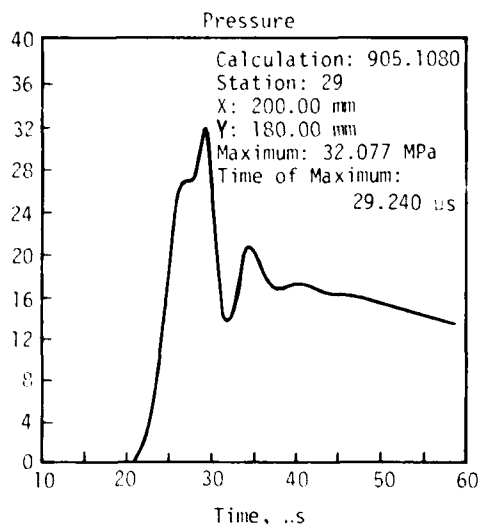
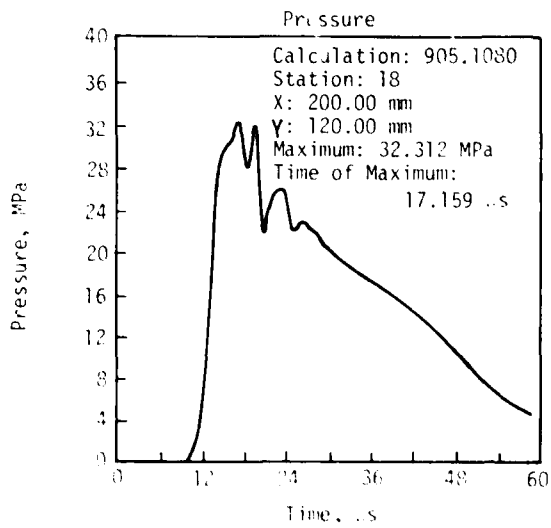


Figure 35. HULL Calculations 905.1080 and 906.1020--Instabilities in Calculations

SECTION IV DABS SIMULATOR CALCULATIONS

The DABS simulator consists in general of a partially buried shock tunnel in which an explosive charge placed against the closed end is used to produce a planar shock wave which propagates down the tunnel and produces a dynamic flow behind the shock. Items of interest in the calculational modeling of the DABS experiment include the proper method for modeling the detonation (a burn algorithm versus an isothermal energy dump), the selection of appropriate cell sizes and boundary conditions, and the representation of target structures and reflecting surfaces.

A number of 1-D and 2-D calculations were performed with the use of the SAP and HULL hydrocodes to investigate these and other items of interest. Several simulator configurations were then modeled and calculated.

PARAMETRIC STUDY OF BLAST WAVE CHARACTERISTICS AS A FUNCTION OF CELL SIZE AND EXPLOSIVE CHARGE DENSITY (SAP HYDROCODE)

The results of a series of SAP 1-D numerical simulations are presented here to provide a data base which can be used to derive an economical technique for predicting blast wave characteristics for DABS experiments.

The fluid behavior for these simulations was governed by the AFWL variable-specific-heat equation of state for air. In all cases Eulerian flow was simulated in a uniform mesh within a Cartesian geometry and in the absence of artificial viscous damping. The left boundary was coincident with the plane of symmetry. Therefore these solutions describe the propagation of planar blast waves in a closed, constant-area tube which initially contains air at one standard atmosphere.

The blast waves were generated by incrementing the internal energy in the cell adjacent to the plane of symmetry between the first and second calculational cycles. Consequently this first cell is comparable to the driver section of a

closed shock tube where both it and the reaction section contain air.

Six calculations* were performed in which both the initial planar energy density of the driver and the cell size were varied. The calculational matrix specified cell widths of 10, 100, and 200 mm at energy levels of 10^6 and 10^{11} ergs/mm² (Fig. 36). In each calculation the histories of hydrodynamic variables were recorded at ranges of 1, 2, 3, and 4 m from the plane of symmetry. In most instances it is desired to predict the blast intensity at some target structure. Therefore these data were recorded at the cell immediately upstream from the nominal station range (Fig. 37) and represent fluid properties at the center of the cell.

When assessing structure response to impulsive blast loadings, four parameters are of particular interest:

1. wave velocity,
2. rate at which the structure is loaded,
3. maximum applied load, and
4. total applied load,

Some typical calculated results are presented in Figure 38 where the waveforms for the same location are compared for three cell sizes.

These parameters are presented graphically as families of functions representing appropriate calculated blast wave characteristics, viz:

1. time of arrival (Fig. 39),
2. rise time (Fig. 40),
3. peak pressure (Figs. 41 and 42), and
4. pressure impulse (Fig. 43).

The accuracy with which a nuclear airblast environment can be simulated is to a great extent dependent on how well these parameters can be controlled.

*Hydrocode Calculations Nos. 908.0011 through 908.0061, Data Report, UNM/CERF AST-44, December 1978.

Calculation Numbers

Explosive Energy Density	Cell Size		
	10 mm	100 mm	200 mm
10^8 ergs/mm ²	908.0011	908.0051	908.0031
10^{11} ergs/mm ²	908.0021	908.0061	908.0041

Figure 36. Computational Matrix

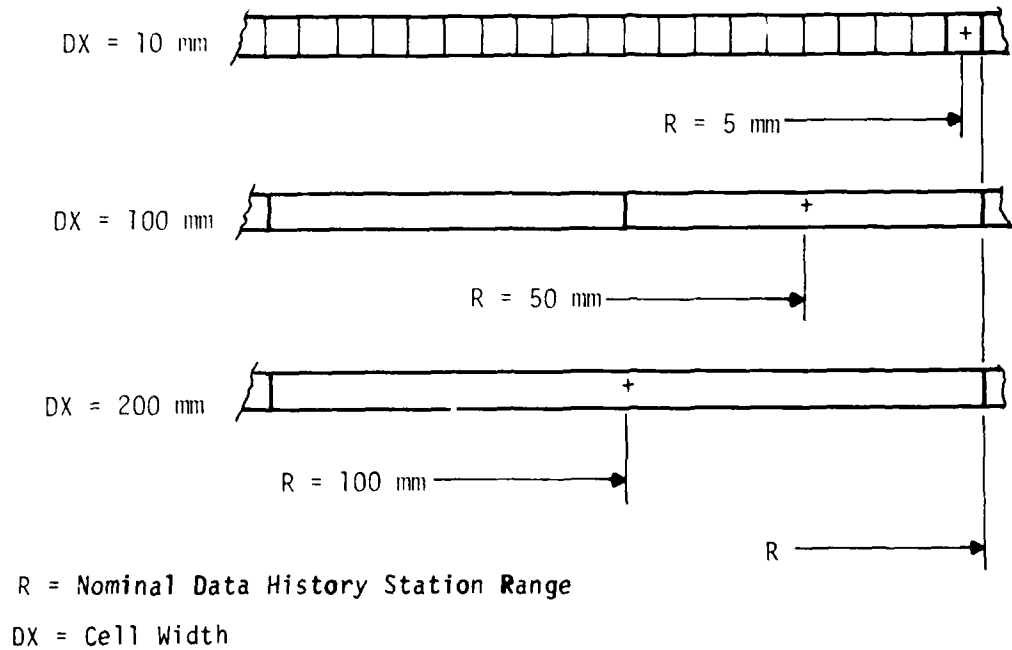


Figure 37. Effective History Station Range

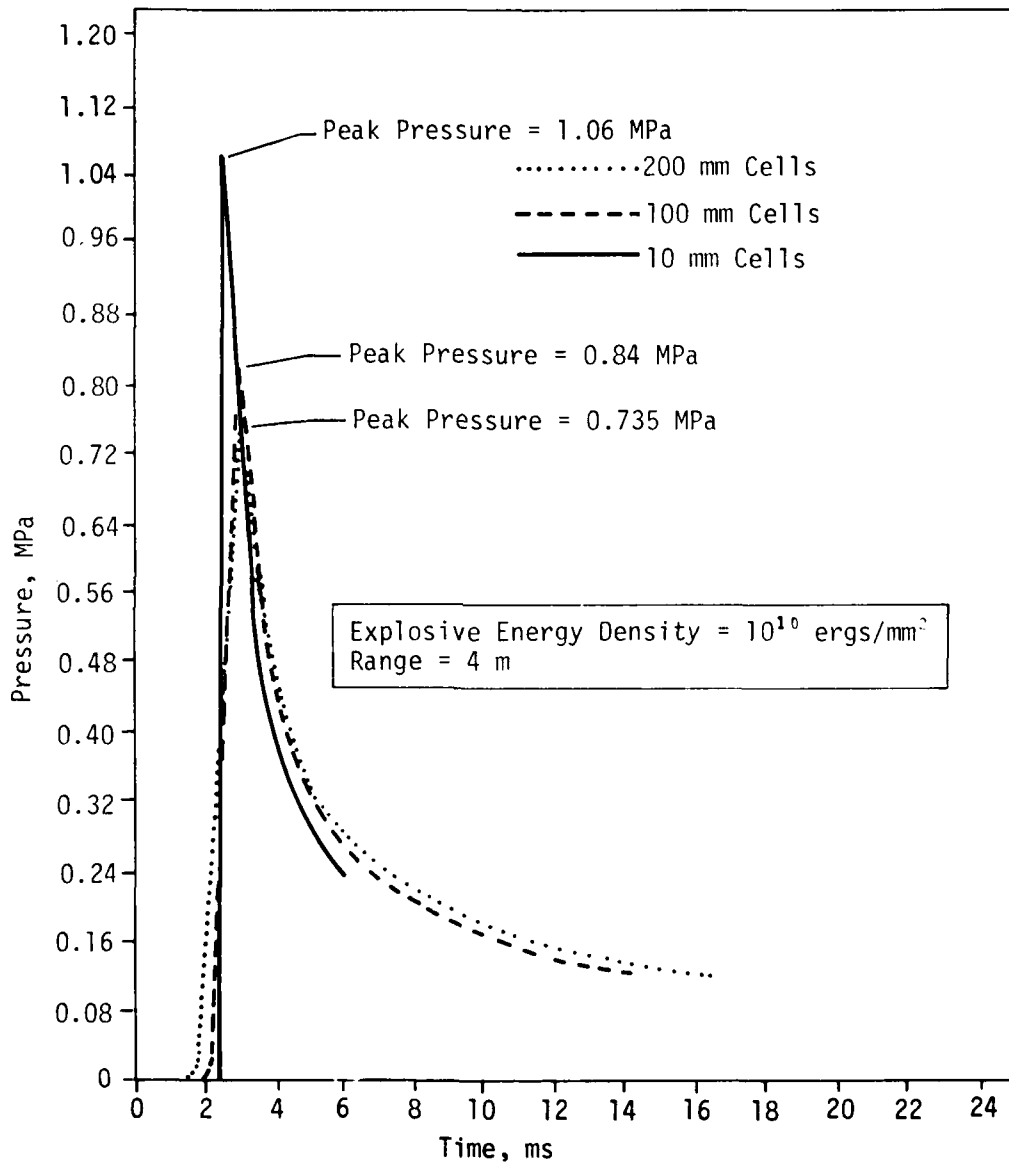


Figure 38. Comparison of Peak Pressures and Waveforms for Different Cell Sizes

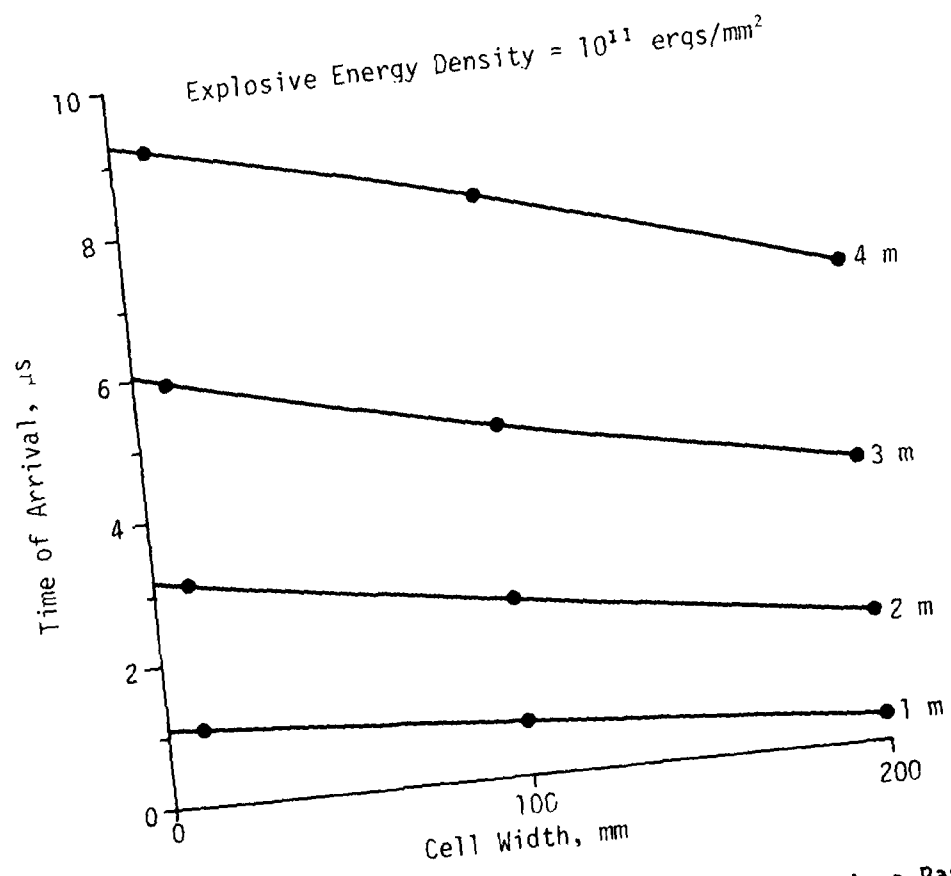
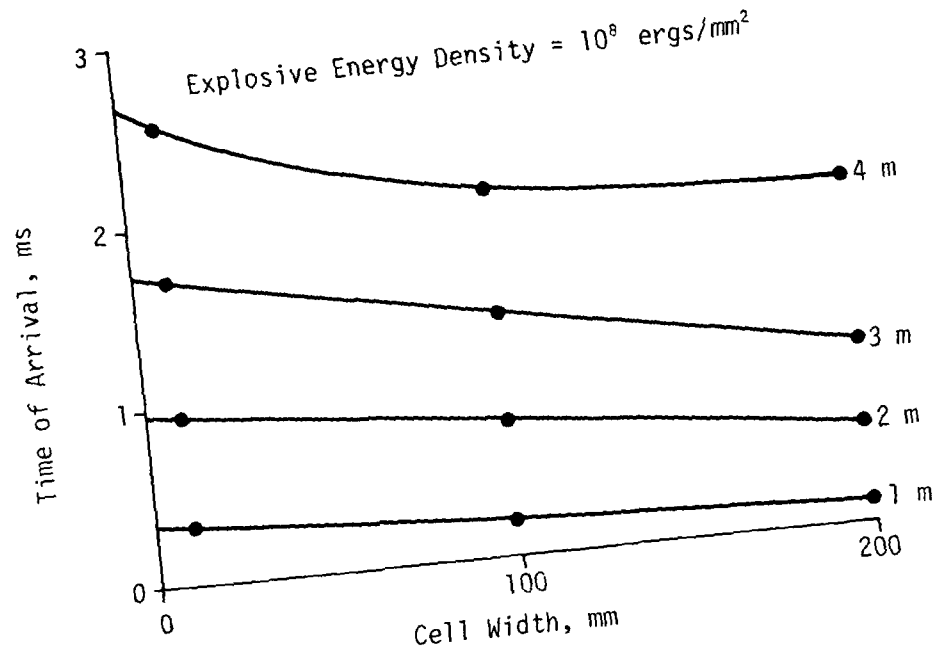


Figure 39. Shock Arrival Time versus Cell Width at Various Ranges

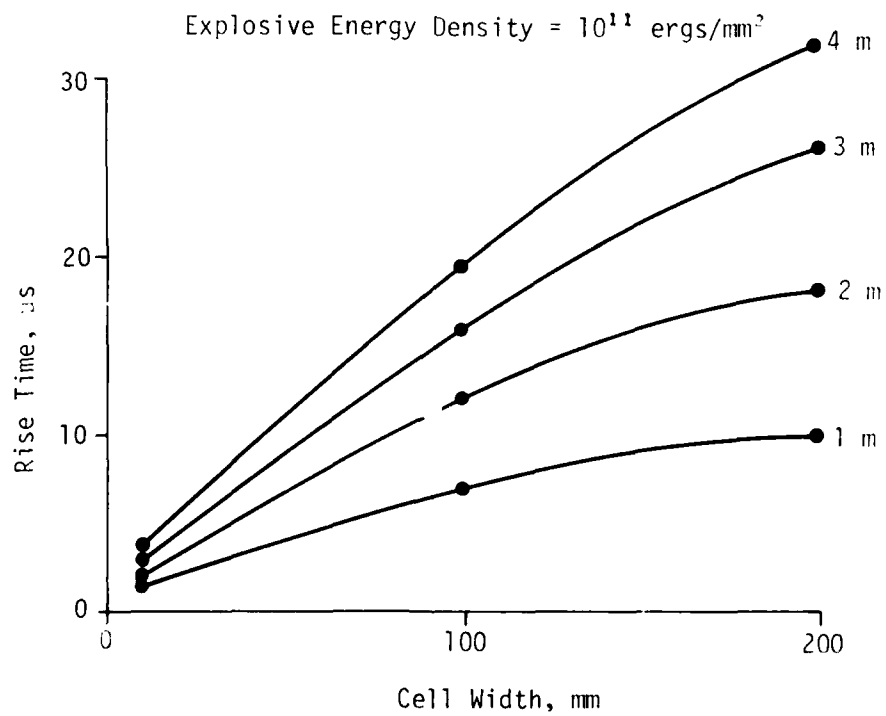
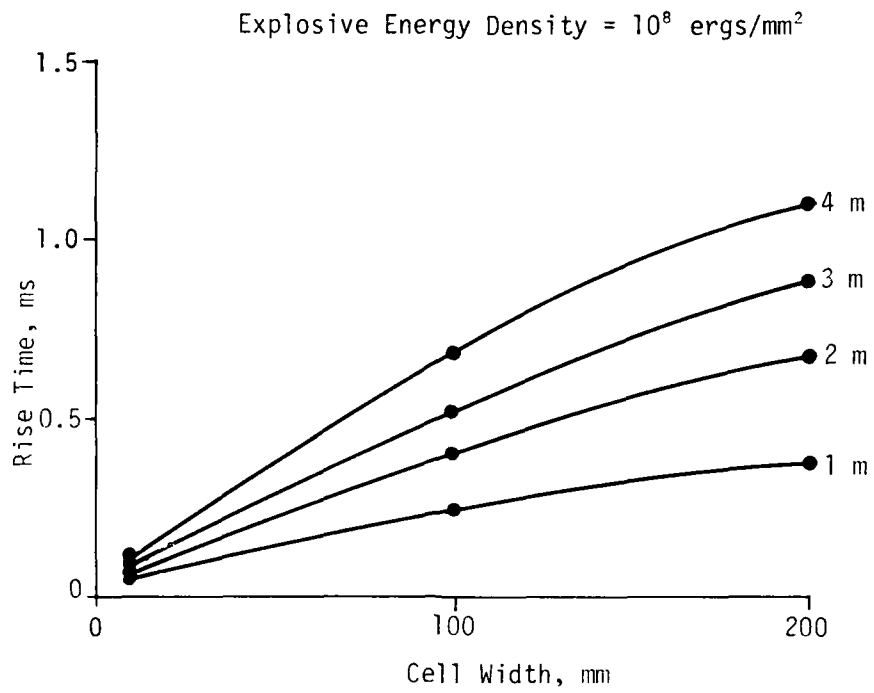


Figure 40. Shock Rise Time versus Cell Width at Various Ranges

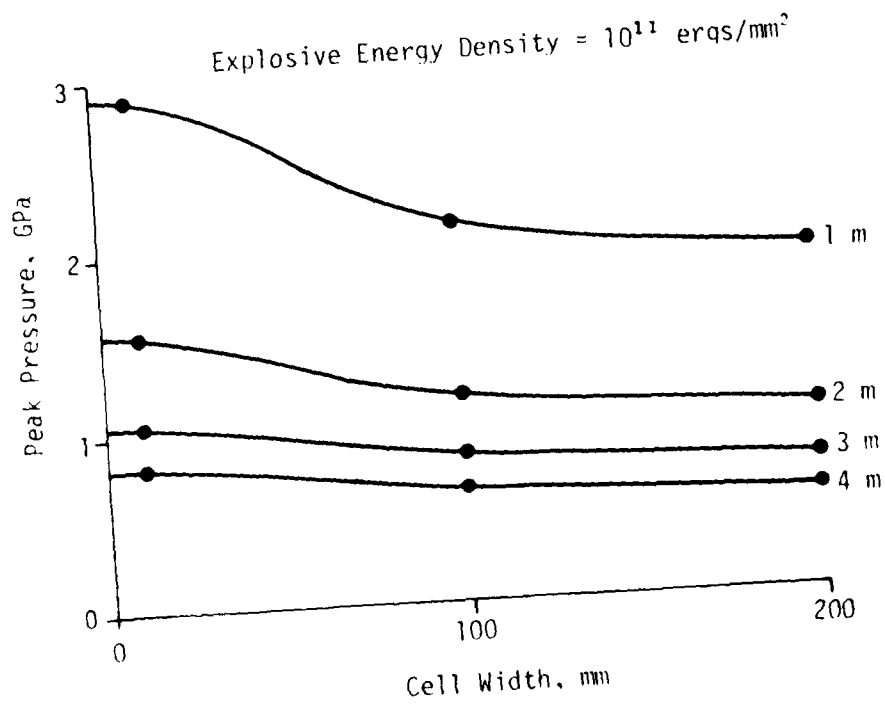
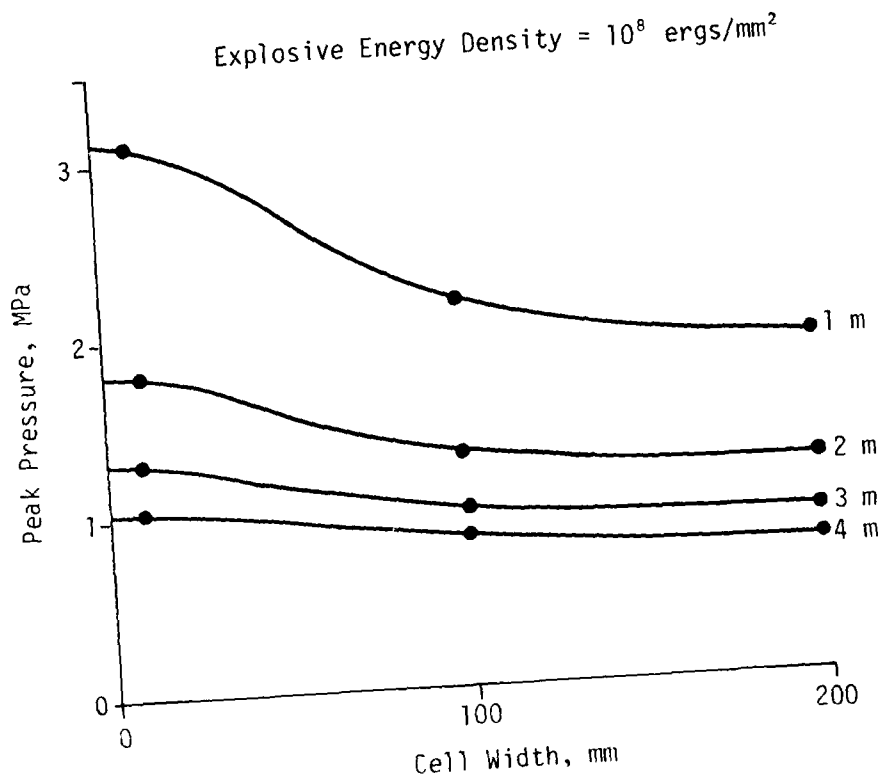


Figure 41. Peak Pressure versus Cell Width at Various Ranges

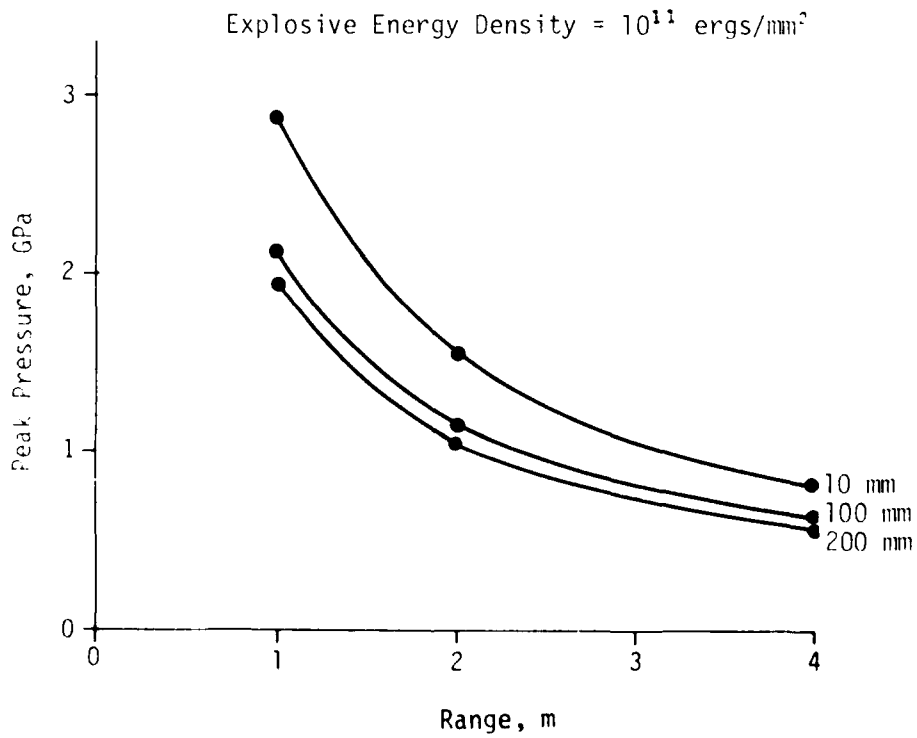
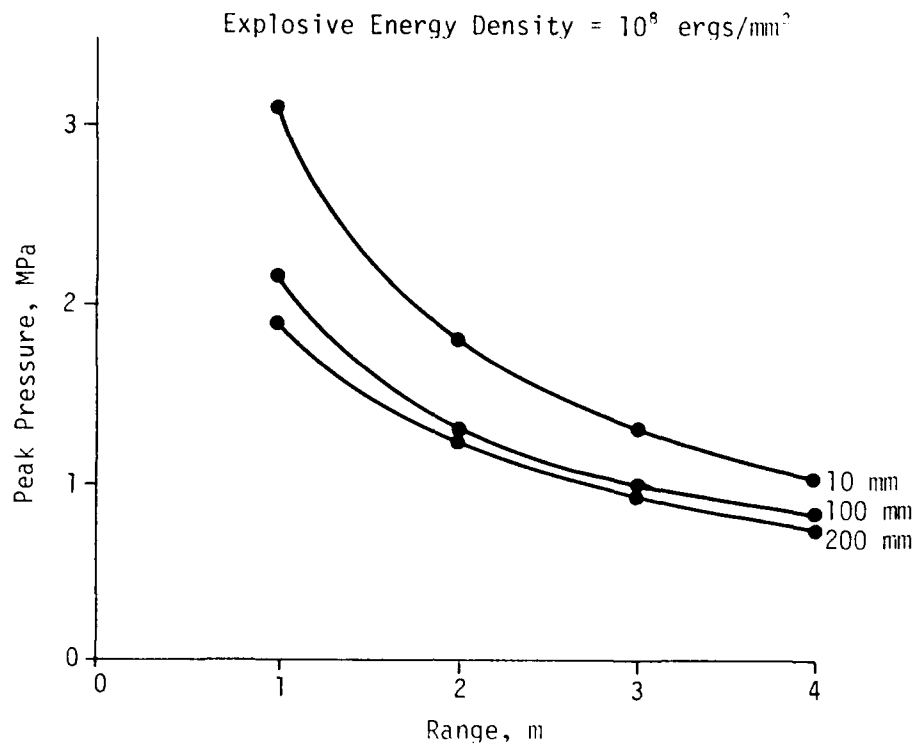


Figure 42. Peak Pressure versus Range at Various Cell Widths

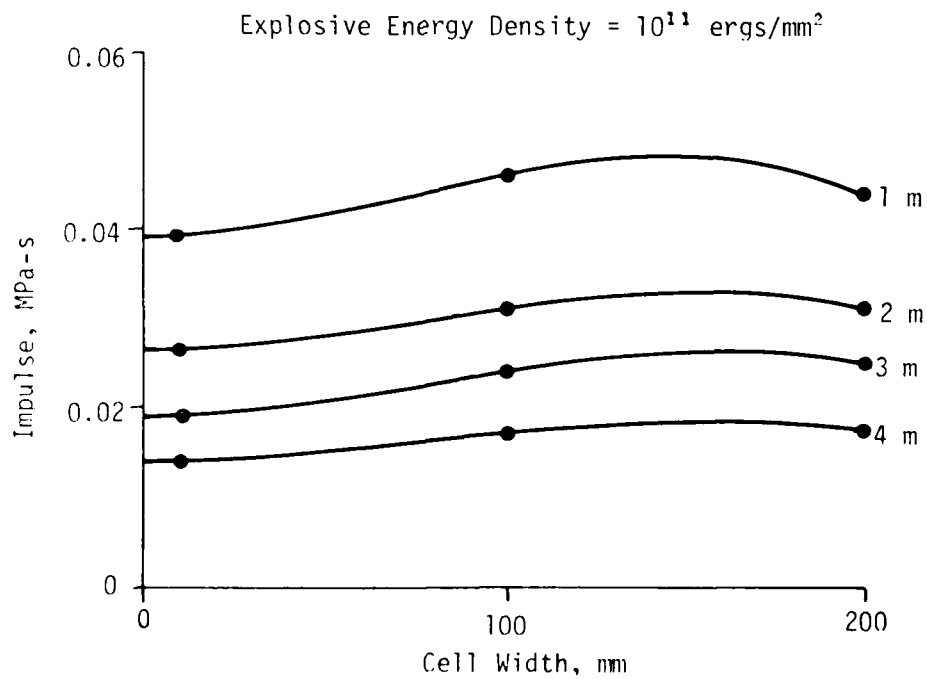
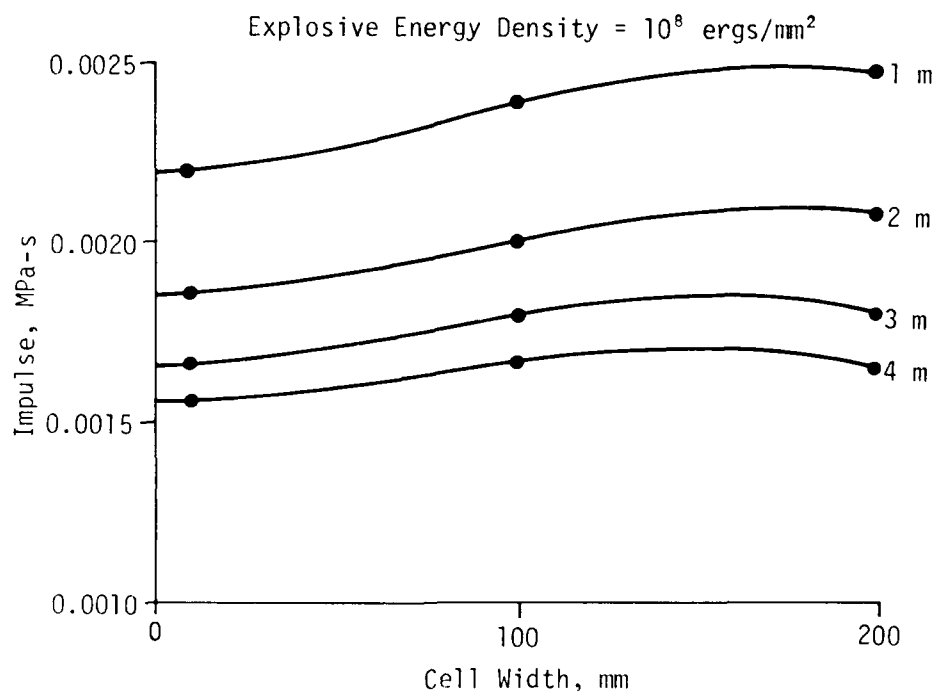


Figure 43. Impulse versus Cell Width at Various Ranges

At ranges up to 3 m shock arrival times exhibited a nearly linear decay as cell width increased (Fig. 39). These solutions indicate, however, that at 4 m this relation no longer holds, particularly for lower strength shocks (peak pressures < 1 MPa) where the effect of cell size on shock velocity may differ significantly.

Some difficulty was encountered in determining rise times from pressure history plots. However, the graphic display of these data sets (Fig. 40) reveals a reasonably uniform influence from an increase of cell width. At all ranges the rate at which rise times lengthen gradually diminishes. As one might expect cell width has the least impact at closer-in ranges where propagation velocities are greatest.

The graphic interpretation of peak pressure data was based on the presumption that as the cell size becomes infinitely small, the calculated peak must asymptotically approach some limiting maximum value. Therefore, when considering peak values as a function of cell width (Fig. 41), it was necessary to arbitrarily introduce an inflection in the curve to satisfy this condition. Due to the character of the data in these limited samplings (three cell widths), it is implied that as the cell becomes very large the peak pressure would approach a lower limit. It is reasonable to contend that in reality this is the case. At both shock strengths it is clear that as range increases, peak pressure becomes markedly less dependent on cell width. The displays of peak pressures versus range (Fig. 42) clearly show that as cell width increases, a rapid convergence to a minimum peak pressure is nearly independent of range.

When considering the presentations of pressure impulse (Fig. 43), one should keep in mind that the accumulations represent relatively short time intervals, 35 ms and 85 μ s for energy levels of 10^8 and 10^{11} ergs/mm², respectively. In the extreme this means that the pressure had decayed to only 57 percent of the peak. Nevertheless there is an indication that the impulse is influenced by cell size, increasing slightly at first and then decreasing when the cell width exceeds 150 mm.

Before using these results to assess the effects of cell size on blast wave characteristics, one should consider certain aspects of this calculational study.

First, the simplistic technique used to generate the airblasts should be evaluated with respect to the simulation of the detonation of an explosive. It is quite possible that a multimaterial model which incorporates the effects of the detonation process could significantly alter these solutions.

Second, the graphical interpretation of functions based on data representing only three cell widths must be considered questionable in some respects. For example, to verify the assumptions made in regard to peak pressure behavior, a broader statistical base is required. Finally, since DABS tests may involve tunnel lengths well in excess of 10 m, calculations of sufficient duration to obtain data at appropriate ranges are recommended.

SIMULATION OF 4.14-MPa REFLECTED AIRBLAST WAVE

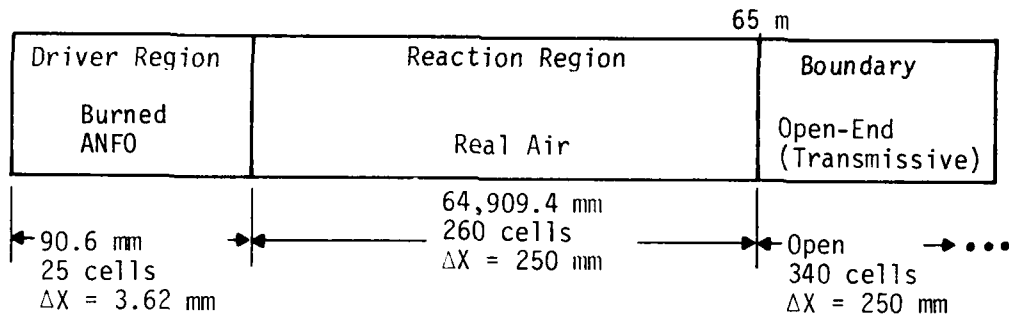
SAP calculation 906.1081* was performed to evaluate the incident airblast wave in an explosive simulation of a 125-kt nuclear airblast wave in support of the early HAVE HOST T series (in-trench) tests. A range was sought which produces a peak pressure of 4.14 Mpa. Calculation 906.1091** then evaluated the flow with a solid, reflecting boundary introduced into the shock tunnel at the 4.14-Mpa range found in calculation 906.1081.

The driver consisted of 25 cells of burned ammonium nitrate and fuel oil (ANFO) with a mass density of 1.38×10^{-3} g/mm³ and an energy density of 2.822×10^{10} ergs/g as shown in Figure 44. Cell thickness was approximately 3.6232 mm for a total driver width of 90.5797 mm. The total driver mass was 12.5 g, and total driver energy was 3.5275×10^{11} ergs. The shock tunnel contained real air with ambient densities of 1.225×10^{-5} g/mm³ and 2.04448×10^9 ergs/g and a cell thickness of 250 mm. SAP method Number 1 (Lagrangian) was selected as the hydrocode to be used because of its multimaterial capability

*Hydrocode Calculation No. 906.1081, Data Report, UNM/CERF AST-26, December 1978.

**Hydrocode Calculation No. 906.1091, Data Report, UNM/CERF AST-27, December 1978.

Incident Wave Geometry--Calculation 906.1081



Reflected Wave Geometry--Calculation 906.1091

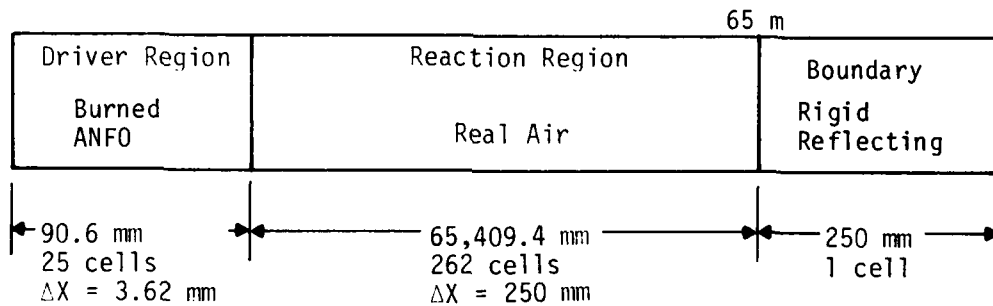


Figure 44. Geometrical Descriptions for Calculations 906.1081 and 906.1091

and because its Lagrangian properties would allow the interaction of detonation products to be traced throughout the calculations. The displacement of this interface at various times for both incident and reflected wave calculations is recorded in Table 4. An artificial viscosity function (Ref. 12) was employed to provide a stable, sharply defined shock front. The mesh geometries for the two calculations are identical in the driver region and also in the reaction region of the shock tunnel. Differences occur at the reflecting boundary which is located at 65,500 mm in calculation 906.1091 as shown in Figure 44. Material and energy deposition are identical for the two calculations.

Pressure history stations were set in calculation 906.1081 at 1-m intervals, starting at 57 m and continuing through 79 m. The calculation was then run far enough to identify that the peak pressure reached a value of 4.14 MPa at the 65-m range at approximately 25.5 ms (Figs. 45 and 46). It was then necessary to extend the open end of the tunnel and allow the calculation to continue until the interface of detonation products passed well beyond the station of interest. Passage of this interface may be noted in Figure 45 as the change in slope of the pressure curve at approximately 45.5 m. It is also verified in Figure 47 as the abrupt change in density at 65 m. The pressure history stations for calculation 906.1091 were complemented with additional stations at 100-mm intervals starting at 64.5 m through 65.4 m to measure the reflected pressure. Calculation 906.1091 was run to 60 ms to allow sufficient time for the detonation products to interact with the reflected wave. The reflected wave, traveling to the left, intercepts the denser detonation products which are still moving to the right, resulting in a secondary reflection wave toward the right. The moment of interception can be seen in Figure 48 in the spikes at a radius of 56 m. This secondary reflection is then reflected in turn at the cavity boundary and appears as the second peak of pressure in Figure 49 with a maximum value of 16 MPa at approximately 44 ms. The moment of arrival of the secondary wave at 65.4 m is shown in Figure 50. The interface boundary reaches a maximum radius of 56.24 m at 39 ms (Table 4) before it starts contracting after the passage of the original reflected wave.

TABLE 4. POSITION OF DETONATION PRODUCTS BOUNDARY

Time, ms	Incident Wave Radius, m	Reflected Wave Radius, m
0	0.0906	0.0906
5	13.6949	13.6949
10	23.5236	23.5236
15	31.6707	31.6707
20	38.7236	38.7236
25	44.9707	44.9707
30	50.5805	50.5790
35	55.6693	55.6623
40	60.3230	56.2114
45	64.5855	55.5395
50	68.5237	54.0469
55	72.1597	51.1936
60	74.2061	48.8432

Each calculation was run to a problem time of 60 ms. Calculation 906.1081 required 5125 cycles and cost \$75. Calculation 906.1091 required 9723 cycles and cost \$120.

The presence of the second reflected peak has been noted in previous APOD calculations used in predicting the test environments for the HAVE HOST T-1 Event.* The corresponding experimental measurements of reflected pressure at the plug of the T-1 event** only hints at the presence of this second reflection. It should be noted that the interface in the calculations is a sharply defined boundary whereas in reality the interface becomes diffused and probably does not stand out to the extent noted in the calculations. This conclusion was confirmed by an Eulerian HULL calculation (reported later in the section).

*Renick, J., et al., *HAVE HOST T-1 Predictions*, Letter Report, Civil Engineering Research Division, Air Force Weapons Laboratory, Kirtland Air Force Base, New Mexico, 12 July 1977.

***HAVE HOST T-1 Quick Look*, Preliminary Report, Civil Engineering Research Division, Air Force Weapons Laboratory, Kirtland Air Force Base, New Mexico, 25 August 1977.

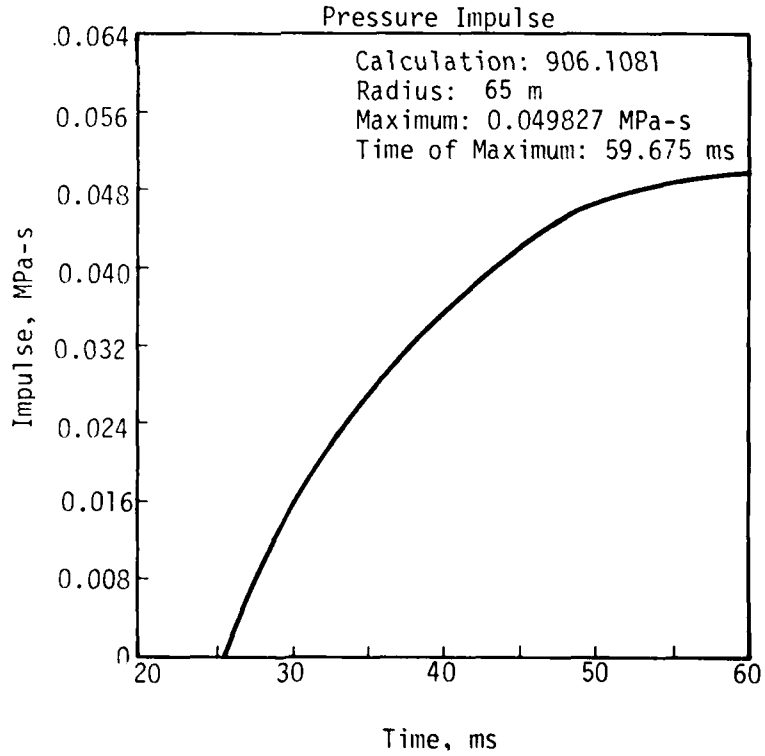
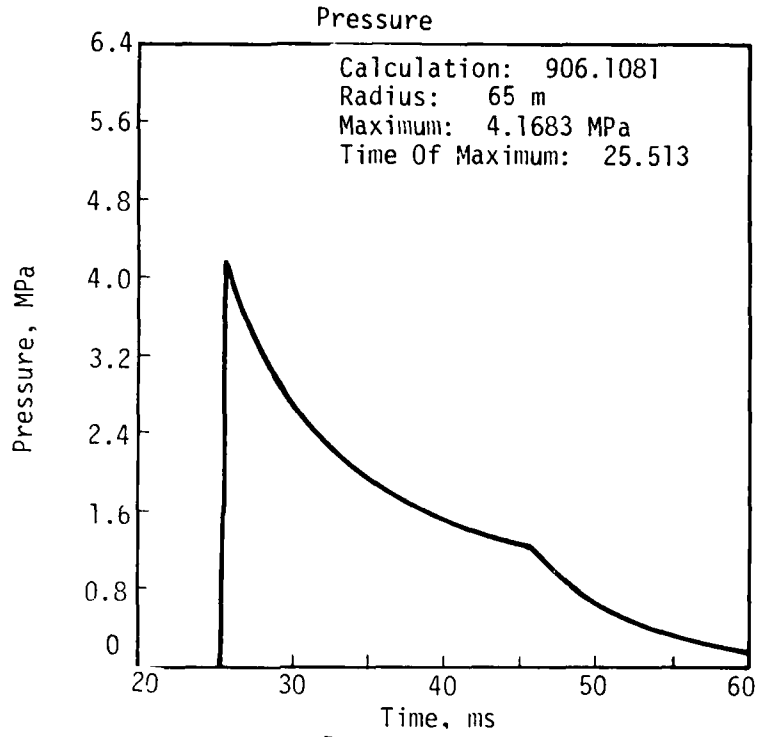


Figure 45. Incident Wave History at 65 m

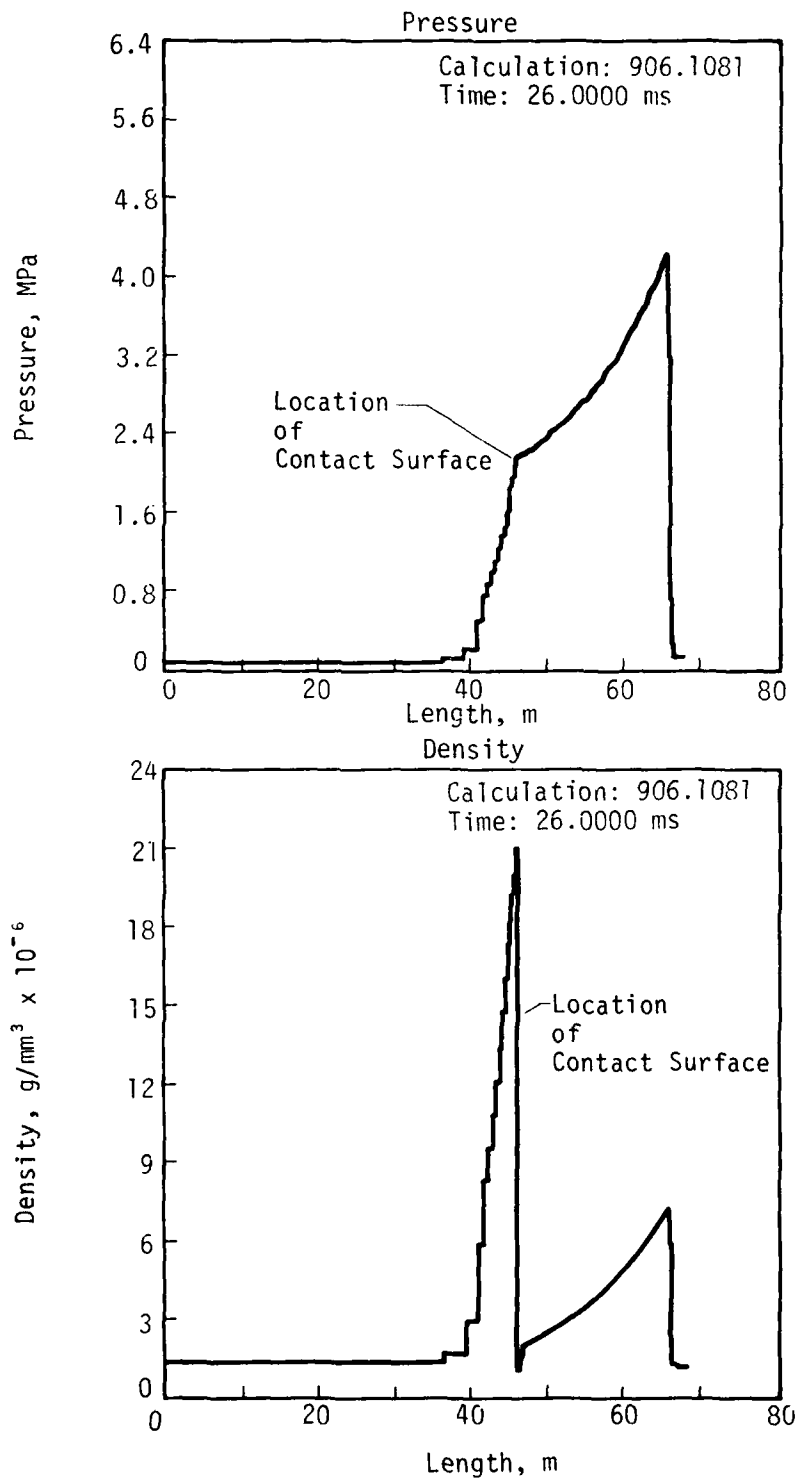


Figure 46. Incident Wave Profiles at 26 ms

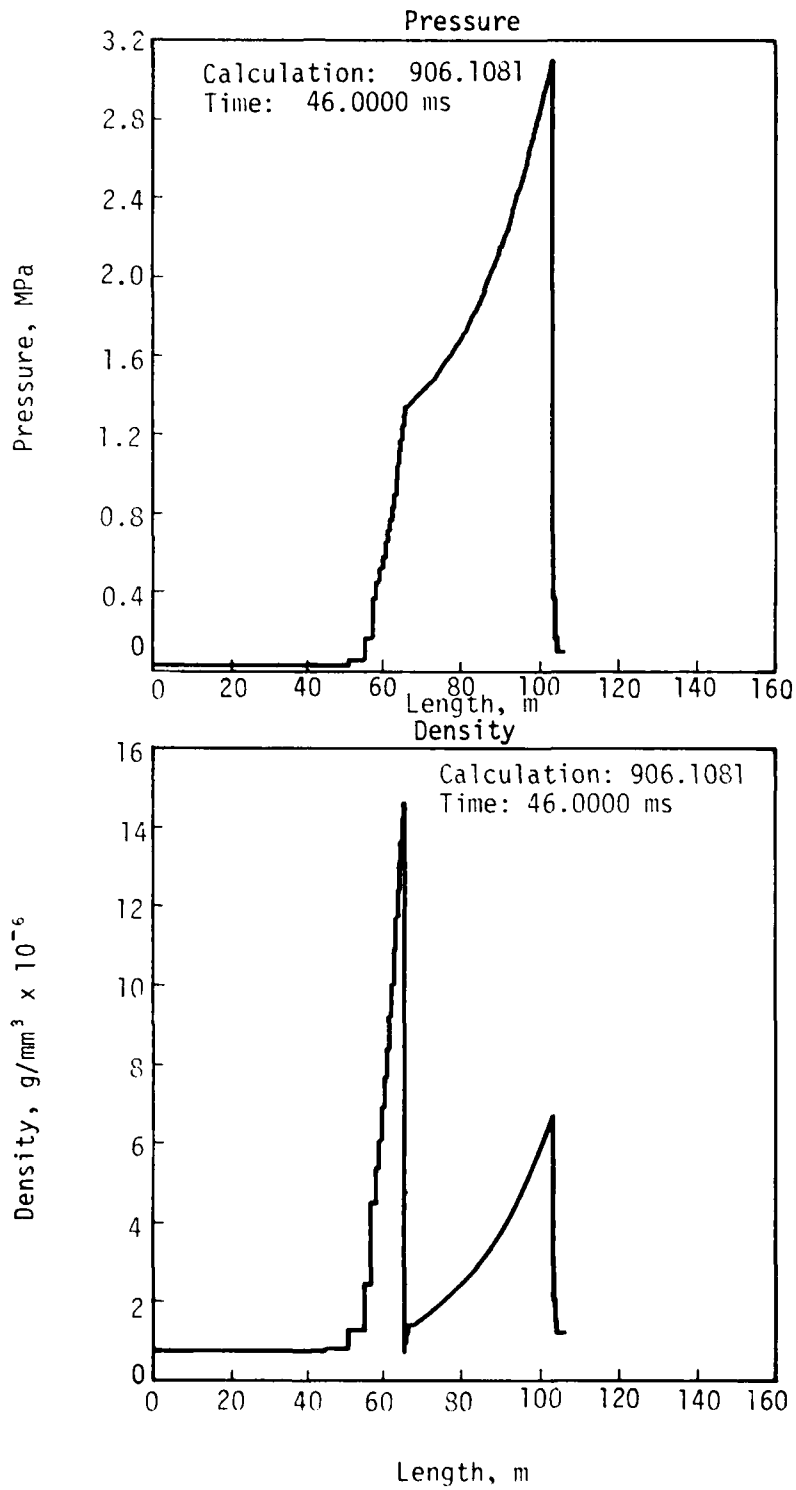


Figure 47. Incident Wave Profiles at 46 ms

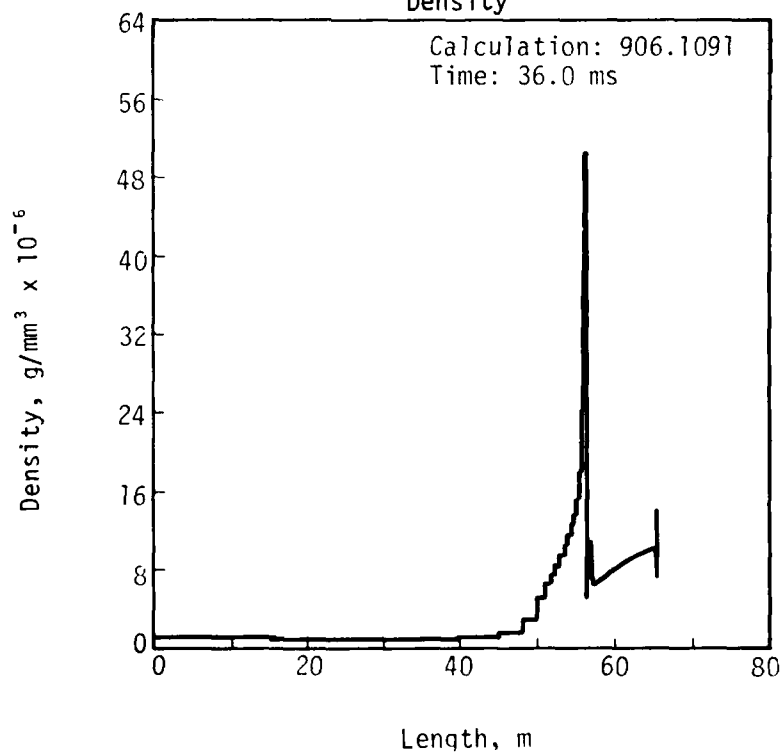
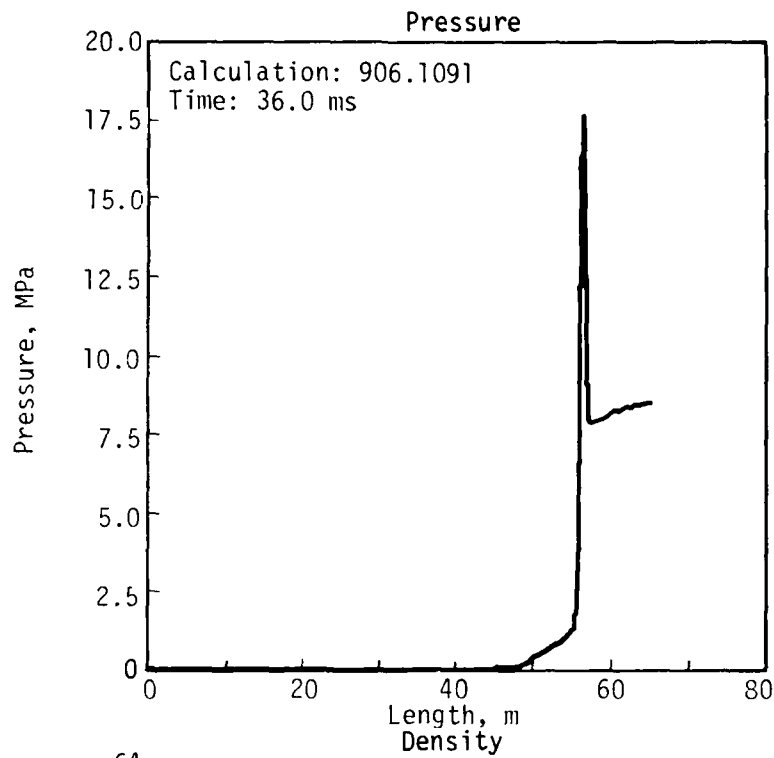


Figure 4C. Reflected Wave Profiles at 36 ms

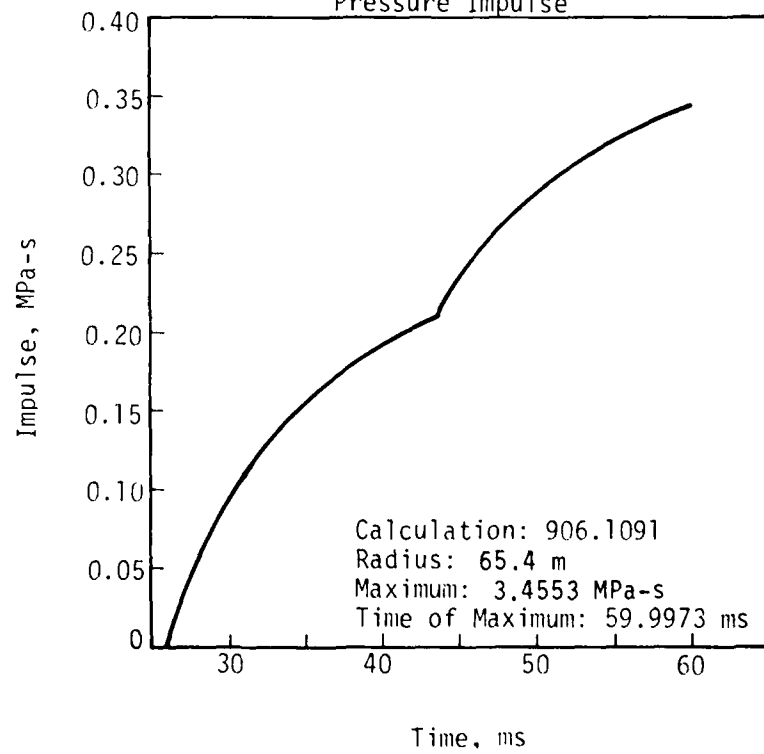
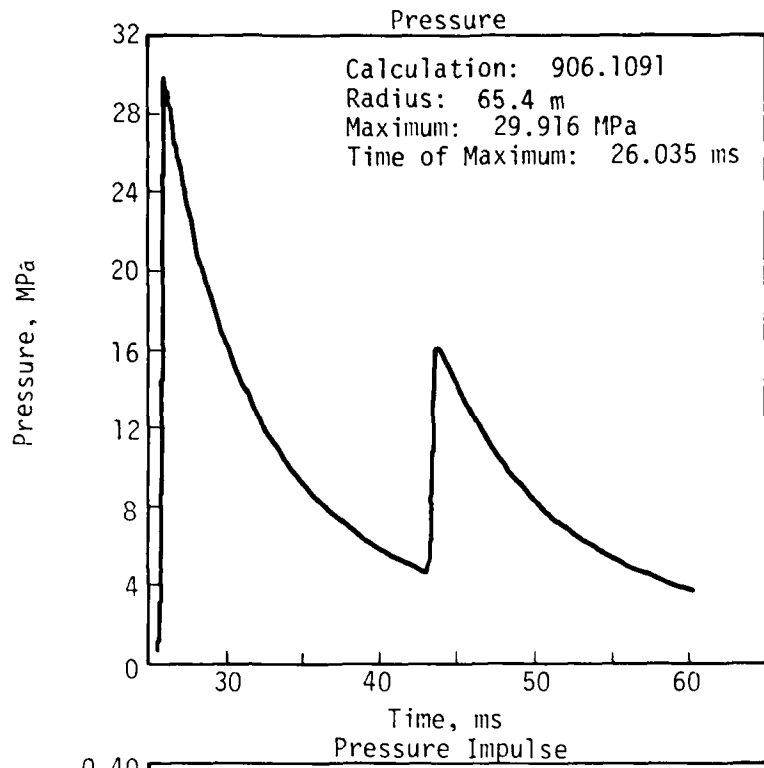
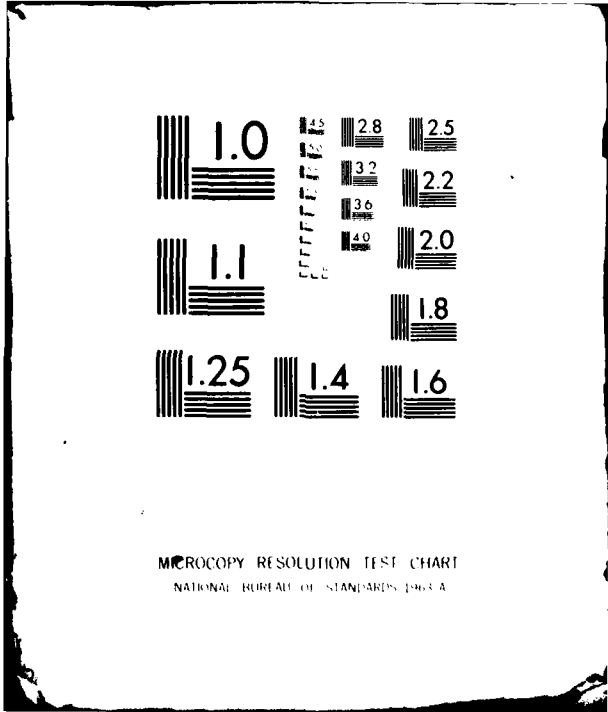


Figure 49. Reflected Wave History at 65.4 m



MICROCOPY RESOLUTION TEST CHART
NATIONAL BUREAU OF STANDARDS, 1963-A

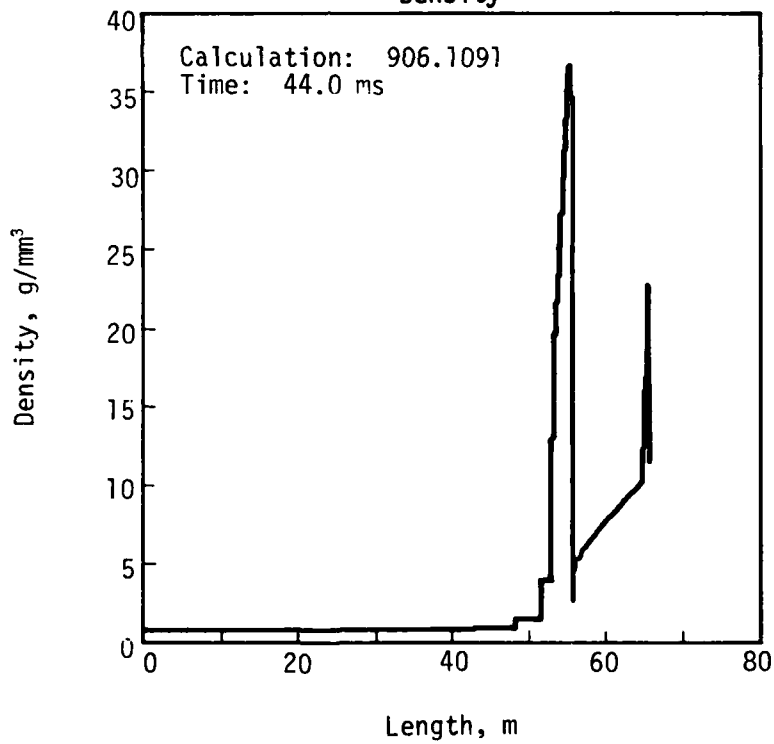
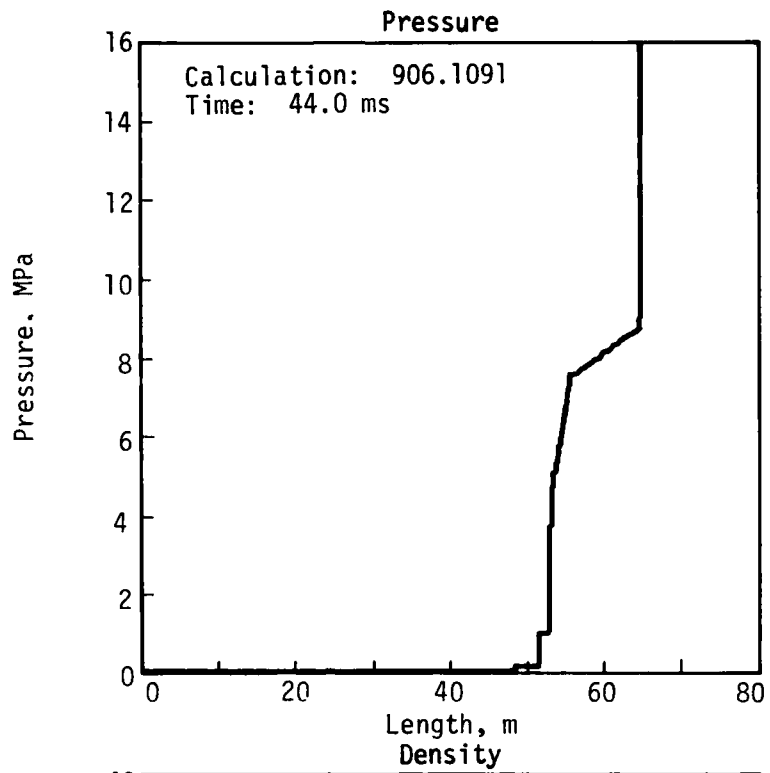


Figure 50. Reflected Wave Profiles at 44 ms

PARAMETRIC STUDY OF SAP LAGRANGIAN HYDROCODE

In the course of varying the mass and energy deposition to achieve the 4.14-MPa incident pressure loading during the previous calculation for the HAVE HOST T series, some unexpected results having to do with the number of cells used to define the explosive driver section and the mass and energy in each were noted. Not all of the results are desirable, and it is important to be able to predict their occurrence. Seven abbreviated trial calculations* were made in the course of finding the proper mass-energy deposition for the driver section to achieve the 4.14-MPa wave. Variations were made in 1) the number of cell divisions within the driver, 2) the total width and mass density of the driver, and 3) the width of the air cells in the shock tunnel. Table 5 provides a listing of all the input parameters as well as a comparative look at the peak pressure at the 5-m station. Three distinct energy levels were used in the study with three calculations at each level. Common to all calculations were the use of the real air EOS in the reaction cavity, the same multi-material Lagrangian version of the SAP hydrocode, and the burned ANFO EOS in the driver section. The ANFO EOS did have modified mass and energy densities as listed in Table 5.

Because previous calculations had employed an energy dump into a single driver cell, this procedure was followed in the initial attempts in this set of calculations. It was noted, however, that the dump into the single cell resulted in unstable oscillations during the late times after the arrival of the initial peak and during the subsequent pressure decay. These oscillations were noted in calculations 906.1011 (Fig. 51), 906.1021, and 906.1031. Another observation made from the use of the single-driver cell was the lack of full downstream dissipation of the driver energy. When multiple cells were employed the peak pressure at downstream stations seemed to peak when

*Hydrocode Calculations Nos. 906.1011 through 906.1071 Data Report, UNM/CERF AST-30, December 1978.

TABLE 5. EFFECTS OF CALCULATION PARAMETERS ON PEAK PRESSURE

Calculation Number	DRIVER SECTION							Air Cell Width, mm	Peak Pressure and Arrival Time at 5 m, Mpa at ms
	Number of Cells	Total Width, mm	Mass Density, g/mm ³ x 10 ⁻³	Energy Density, ergs/g	Total Mass, g	Total Energy, ergs			
906.1011	1	100.0	2.058	2.822 x 10 ¹⁰	20.58	5.808 x 10 ¹¹	1000	16.335 at 1.369	
906.1031	1	100.0	2.058	2.822 x 10 ¹⁰	20.58	5.808 x 10 ¹¹	500	16.859 at 1.348	
906.1041	10	100.0	2.058	2.822 x 10 ¹⁰	20.58	5.808 x 10 ¹¹	100	18.788 at 1.106	
906.1071	25	90.6	1.380	2.822 x 10 ¹⁰	12.50	3.528 x 10 ¹¹	500	12.887 at 1.356	
906.1081	25	90.6	1.380	2.822 x 10 ¹⁰	12.50	3.528 x 10 ¹¹	250	13.316 at 1.320	
906.5081 (with Burn)	25	90.6	1.380	2.822 x 10 ¹⁰	12.50	3.528 x 10 ¹¹	250	20.002 at 1.059	
906.1021	1	75.5	1.380	2.822 x 10 ¹⁰	10.43	2.942 x 10 ¹¹	1000	10.598 at 1.783	
906.1061	10	75.5	1.380	2.822 x 10 ¹⁰	10.43	2.942 x 10 ¹¹	500	12.307 at 1.375	
906.1051	25	75.5	1.380	2.822 x 10 ¹⁰	10.43	2.942 x 10 ¹¹	500	11.994 at 1.380	

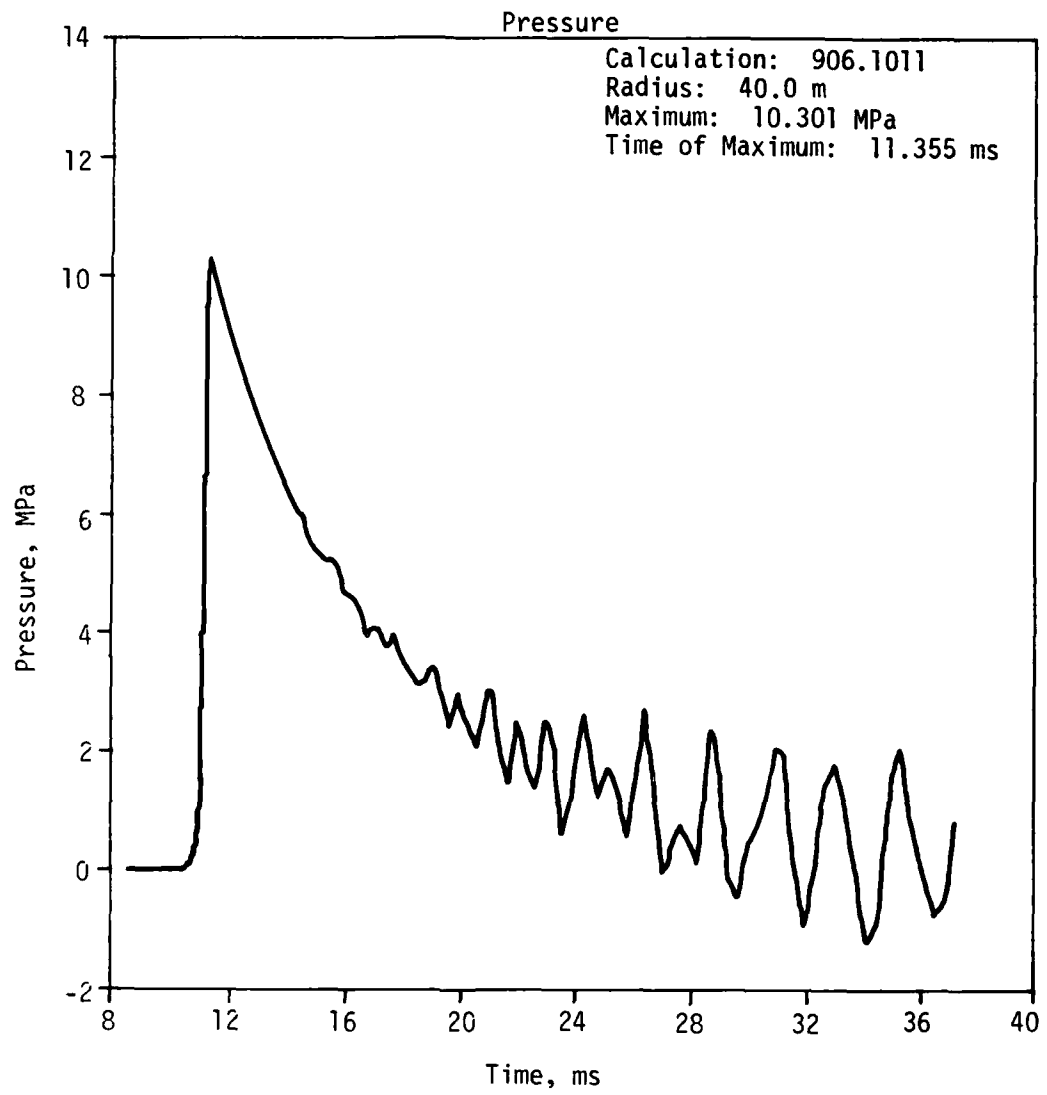


Figure 51. Unstable Oscillations Produced by SAP Calculations

approximately 10 cells were used in the driver. (Compare calculations 906.1011 versus 906.1041 in Table 5 and then 906.1021 versus 906.1061.)

It was also observed that cell size within the reaction cavity had a definite effect on the magnitude of the peak pressure produced downstream. Figures 52, 53, and 54 are plots of peak pressure versus station radii for the three groups of energy levels. The energy level is constant for all calculations within a group. The legend on the figures identifies the particular curve according to its pressure at the 5-m location. In all three group plots the highest peak pressure occurs in the calculation with the smallest air cell width and decreases to the lowest peak with the largest cell width.

Of special interest are calculations 906.1081 and 906.5081.* Calculation 906.1081 is the final version used in the 4.14-MPa wave calculation. Calculation 906.5081 uses the identical input parameters as calculation 906.1081 with the sole exception of using a burn subroutine to release the driver energy rather than using an energy dump. In Figure 53 the peak pressures at all stations for calculation 906.5081 are from 30 to 65 percent higher than the corresponding stations for calculation 906.1081. In both the energy dump and burn methods a pressure differential exists initially between the last driver cell and the first air cell. The burn subroutine begins adding energy at the other end of the driver which establishes a second pressure front at the rear of the driver section. This leads to the possibility of an early reflection off the backwall to boost the outgoing pressure wave above the values noted in the no-burn process.

From these parametric calculations it can be concluded that a simple isothermal energy dump is not adequate for the accurate modeling of a detonation process occurring across some significant thickness of explosive material. It can, however, be used for qualitative calculations where an exact modeling of the energy source is not important.

*Hydrocode Calculation No. 906.1081, Data Report, UNM/CERF AST-26, December 1978.

Hydrocode Calculation No. 906.5081, Data Report, UNM/CERF AST-28, December 1978.

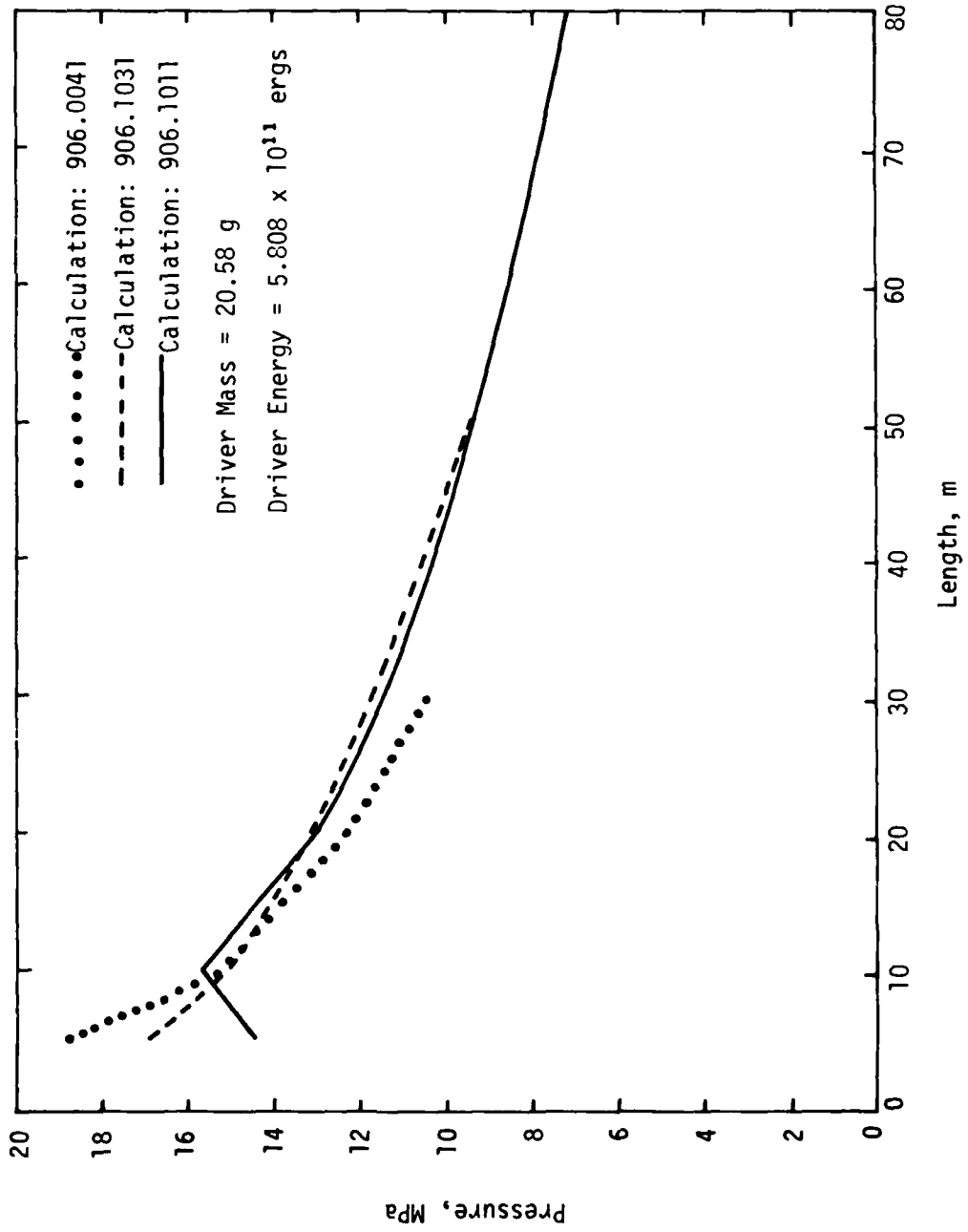


Figure 52. Peak Pressure versus Length (Group I)

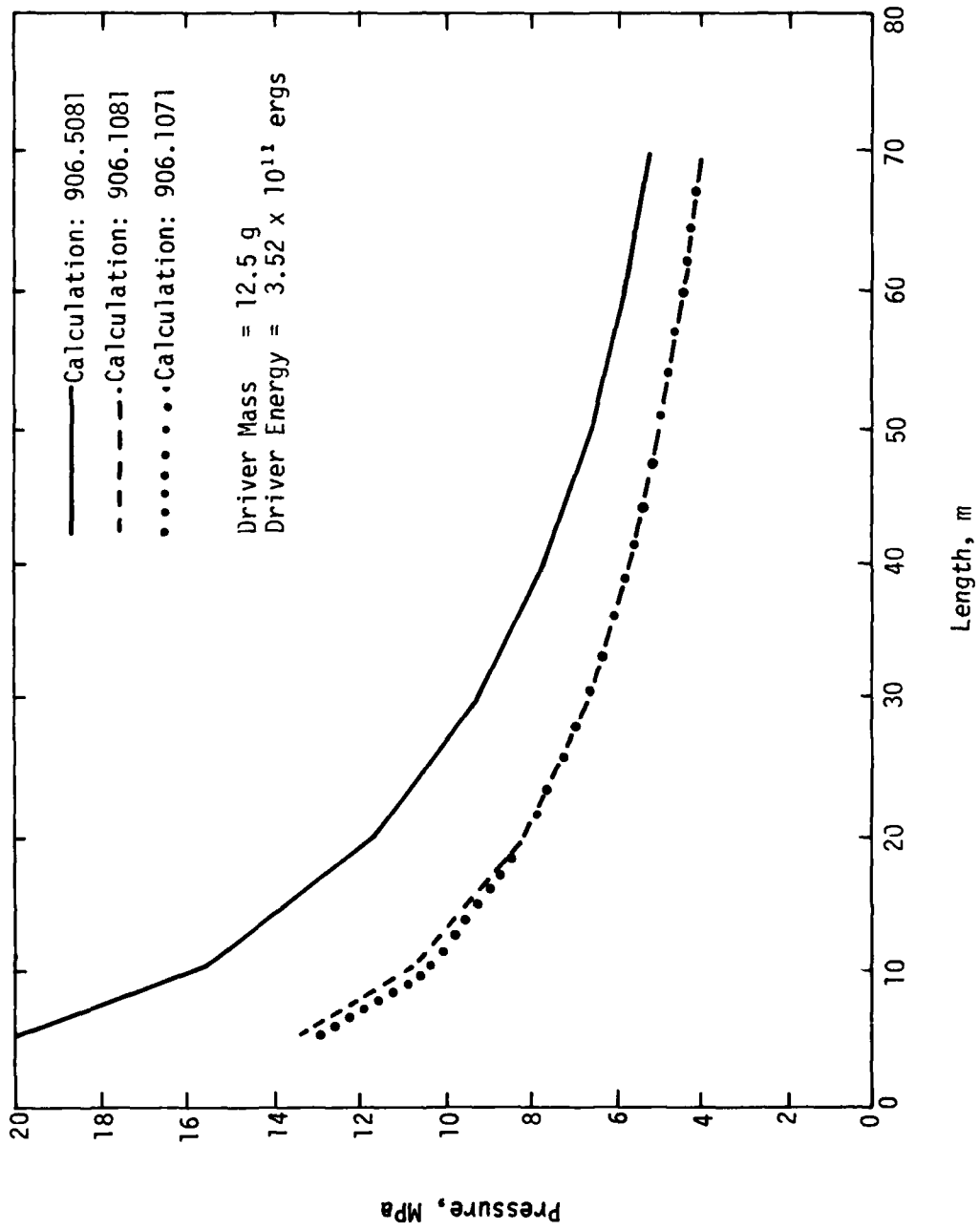


Figure 53. Peak Pressure versus Length (Group II)

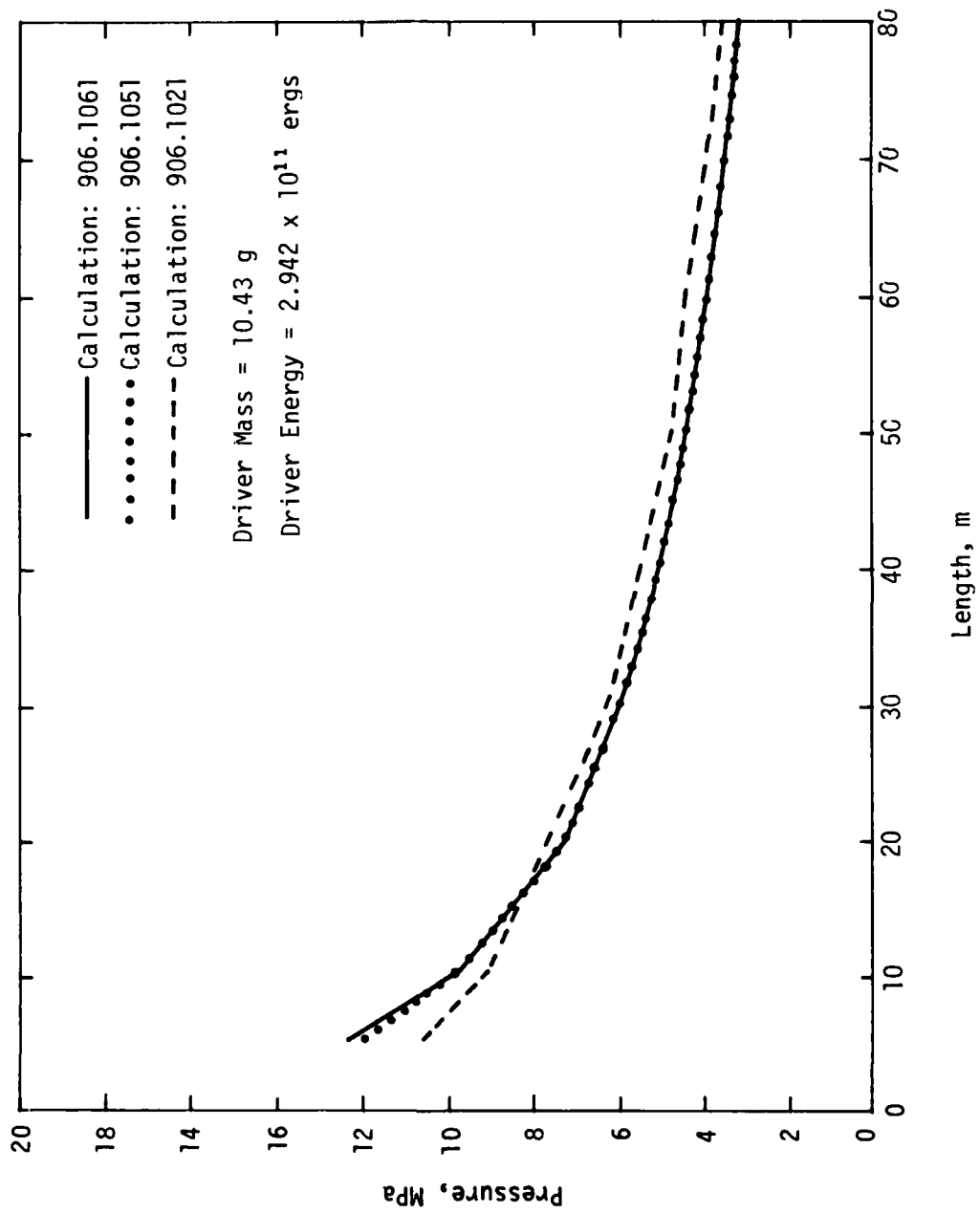


Figure 54. Peak Pressure versus Length (Group III)

EVALUATION OF DIFFUSION LIMITATION IN HULL CODE

Airblast waves generated in explosively driven shock tunnels and test cavities are essentially high-strength planar shock waves which, it can be assumed, are representative of the interior ballistics encountered in typical shock tube experiments. The contact surfaces* which accompany shocks of this kind can play an important part in complex shock interactions during the evolution of the wave system. The purpose of the numerical simulation described here (calculation 906.0040**) was to evaluate the diffusion limitation scheme which is automatically implemented in HULL for multimaterial models. Since the HULL code simulates flow in a Eulerian frame of reference, some mechanism of this kind is required if contact discontinuities are to be realistically preserved.

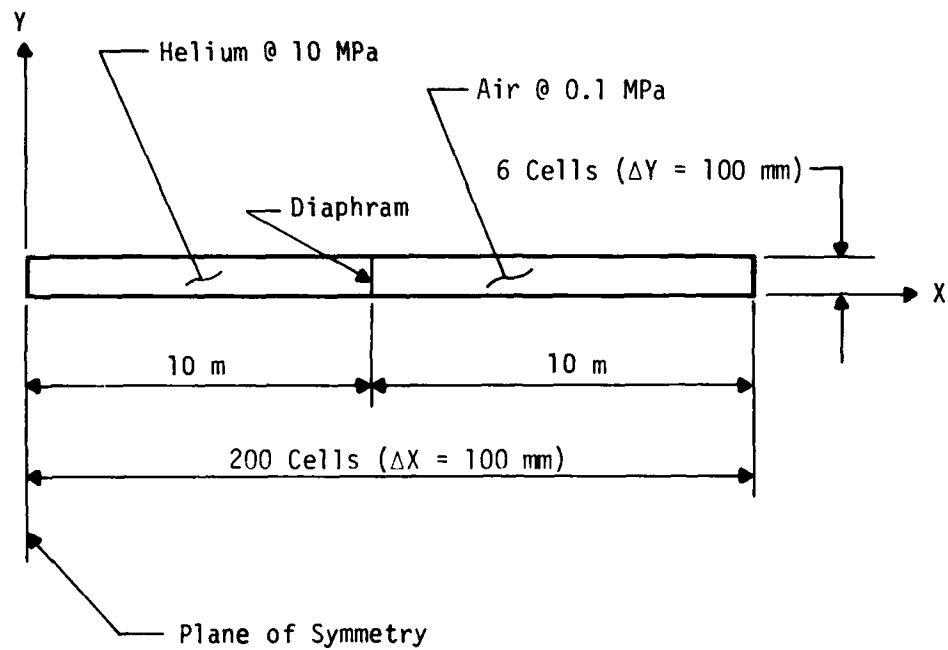
A model was chosen which was readily amenable to a closed form analytical solution. In this instance a 20-m closed shock tube with the diaphragm at midlength was simulated (Fig. 55). With these proportions the primary shock and contact surface can diverge suitably before any reflections take place (Fig. 56). This configuration was modeled in a Cartesian coordinate system in which the closed end of the high pressure chamber was at the plane of symmetry. Since flow in this case is one-dimensional, only the minimum number of cells (6) required by the HULL code were used in the transverse or "radial" direction. All cells were 100 by 100 mm, and all boundaries were reflective.

Helium, pressurized to 100 atmospheres, was selected as the driver gas and air at standard sea level conditions as the reaction gas. Initial conditions for the driver (Region 4, Fig. 56) were assumed to be the result of an isentropic compression (Table 6, Ref. 16). Instantaneous removal of the diaphragm

16. Liepmann, H. W., and Roshko, A., *Elements of Gas Dynamics*, pp. 62-83, Wiley, 1957.

* A surface which separates the driver gas and reaction gas in a shock tube. It is in reality a region but is often theoretically idealized to be a discrete material interface.

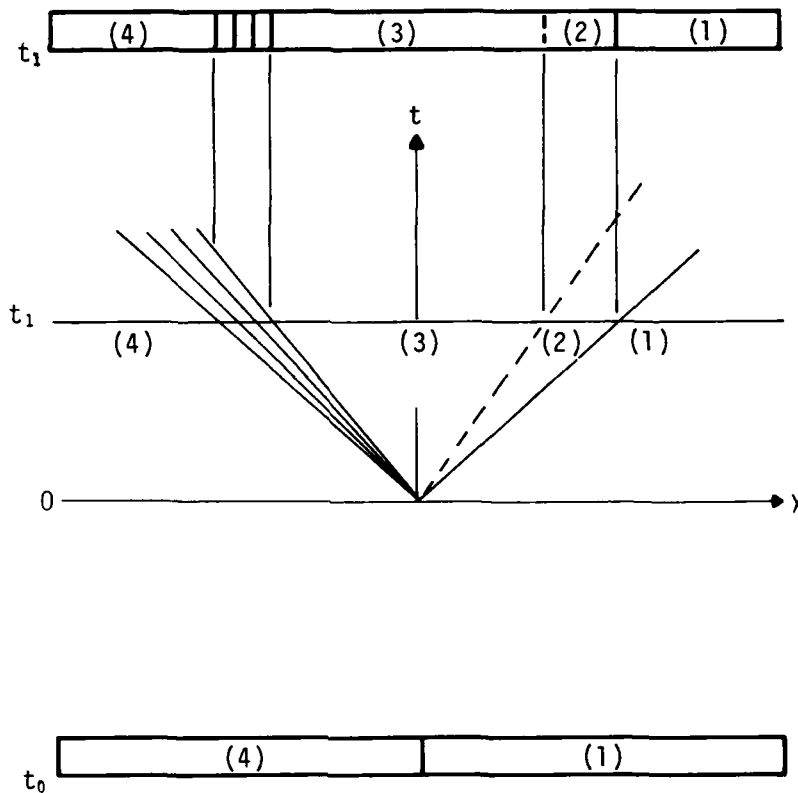
**Hydrocode Calculation No. 906.0040, Data Report, UNM/CERF AST-37, December 1978.



Geometry -- Cartesian

Boundary Conditions--Reflective

Figure 55. Shock Tube Geometry--Calculation 906.0040



Regions (3) and (4) Contain Helium
 Regions (1) and (2) Contain Air
 Diaphragm Pressure Ratio (P_4/P_1) = 1.00
 Shock Strength (P_2/P_1) = 33.66

Figure 56. Wave System Diagram--Calculation 906.0040

TABLE 6. DRIVER REGION INITIAL CONDITIONS^a--
HULL CALCULATION 906.0040

$$\rho_4 = \rho_0 \left(\frac{P_4}{P_0} \right)^{\gamma-1} = 2.679 \times 10^{-6} \text{ g/mm}^3$$

$$P_4 = 100 P_0 = 10 \text{ MPa}$$

$$\varepsilon_4 = \frac{P_4}{[\rho_4 (\gamma - 1)]} = 5.598 \times 10^{10} \text{ ergs/g}$$

$$T_4 = T_0 \left(\frac{P_4}{P_0} \right)^{\frac{(\gamma-1)}{\gamma}} = 1849^{\circ} \text{ K}$$

where $P_0 = 0.1 \text{ MPa}$

$$\gamma = \frac{5}{3}$$

$$\rho_0 = 1.6905 \times 10^{-7} \text{ g/mm}^3$$

$$T_0 = 2.93^{\circ} \text{ K}$$

^a Helium isentropically compressed to 100 atmospheres.

separating Regions 4 and 1 was simulated by using these values to describe the initial state of the driver gas. A solution for the fluid response of this model was recorded every 100 μ s for a period of 3 ms.

To obtain the closed form analytical solution based on shock tube theory the computer program SHOK2B (Appendix C) was written. Given the initial conditions for the driver and reaction gases (Regions 4 and 1) and the desired solution time, this program first solves the basic shock tube equation for the shock strength (P_2/P_1) which is defined implicitly as a function of the diaphragm pressure ratio (P_4/P_1). The remaining state variables are then calculated for Regions 2 and 3. Finally the positions of primary shock front, contact surface, and expansion wave are determined.

The HULL numerical solution density, specific internal energy, and pressure profiles at 3 ms is shown in Figures 57 through 59. For the purpose of comparison the analytical solution has been overlaid. It can be seen that these solutions are in remarkably close agreement. The gradients in Region 2 in both the density and energy profiles (Figs. 57 and 58) show the extent to which HULL has permitted diffusion to take place at the contact surface. The HULL solution locates the contact surface approximately 14.1 m as opposed to the analytical value of 14.4 m.

From this calculation it can be concluded that the HULL diffusion limitation scheme can creditably simulate the contact discontinuity of the simplistic shock tube environment. Since in reality such a discontinuity cannot be sustained (Ref. 17), a diffusion does occur. The truth then may very well lie somewhere between this HULL prediction and the theoretical case which presumes no diffusion.

Although blast effects in explosively driven test facilities are essentially analogous to the 1-D wave motions and phenomena of the shock tube, certain physical factors were overlooked here. For example, the explosive energies involved are equivalent to diaphragm pressure ratios that may be orders of magnitude greater than can be achieved in a diaphragm shock tube experiment.

17. Bradley, J. N., *Shock Waves in Chemistry and Physics*, pp. 103-4, Wiley, 1962.

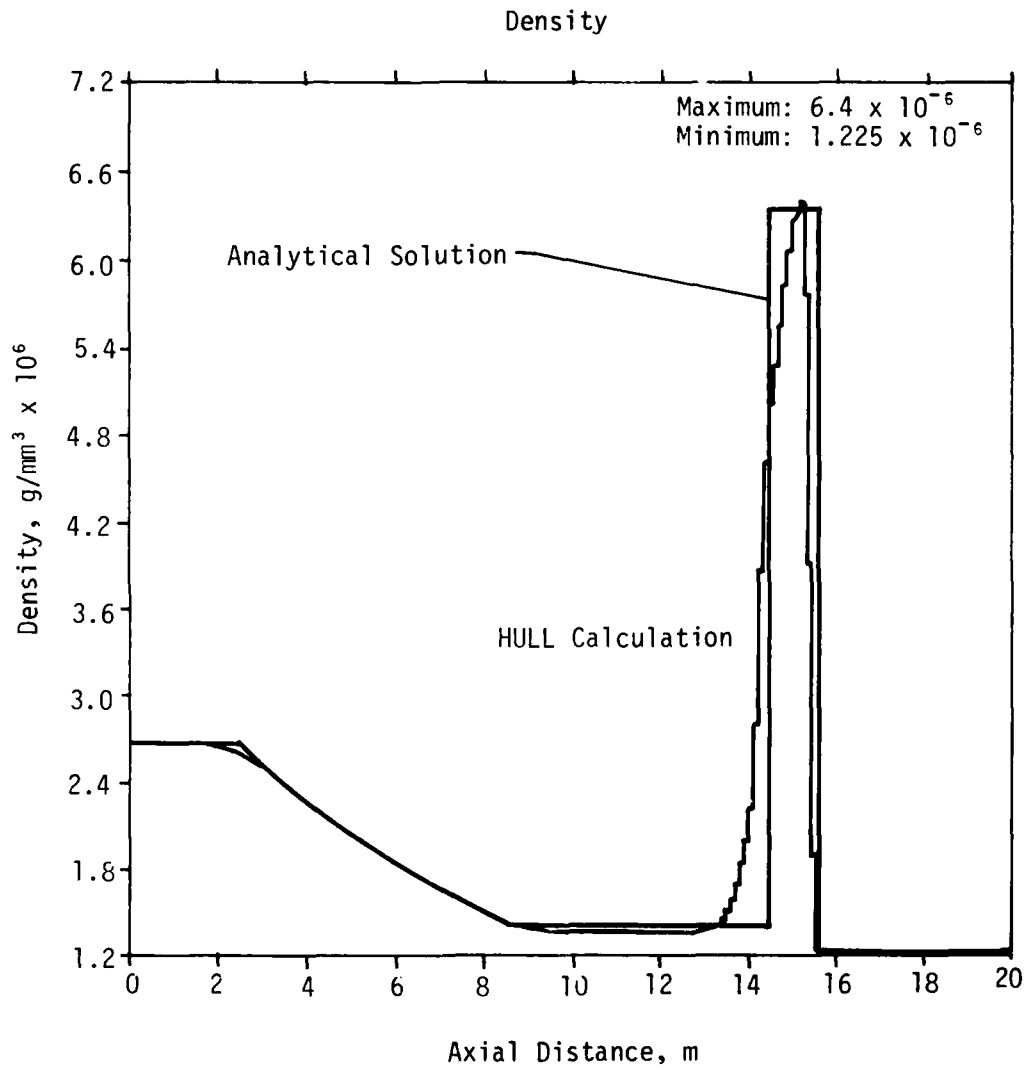


Figure 57. Axial Density Profile--HULL Calculation 906.0040 at 3 ms

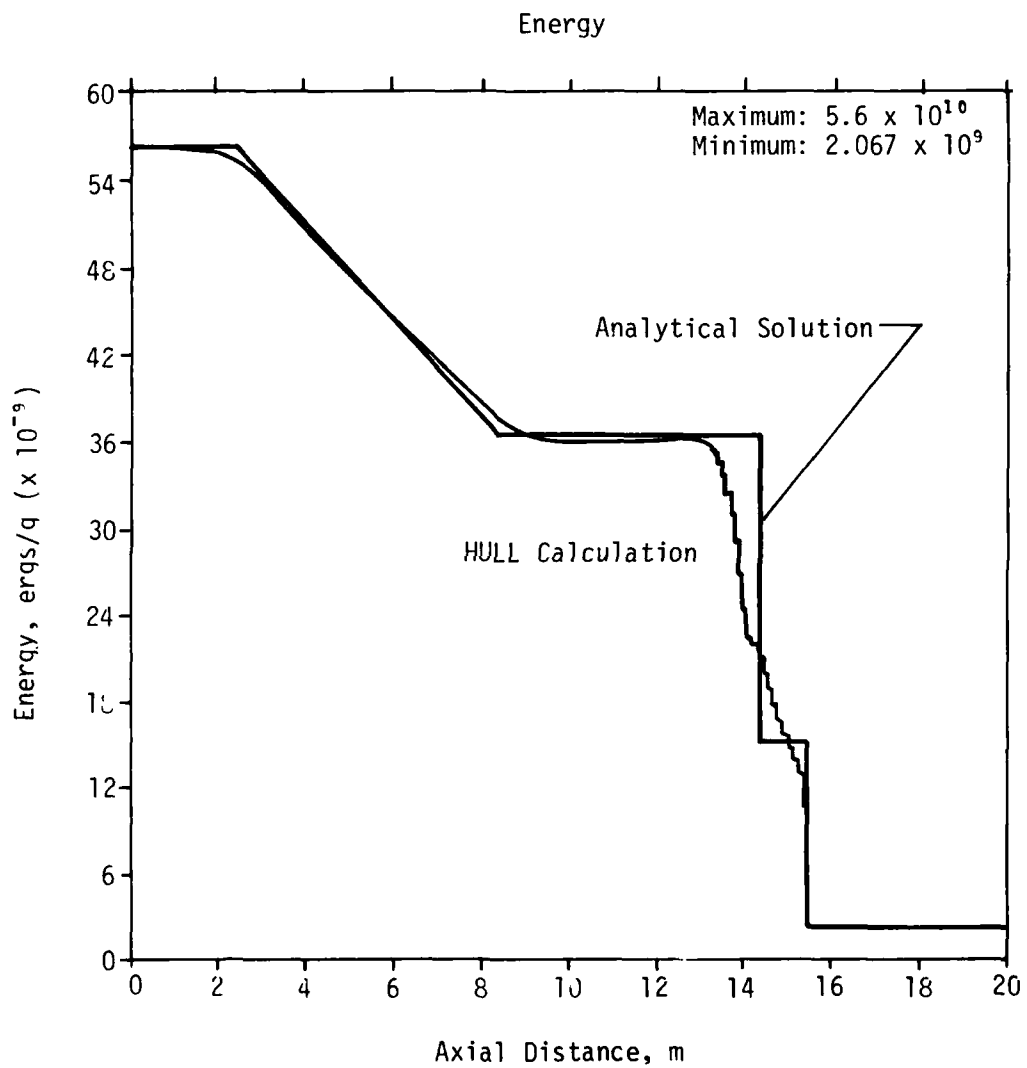


Figure 58. Axial Energy Profile--Calculation 906.0040 at 3 ms

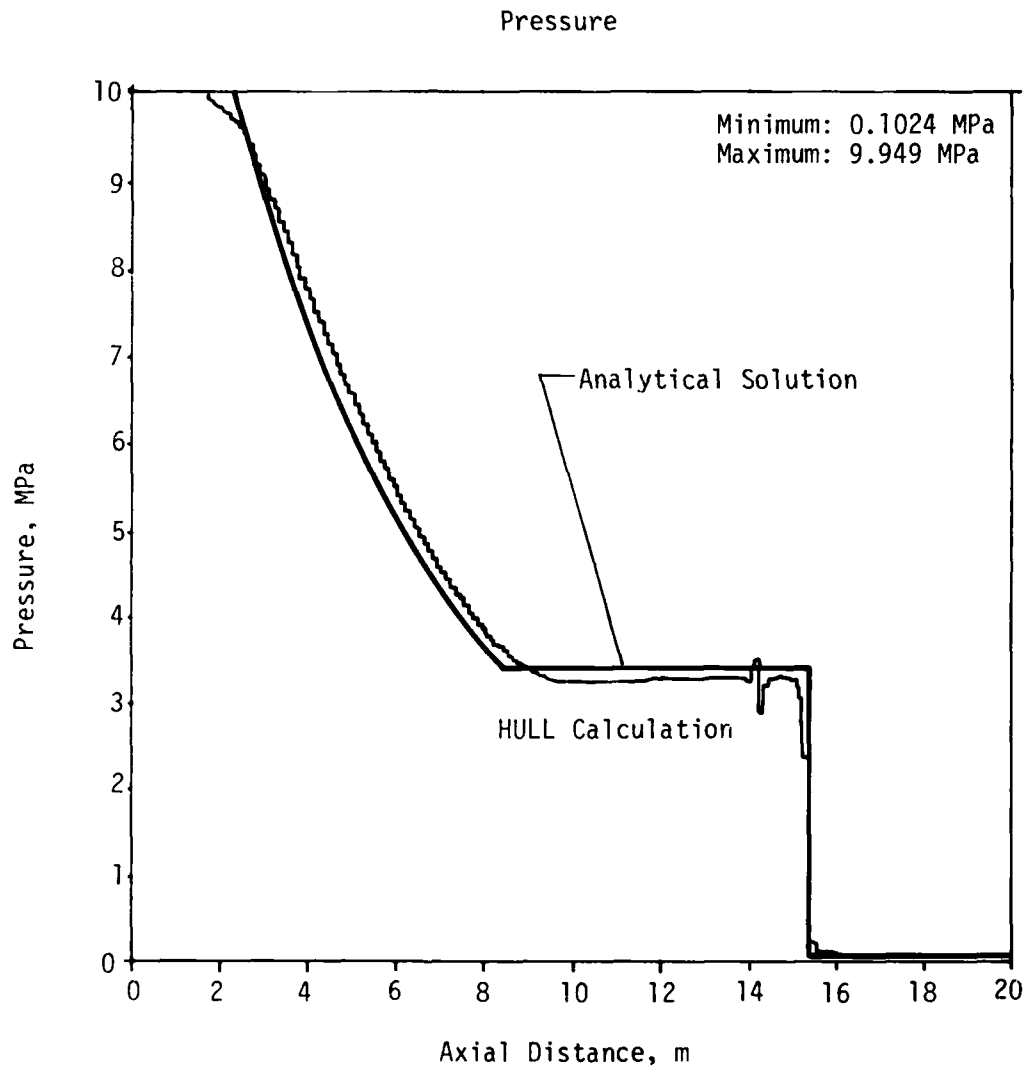


Figure 59. Axial Pressure Profile--Calculation 906.0040 at 3 ms

Also, the typical test configuration is such that the driver section is relatively short. This condition will most certainly lead to complex wave interactions involving reflections, refractions, overtaking situations, and possibly the generation of contact regions of variable entropy. Finally, of course, it is to be expected that the explosive burning processes would contribute significantly to the experimental environment.

A number of closed-form analytical solutions for various wave interactions are available (Ref. 18). It is therefore recommended that HULL simulations of some of the more straightforward cases be evaluated.

HULL NUMERICAL SIMULATION OF NORMAL REFLECTION OF 4.14-MPa PLANAR SHOCK WAVE

HULL calculation 906.1090* predicts the blast effects in an explosively driven shock tunnel. It was part of a calculational study to determine driver specifications for HAVE HOST experiments. The specifications for this model duplicated those for a 1-D SAP Lagrangian calculation (calculation 906.1091**). For all practical purposes it simulates a 65.4-m closed shock tunnel which is represented in a Cartesian coordinate system (Fig. 60). All boundaries of the rectangular mesh are reflective.

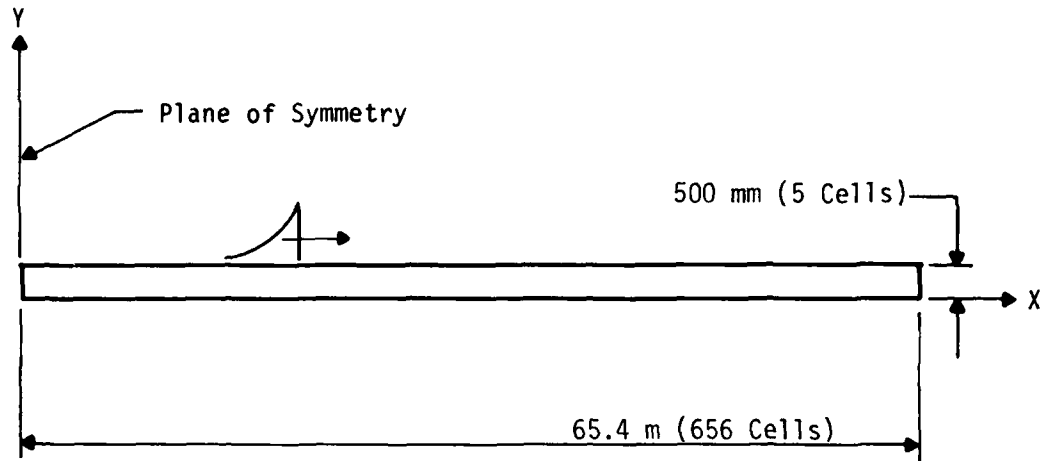
The explosive driver initially occupied the column of cells adjacent to the left boundary so as to generate the planar blast wave. This explosive was then considered to be motionless and in a completely burned state with a specific internal energy of 2.822×10^{10} ergs/g and a mass density of 8.5×10^{-4} g/mm². To obtain an incident peak pressure of 4.14 MPa at 65.4 m the thickness of the driver was set at 90.5797 mm (i.e., a planar energy density of 2.17×10^9 ergs/mm²). The behavior of this burned explosive gas governed by the HULL EOS for burned ANFO. The remainder of the mesh was

18. Glass, I. I., and Hall, J. G., *Handbook of Supersonic Aerodynamics*, Vol. 6, Section 18, NAVORD Report 1488, pp. 81-101, December 1959.

* Hydrocode Calculation No. 906.1090, Data Report, UNM/CERF AST-36, December 1978.

** Hydrocode Calculation No. 906.1091, Data Report, UNM/CERF AST-27, December 1978.

Geometry--Cartesian



Boundary Conditions--Reflective

Initial Conditions

Equation of State	ΔX , mm	Internal Energy, ergs/g	Density, g/mm ³
Burned ANFO	0 to 90.5797	2.822×10^{10}	8.5×10^{-4}
Real Air	90.5797 to 65,400	2.0448×10^9	1.225×10^{-6}

Figure 60. Model Specifications--HULL Simulation 906.1090

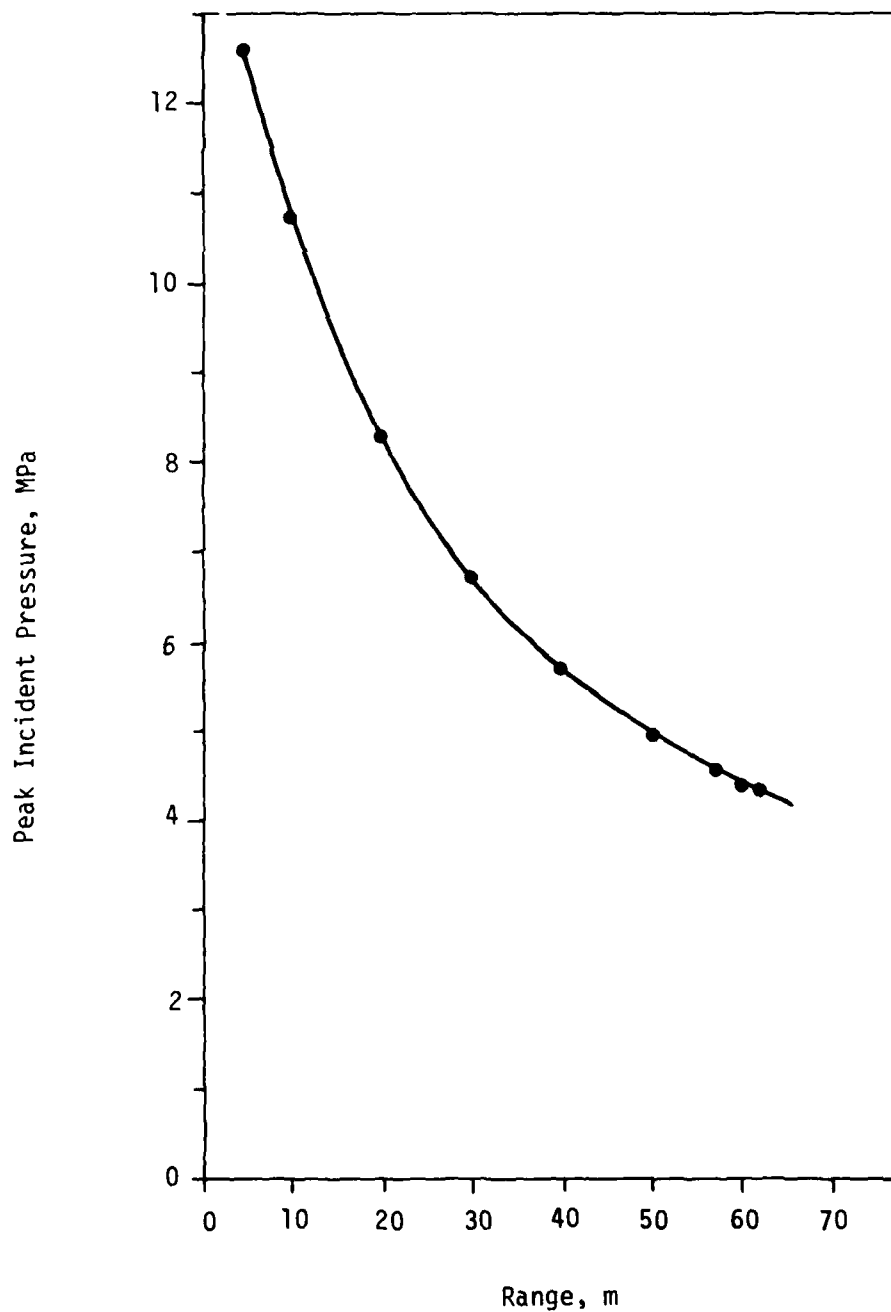


Figure 61. Calculated Peak Pressure--Calculation 906.1090

defined as real air (i.e., variable specific heats) at conditions corresponding to 1 standard atmosphere at sea level. Calculated peak pressure as a function of range is shown in Figure 61.

This model represents a typical case of interior shock physics where the exploded gas is separated from the air in the tunnel by a membrane which is instantaneously removed (Ref. 14, pp. 173-176). Since the contact surface (membrane) is quite close to the closed end, the rarefaction reflects quite early and a complex sequence of wave interactions and reflections takes place. Of particular importance here is the overtaking of the primary shock by the reflected rarefaction. The outcome of such an interaction is dependent on the relative strength of the rarefaction. Glass and Hall (Ref. 18) have addressed this subject and described the various wave systems which can result. In all cases, the attenuation of the shock gives rise to a variable entropy field in the form of a contact region rather than a contact surface.

Pressure histories at 60 and 65.4 m (Figs. 62 and 63) depict the character of the incident and reflected shock waves. A peak reflected pressure at the right boundary of 39 MPa is equivalent to a peak pressure ratio of 9.4. This value is considerably higher than the theoretical (7.5); however, it should be noted that this calculation did not include any artificial viscous damping. The pressure profile just prior to incidence (Fig. 64) clearly shows the erosive effects of overtaking rarefactions. This waveform can be compared directly with Figure 46 which clearly reveals the presence of the original contact surface which is rigorously preserved by the Lagrangian calculation. Experimental data show this Eulerian HULL calculation to be more representative of real world effects.

The HULL code diffusion limiter would tend to preserve the original contact surface. However, since the driver section is very short there is ample time for the development of a complex wave system involving a succession of reflections and refractions as one wave overtakes another. These interactions can lead to the creation of additional discontinuities. It is somewhat less than clear as to the extent this solution reflects either theory or reality.

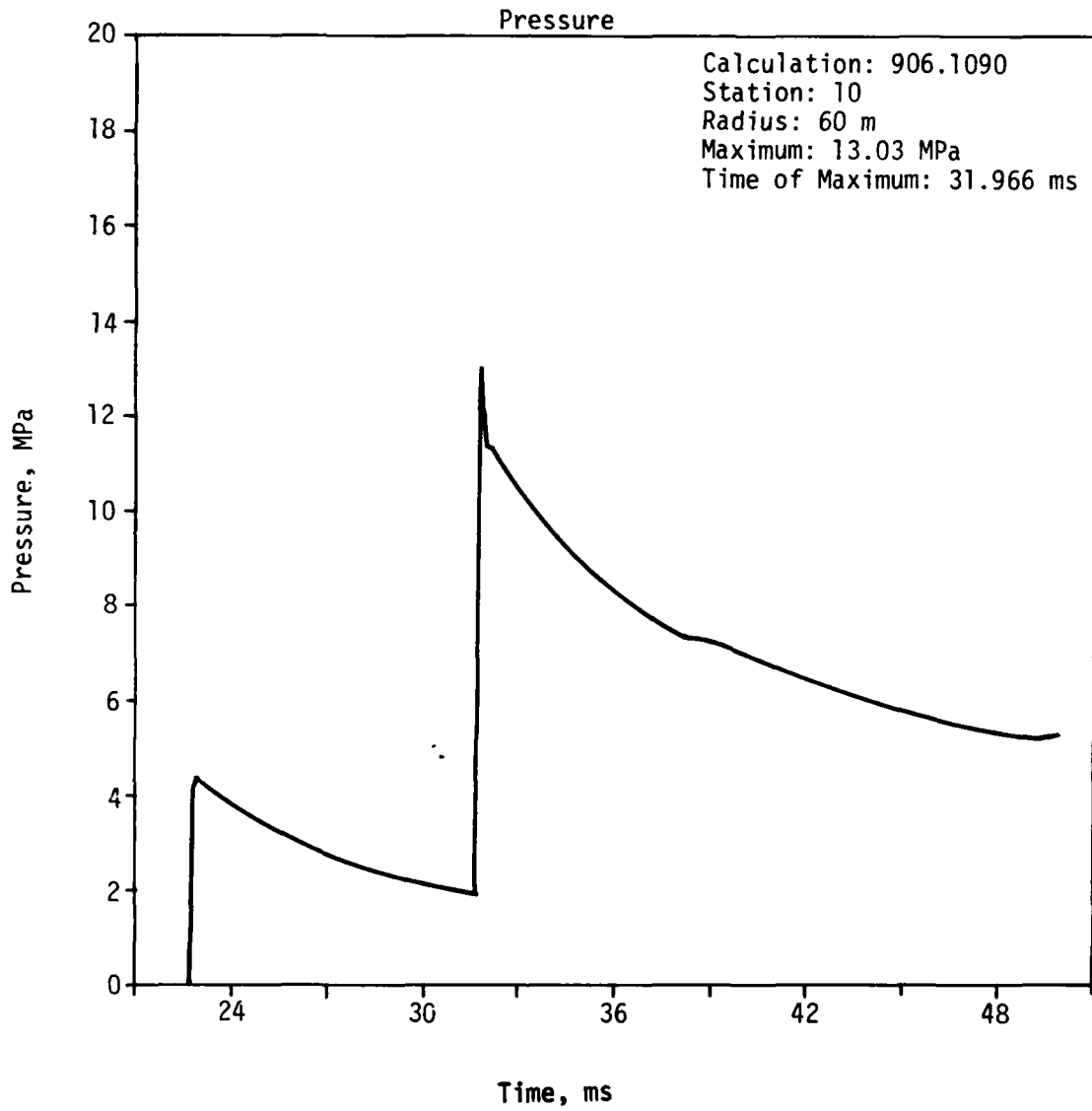


Figure 62. Pressure History at 60 m--Calculation 906.1090

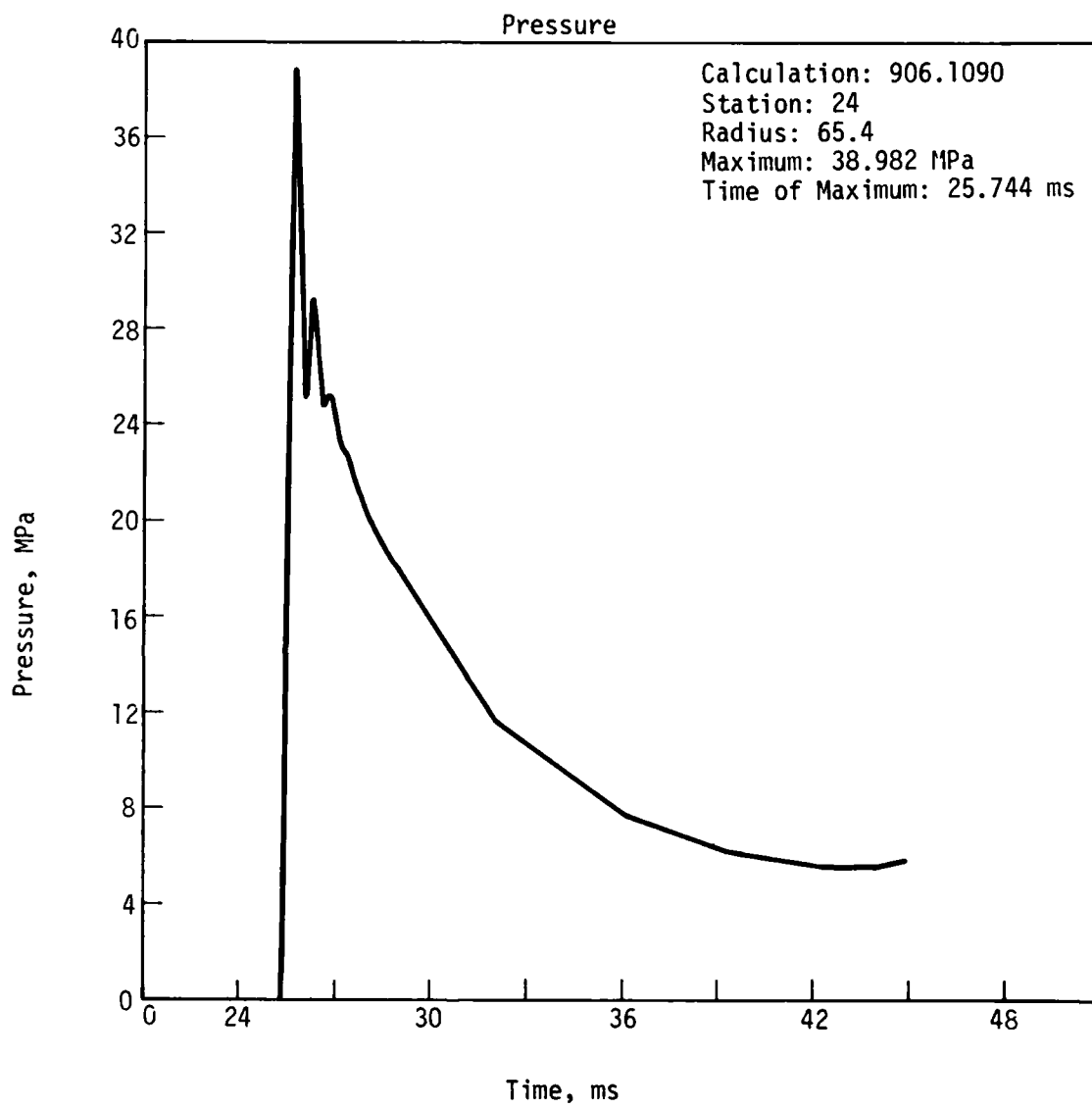


Figure 63. Pressure History at 65.4 m--Calculation 906.1090

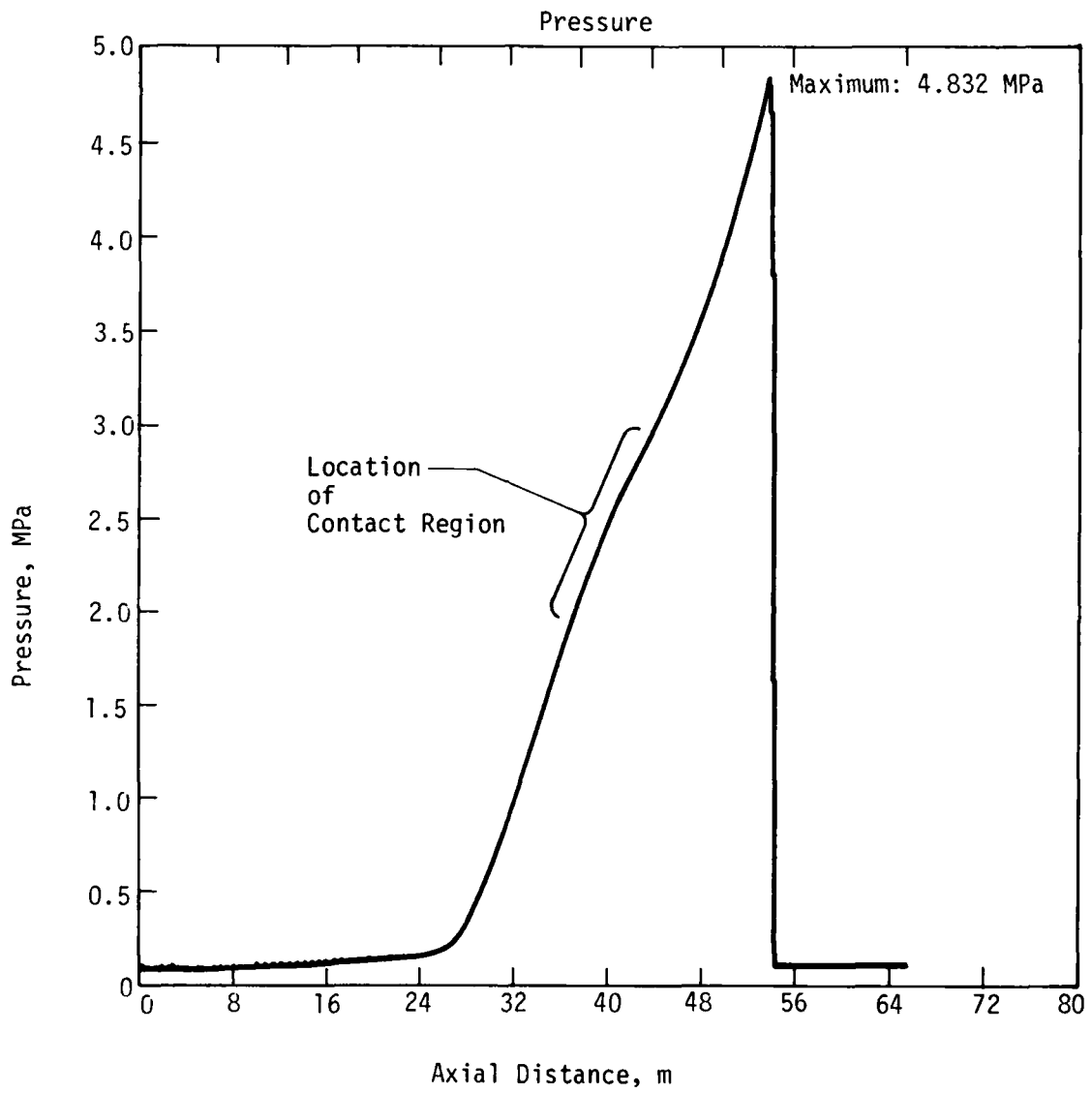


Figure 64. Axial Pressure Profile at 20 μ s--Calculation 906.1090

Any evaluation must take into account another aspect of blast environments encountered in explosively driven shock tunnels. In this simulation, for example, the initial pressure in the driver section is approximately 6000 MPa. This is equivalent to a diaphragm pressure ratio of 60,000. It is not at all certain that classical shock tube theory is valid in these higher pressure regimes and it may well be that numerical solutions such as this can only be analyzed in the light of the results from well-instrumented and controlled high-pressure experiments.

If one makes a reasonable allowance for the absence of artificial viscous damping, an estimated reflected peak pressure of 30 MPa compares favorably with an analytical value of 31.05. Finally, examination of the pressure, density, and energy profiles representing the solution at 20 ms (Figs. 64, 65, and 66) reveals a discontinuity at 40 m. This may indicate the presence of a contact region which is generated as a rarefaction erodes the shock wave.

HULL SIMULATION OF TYPICAL DABS EXPERIMENT

HULL calculation 908.0010* was an attempt to simulate the blast effects numerically which are typical of those experienced during recently fielded large DABS experiments. The DABS test facility is an explosively driven, partially buried shock tunnel which is used to impose dynamic airblast loadings on scaled target structures. This calculation was part of a parameter study to establish design guidelines to be used in preparing specifications for future experiments.

The working medium for this simulation was modeled as air, the behavior of which was governed by the AFWL variable specific heat EOS (Ref. 19). The shock tunnel was represented in a Cartesian coordinate system as the space between two parallel and reflective X-Z planes which are 4.1 m apart (Fig. 67). Consequently this solution simulates only a 2-D fluid response.

19. Needham, C. E., *Nuclear Blast Standard (1 kt)*, AFWL-TR-73-55 (Rev.), Air Force Weapons Laboratory, Kirtland Air Force Base, New Mexico, 1975.

* Hydrocode Calculation No. 908.0010, Data Report, UNM/CERF AST-42, December 1978.

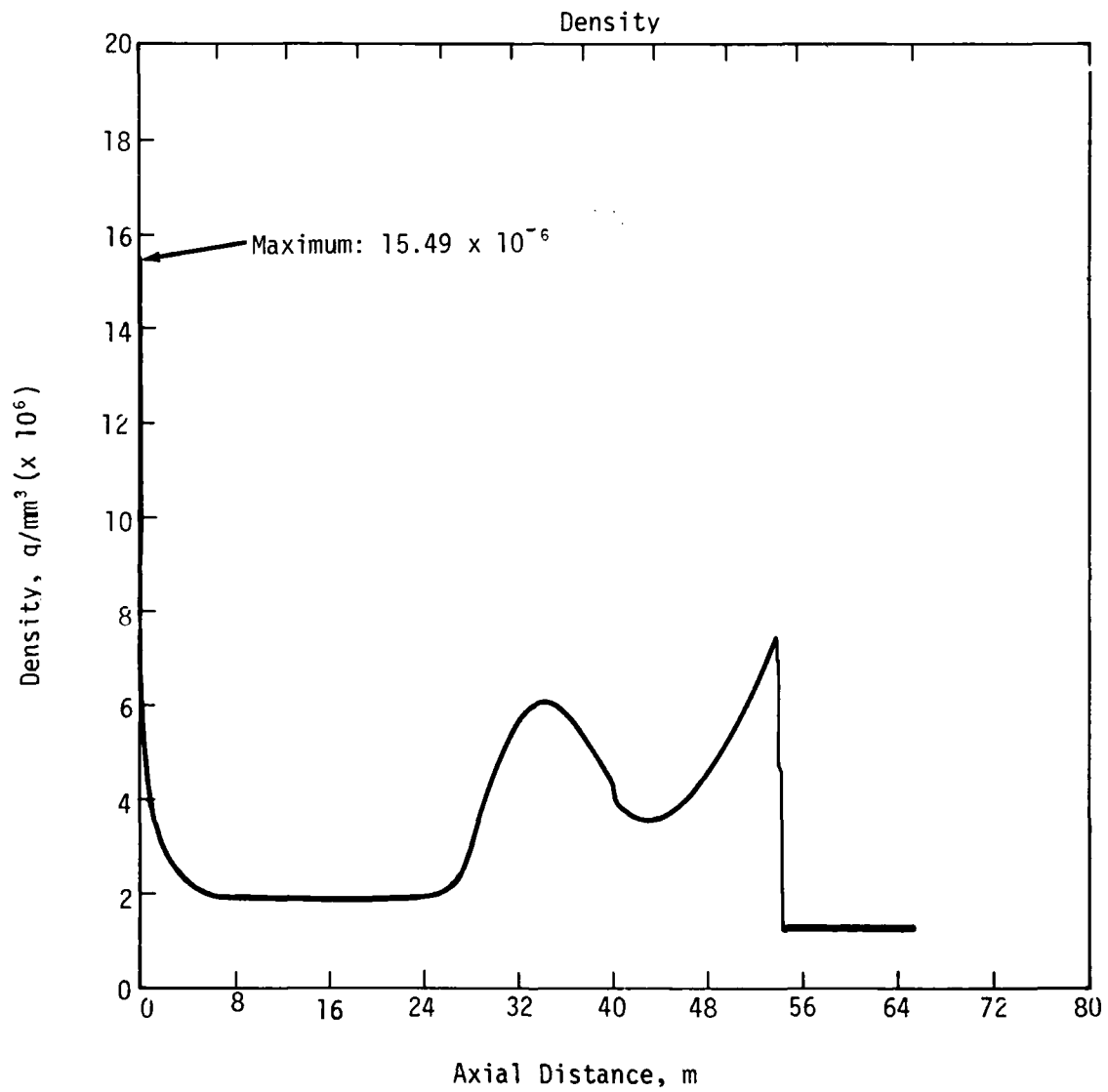


Figure 65. Axial Density Profile at 20 ms--Calculation 906.1090

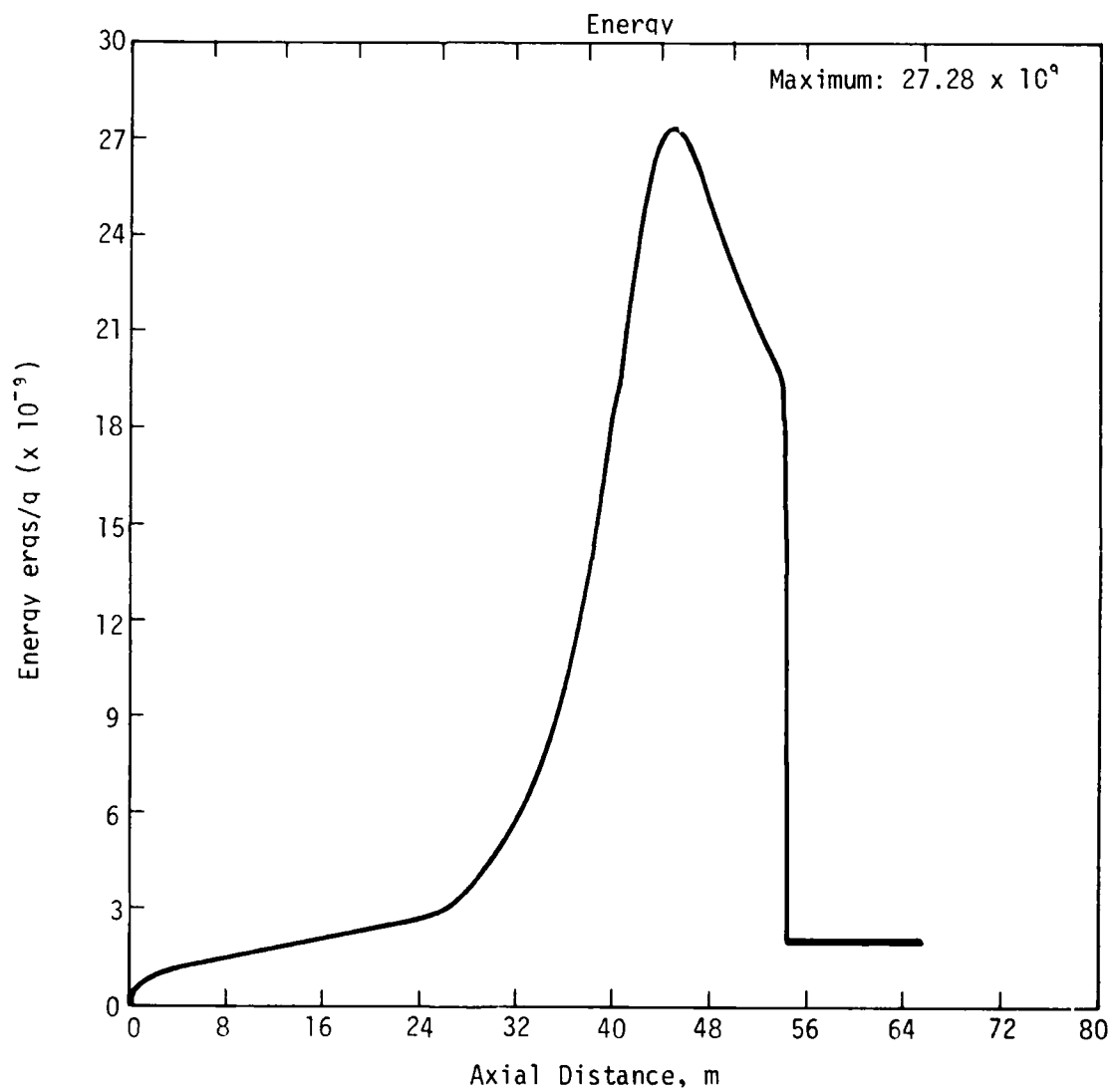
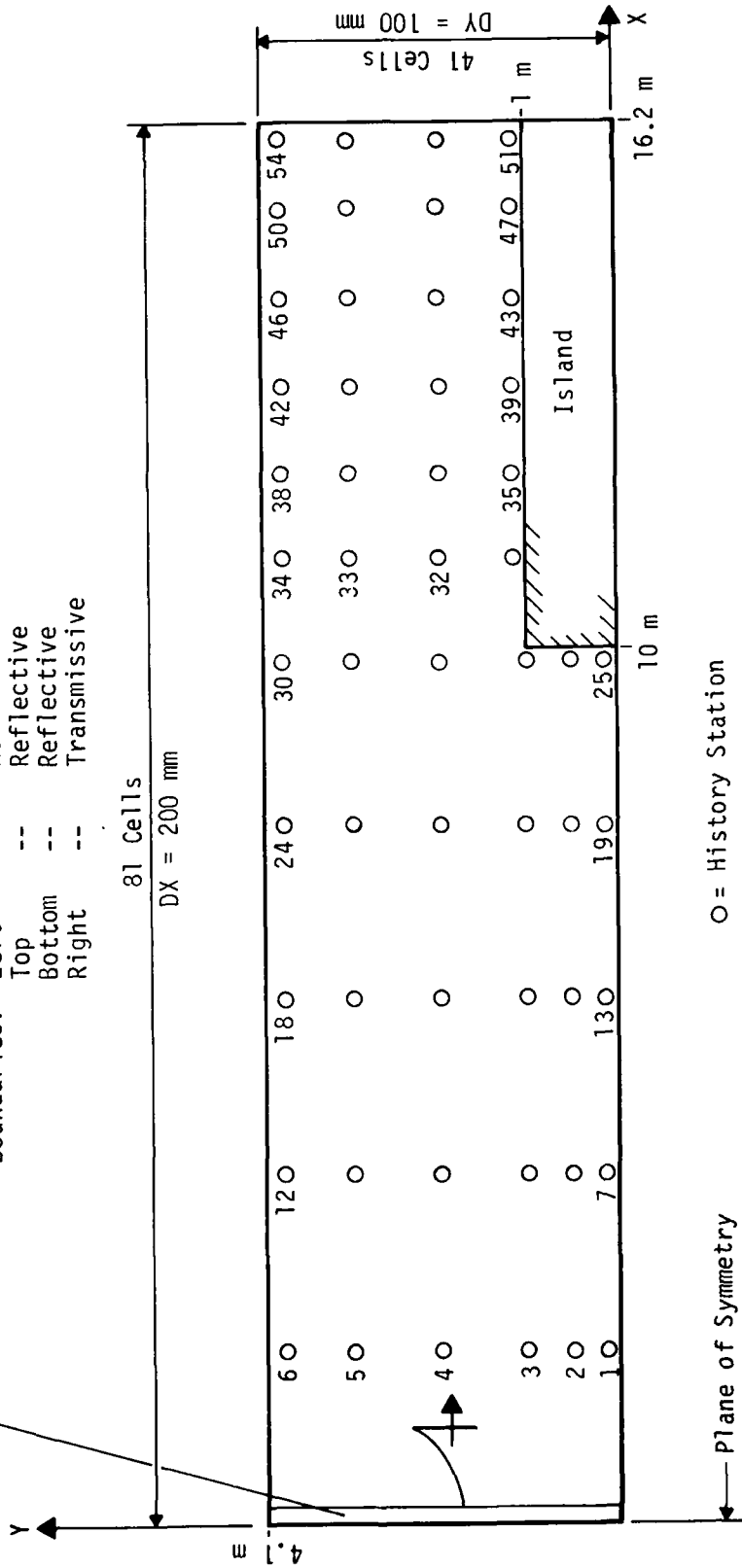


Figure 66. Axial Energy Profile at 20 ms--Calculation 906.1090

Energy Deposition = 1.195×10^9 ergs/mm² to provide 3.448 MPa peak incident pressure at the 10-m range

Boundaries: Left -- Reflective
 Top -- Reflective
 Bottom -- Reflective
 Right -- Transmissive



O = History Station

Plane of Symmetry

Figure 67. Simulation Model--HULL Calculation 908.0010

The explosive driver was located at the closed end of the tunnel (plane of symmetry) and was initially configured as being 200 mm thick from floor to ceiling. The open end of the tunnel is simulated with a transmissive boundary which is 16 m from the plane of symmetry. The rectangular target structure is modeled by a 1- by 6-m "island" (a region of the mesh which is filled with a motionless fluid of infinite strength). In short all tunnel and structure surfaces are modeled as perfectly rigid material interfaces (i.e., perfectly reflective).

The instantaneous release of explosive energy was simulated by a one-time deposition between the second and third calculational cycles. This energy deposition was made in the column of cells adjacent to the plane of symmetry and corresponds to a planar energy density of 1.195×10^9 ergs/mm².

The energy deposition was chosen to generate a blast wave which would deliver a peak incident pressure of approximately 3.448 MPa at a range corresponding to the vertical front face of the target structure (10 m). Dimensions for the tunnel as well as the position of the structure were patterned after the HAVE HOST S-1 experiment.

This model is essentially analogous to the case for a nonuniform (decaying) shock where the front is overtaken by a rarefaction which remains in contact indefinitely. When the instantaneous energy deposition is made, the closed end of the tunnel (plane of symmetry) for all practical purposes represents a piston which has suddenly stopped. This, of course, gives rise to an expansion wave which at 0.2 ms (the approximate shock arrival time at 2 m) has already overtaken and begun to erode the primary shock. By the time the shock has reached the target structure (10 m) the peak incident pressure has decayed to 3.73 MPa. This calculated rate of decay compares quite well with the analytical solution (Fig. 68) where the shock strength is inversely proportional to the square root of time.

The shock wave impinges on the structure front face at normal incidence and results in a calculated peak reflected pressure at the base (Station 25) of

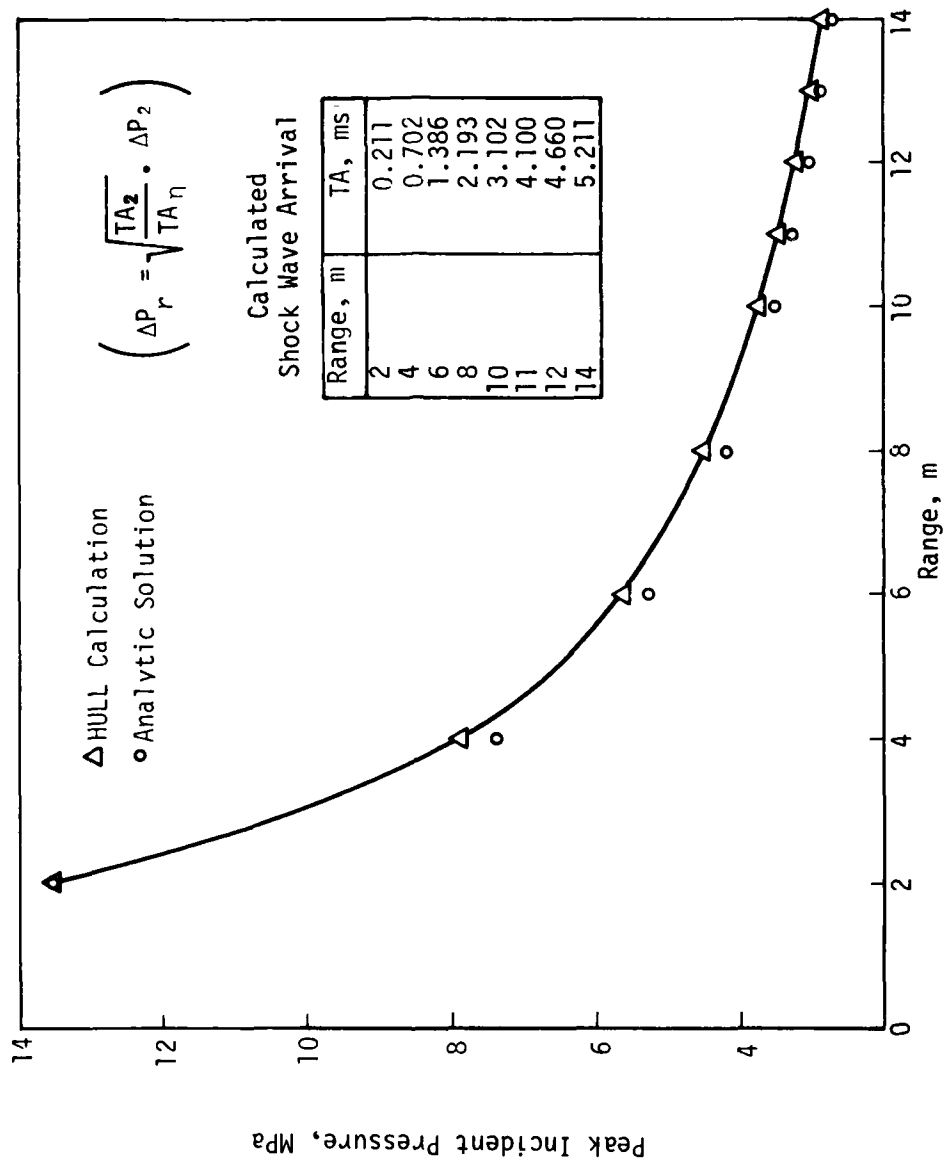


Figure 68. Incident Pressure versus Range

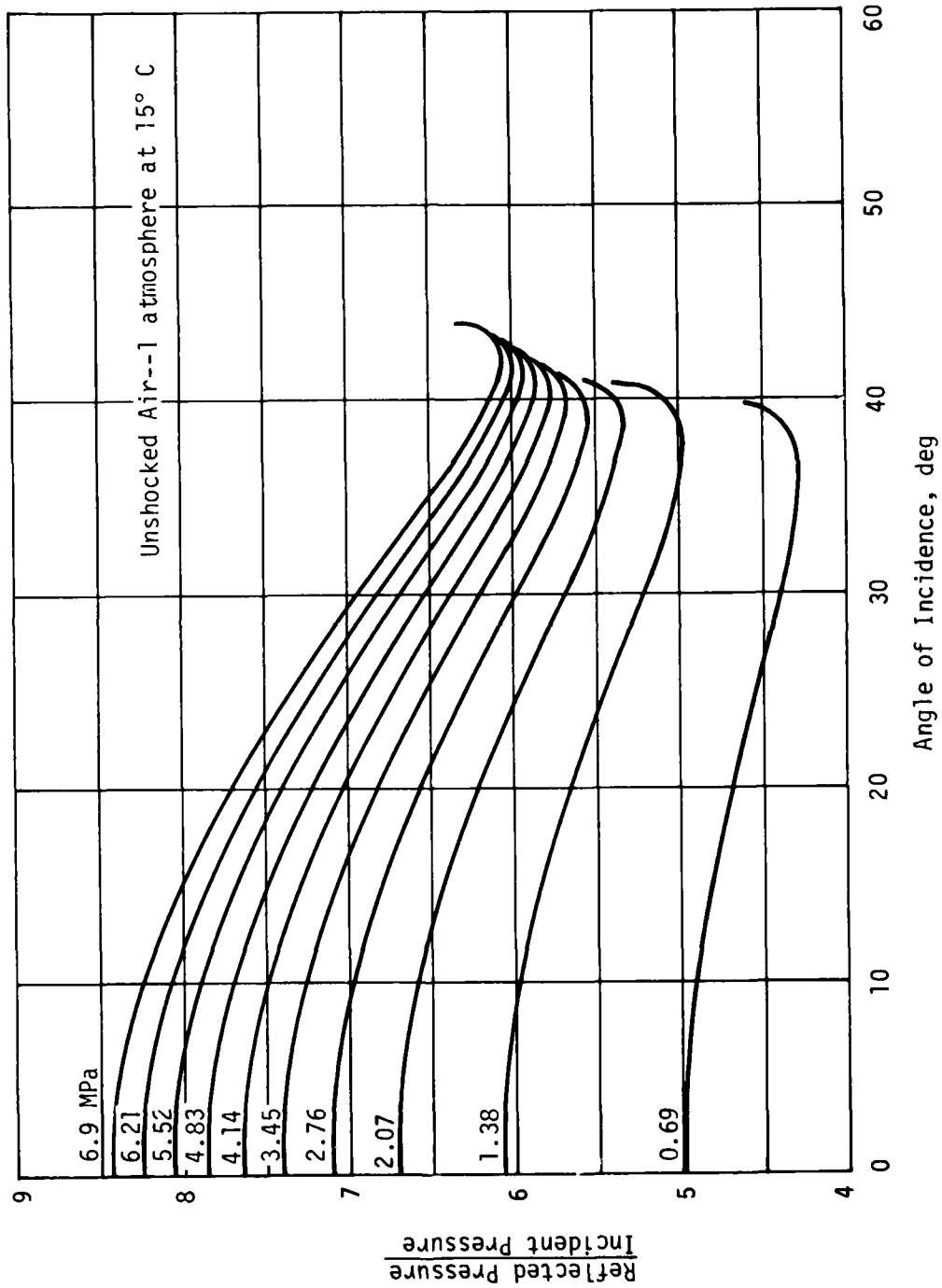


Figure 69. Reflected Pressure Ratio versus Angle of Incidence for Various Incident Pressures

23.1 MPa. This corresponds to a peak pressure ratio of 6.2 as opposed to a more analytically exact value of 7.5 (Fig. 69).* This discrepancy is believed due principally to the unrealistic prescription of properties behind the shock front. The arbitrary deposition of energy can give rise to momentum and thermodynamic states which are not appropriate for shocks in real air.

Diffraction of the planar blast wave is accompanied by a rarefaction which propagates downward from the top corner of the front face of the target structure. As a result reflected peak pressures on this surface are significantly attenuated. For example, the calculated peak at the corner (Station 27) was 13 MPa or nearly 43 percent less than the value recorded at floor level. At a height of 450 mm (Station 26) a peak of 21.6 MPa was observed. This gradient is due in large measure to the pseudoviscous damping of the relatively coarse mesh (200- by 100-mm cells). Rise times of approximately 0.5 ms permit significant erosion of reflections at this surface (Fig. 70).

As the blast continues to engulf the structure, heated fluid from the high-pressure region in front of the structure flows upward to develop a secondary oblique shock wave which impinges on the tunnel roof at approximately 6.2 ms (Fig. 71a). The resulting reflected shock arrives at the top surface of the structure at approximately 8.5 ms (Fig. 71b). Peak reflected pressures at this surface range from 71 to 82 percent of the incident peaks (Fig. 72).

The simplistic model used for this calculation precludes all but a qualitative evaluation of results. Some real-world conditions and phenomena that could significantly affect the solution which were not considered are

1. Explosive materials and processes
2. Soils and structure strains
3. Three-dimensional (side) effects

Of particular interest in DABS tests is the likelihood and extent of target structure loadings which are due solely to the proximity of interior tunnel

* Chown, W. H., "Calculation of Regular Reflection of Oblique Shocks Using the AFWL Equation of State for Air," Internal Memorandum to Lt. Col. J. J. Osborn, Air Force Weapons Laboratory, Kirtland Air Force Base, New Mexico, September 7, 1973.

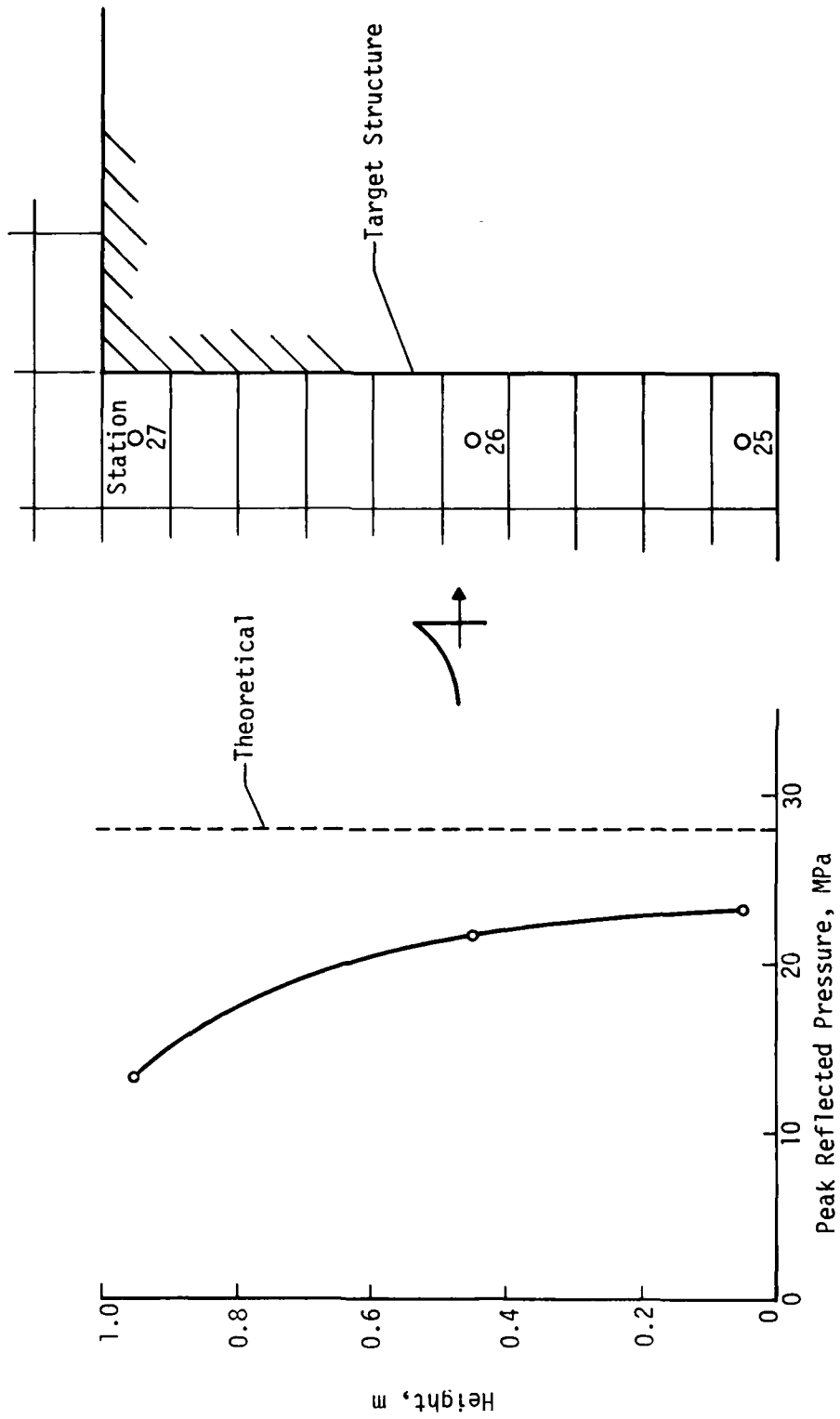


Figure 70. Normal Reflections at Front Face of Target Structure

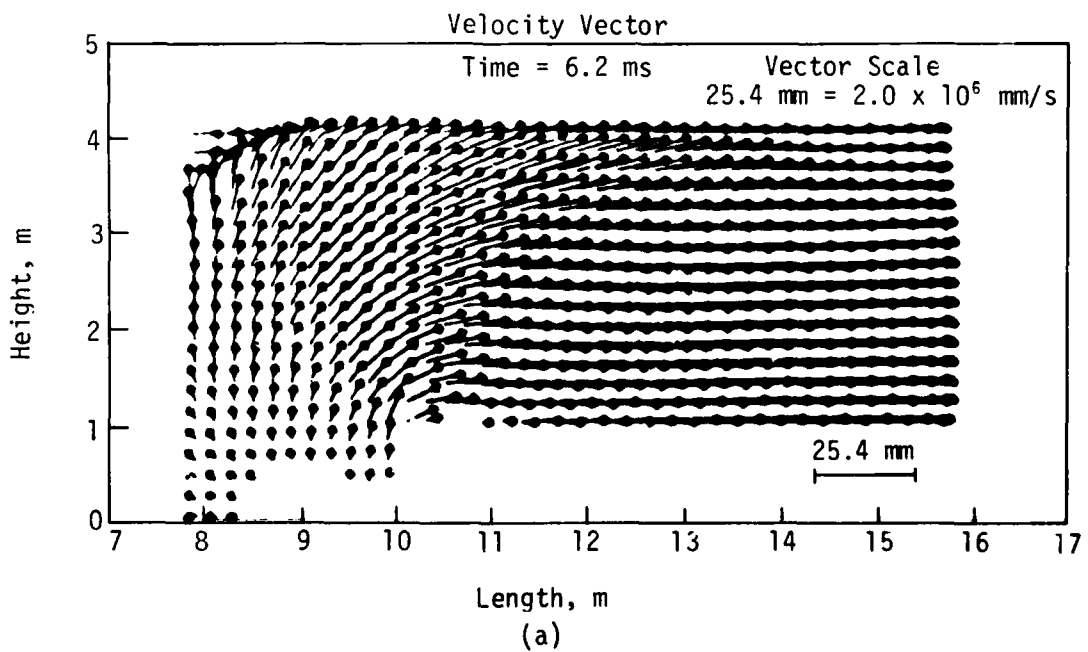
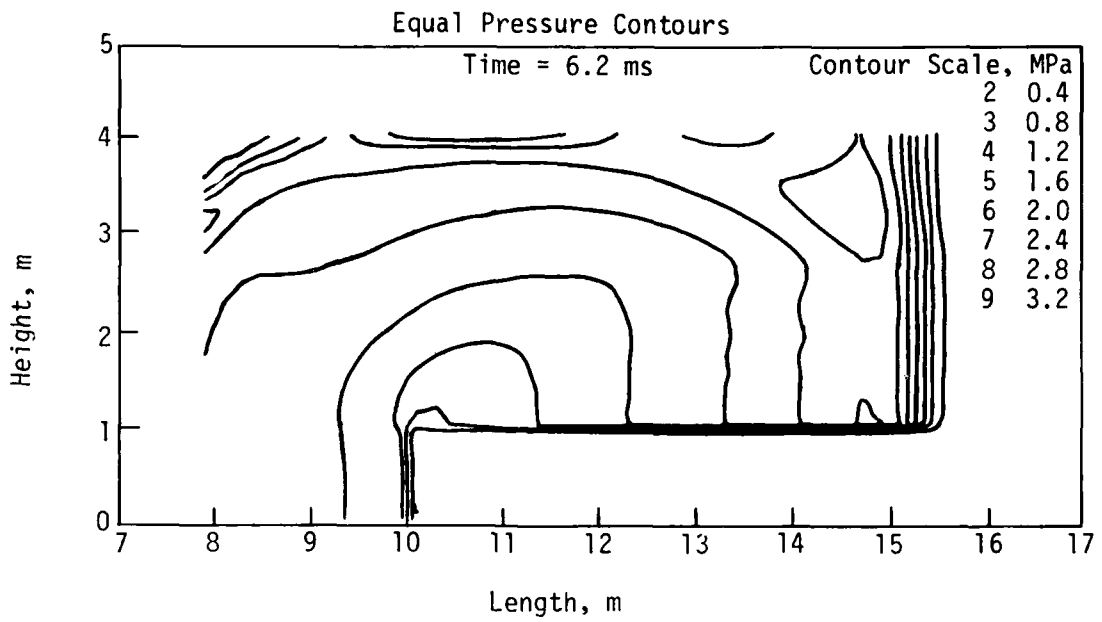


Figure 71. HULL Simulation--DABS Parameter Study
(Calculation 908.0010) (1 of 2)

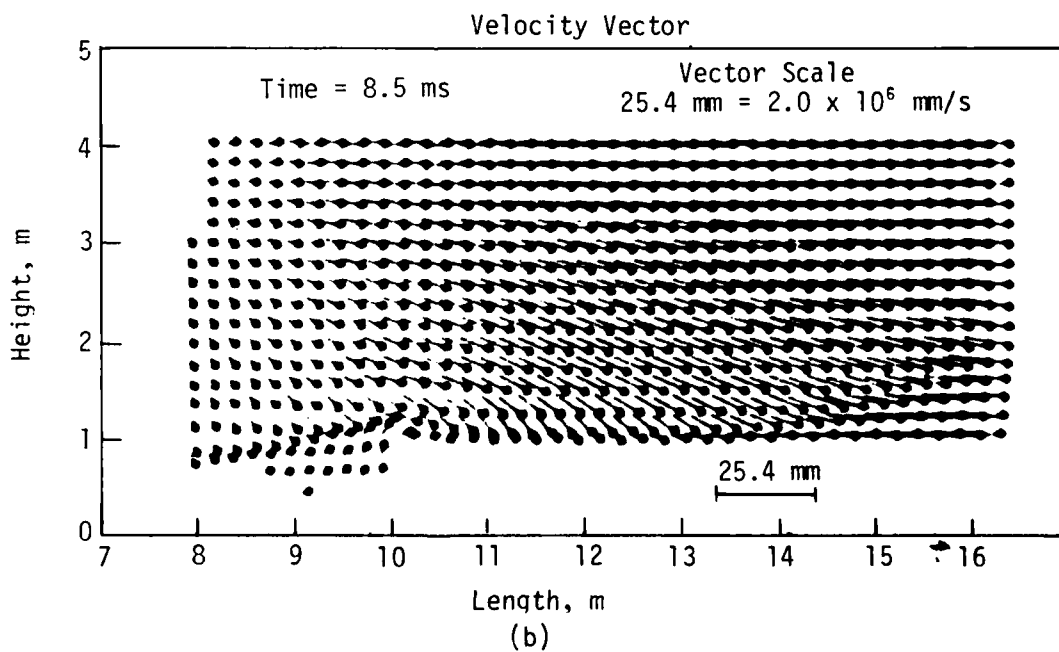
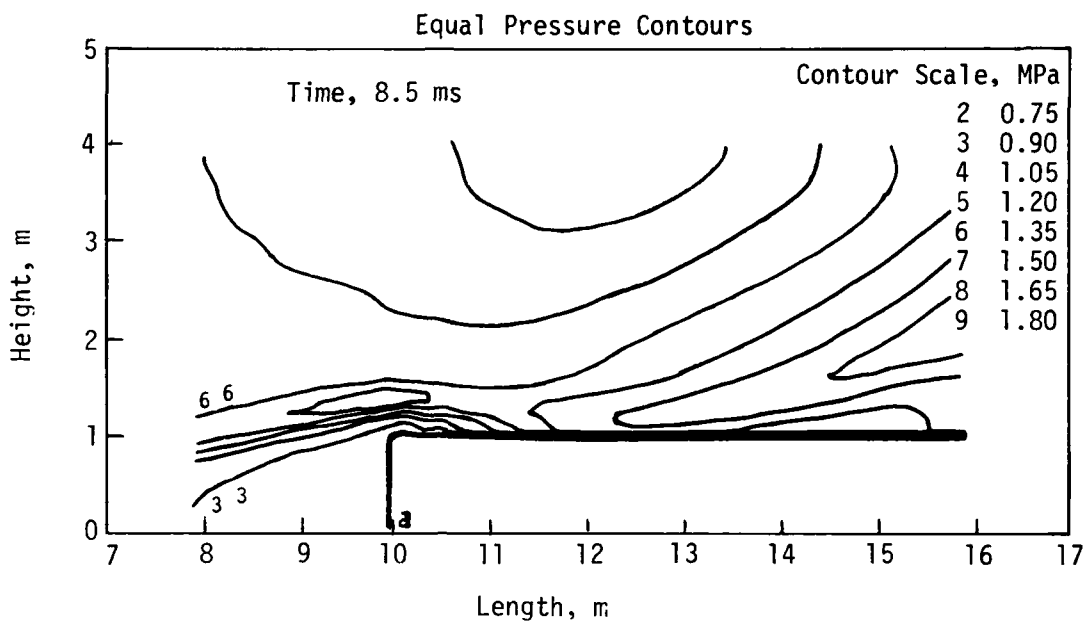


Figure 71. HULL Simulation--DABS Parameter Study
(Calculation 908.0010) (2 of 2)

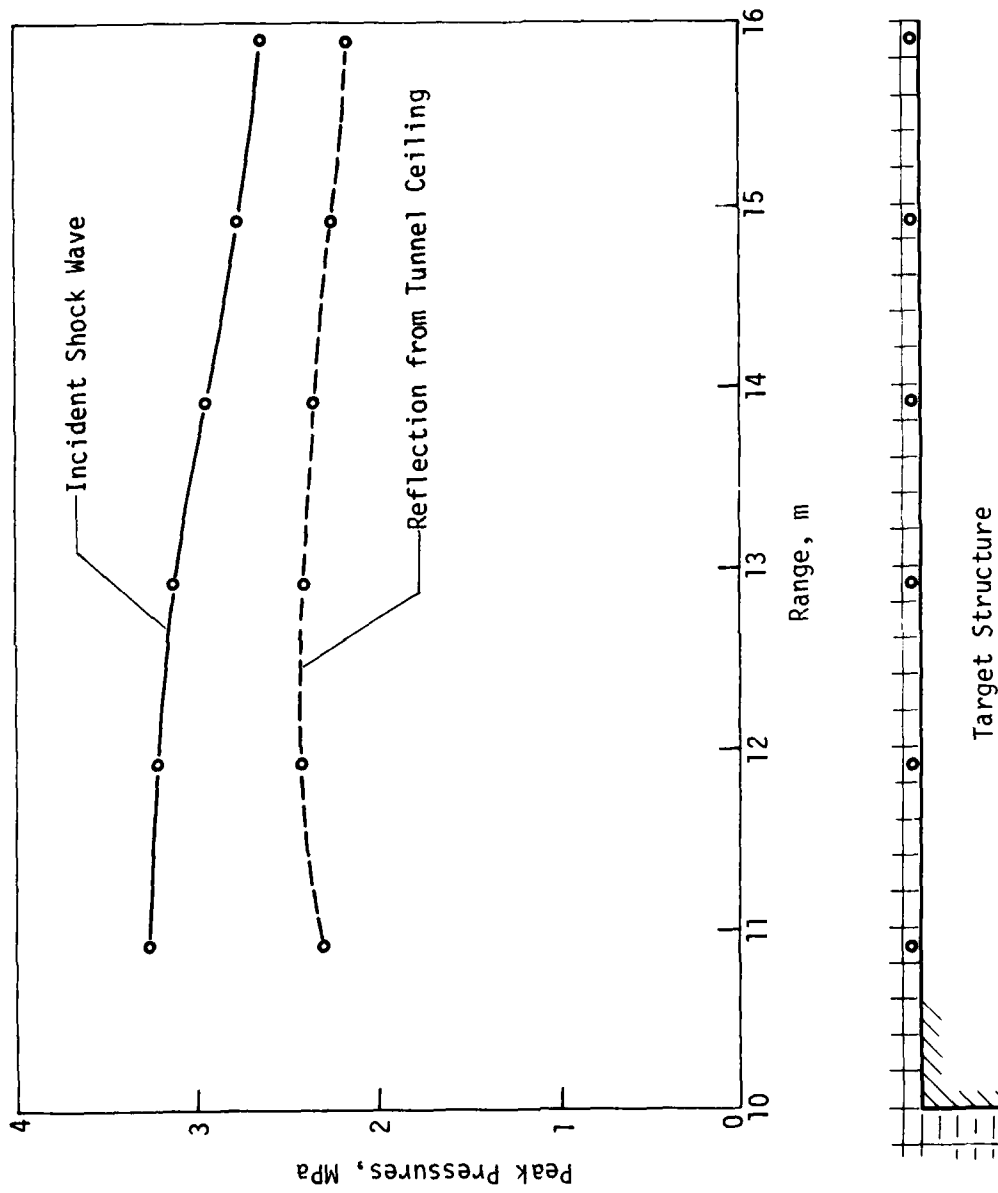


Figure 72. Peak Pressures at Top of Target Structure

surfaces. On the presumption that in actuality dimensional changes during the diffraction phase are minimal this solution indicates that reflected shocks within such a test facility may contribute substantially to the airblast environment. Reflections from the tunnel ceiling have caused repressurizations at the top of the target structure which correspond to impulse load increases in the neighborhood of 20 percent.

The low peak reflected pressures obtained with this numerical simulation suggest that other characteristics of the solution may not provide a reliable data base for establishing design parameters. It is recommended that the model specifications be revised to more realistically represent the experimental environment insofar as is practical. In addition to refining the material models and soil-air interface behavior a significantly finer mesh may be necessary.

SECTION V CONCLUSIONS AND RECOMMENDATIONS

The state of the art in modeling explosive simulation experiments with hydrodynamic computer codes has advanced markedly during the past several years. Several calculational tools are available ranging from simple 1-D similarity solutions to complex 2-D Eulerian hydrocodes with a variety of geometries and boundary conditions.

Methods for modeling the HEST simulator have increased the qualitative understanding of the complex explosion mechanisms and shock interactions which occur within the HEST explosion cavity. HEST designers can now use these calculational tools to better understand where to place explosive arrays and instrumentation for improved HEST performance. For example, the most uniform and widely dispersed arrangement of the explosive material that is practical should be used when designing a HEST explosion cavity. Instruments should be placed at locations which avoid the shock focusing effects from individual strands of detonating cord.

Quantitative HEST prediction models will require the use of an equation of state for the plastic foam materials used to form the HEST explosion cavity (which is currently under development) and a more precise means for modeling the release of explosive energy into the HEST explosion cavity. "Burn" models are not currently available for either detonating cord or for ammonium nitrate-based "slurry" explosives. The use of an isothermal energy deposition has proven to be quantitatively inadequate as a means of modeling explosion processes. It can, however, be used for the qualitative evaluation of such parameters as geometrical effects, shock reflections from various structures, boundary conditions, and so on.

The DABS simulator can be realistically modeled using the above mentioned calculational tools. Again, as in HEST, quantitative predictions must await the development of accurate "burn" routines for the nonidealized explosive materials used for the DABS driver. Qualitative calculations, however, are very useful for describing the shock interaction with downstream target

structures. Calculated peak pressures and shock rise times are quite dependent on the cell sizes used. Increasing the number of cells, however, substantially increases the cost of the calculation. The prudent selection of cell size and/or mesh rezoning for a proposed calculation is essential.

Computer costs for hydrocode calculations of explosive simulation tests can range from \$10 to \$120 for 1-D calculations and from \$100 to \$1000 for 2-D calculations although more complex 2-D problems can be encountered which may cost many times this amount. These relatively low costs would indicate the practicality of increased computer calculations and modeling for the design, prediction, and analysis of nuclear airblast simulation experiments which use high explosives.

Recommendations for future work include the development of equations of state and "burn" routines for the nonideal explosive materials involved in simulator explosion processes. Specific calculations of well-defined and controlled experiments will be required to validate these improvements. The continuation of the development of the 1 1/2-D version of SAP should be given high priority so calculations of problems having nearly 1-D geometry can be calculated without long and costly 2-D computations. Finally, calculations of specific explosive configurations currently being used in the ongoing research in nuclear blast simulator technology should be accomplished using the appropriate calculational tools to provide guidance to designers of simulation experiments.

REFERENCES

1. Auld, H. E., D'Arcy, G. P., and Leigh, G. G., *Simulation of Airblast-Induced Ground Motions (Phase I)*, AFWL-TR-65-11, Air Force Weapons Laboratory, Kirtland Air Force Base, New Mexico, April 1965.
2. Auld, H. E., D'Arcy, G. P., and Leigh, G. G., *Simulation of Airblast-Induced Ground Motions (Phase II)*, AFWL-TR-65-26, Vol. I, Air Force Weapons Laboratory, Kirtland Air Force Base, New Mexico, April 1965.
3. Martens, Daniel P., and Bradshaw, Joel C., *Dynamic Airblast Simulator Parametric Test Series, Events I-A, I-B, I-C, I-D, and I-E Data Report*, AFWL-TR-76-018, Air Force Weapons Laboratory, Kirtland Air Force Base, New Mexico, November 1976.
4. Bratton, J. L., and Pratt, H. R., *Simulation of Airblast-Induced Ground Motions (Phase III)*, AFWL-TR-66-85, Air Force Weapons Laboratory, Kirtland Air Force Base, New Mexico, October 1967.
5. Sakurai, A., "On the Propagation and Structure of the Blast Wave, I," *Journal of the Physical Society of Japan*, Vol. 8, No. 5, September-October 1953.
6. Richtmyer, Robert D., and Morton, K. W., *Difference Methods for Initial-Value Problems*, 2nd Edition, Interscience Publishers.
7. Whitaker, W. A., et al., *Theoretical Calculations of the Phenomenology of HE Detonations*, AFWL-TR-66-141, Vol. 1, Air Force Weapons Laboratory, Kirtland Air Force Base, New Mexico, November 1966.
8. Graham, D. C., Gaby, L. P., II, and Rhoades, C. E., Jr., *SAIL, An Automated Approach to Software Development and Management*, AFWL-TR-77-78-80, Air Force Weapons Laboratory, Kirtland Air Force Base, New Mexico, October 1976.
9. Fry, M. A., et al., *The HMLE Hydrodynamics Computer Code*, AFWL-TR-66-183, Air Force Weapons Laboratory, Kirtland Air Force Base, New Mexico, September 1976.
10. Hilsenrath, J., Green, M. S., and Beckett, C. W., *Thermodynamic Properties of Highly-Ionized Air*, SWC-TR-56-35, National Bureau of Standards, Washington, DC, April 1957.
11. Doan, L. R., and Nickel, G. H., *A Subroutine for the Equation of State of Air*, RTD (WLR) TM-63-2, Air Force Weapons Laboratory, Kirtland Air Force Base, New Mexico, May 1963.
12. Needham, C. E., *Development of an Artificial Viscosity Function*, AFWL-TR-77-53, Air Force Weapons Laboratory, Kirtland Air Force Base, New Mexico, August 1977.
13. Gagnon, L. W., *HEST Over Rectangular Slab (HORS)--Phase I*, AFWL-TR-78-238, Air Force Weapons Laboratory, Kirtland Air Force Base, New Mexico, March 1979.
14. Kinney, G. F., *Explosive Shocks in Air*, McMillan, p. 57, 1962.
15. Courant and Friedrichs, *Supersonic Flow and Shock Waves*, Interscience Publishers, New York, pp. 334-335, 1948.

REFERENCES (Concluded)

16. Liepman, H. W., and Roshko, A., *Elements of Gas Dynamics*, Wiley, 1957.
17. Bradley, J. N., *Shock Waves in Chemistry and Physics*, Wiley, pp. 103-104, 1962.
18. Glass, I. I., and Hall, J. G., *Handbook of Supersonic Aerodynamics* Vol. 6, Section 18, NAVORD Report 1488, pp. 81-101, December 1959.
19. Needham, C. E., *Nuclear Blast Standard (1 kt)*, AFWL-TR-73-55 (Rev.), Air Force Weapons Laboratory, Kirtland Air Force Base, New Mexico, 1975.

APPENDIX A
COMPUTER LISTING OF ONE-DIMENSIONAL SIMILARITY SOLUTION
PROGRAM FOR A PLANAR BLAST WAVE PROBLEM
(BASIC LANGUAGE)

```

1000 PAGE
1010 IMAGE 16T, 25A, 4E
1020 IMAGE 16T, 25A, 6D, 3D, 4A
1030 IMAGE 16T, 24A, 5E, 12A
1040 IMAGE 2X, 3A, 5X, 3(1A, 6X), 1X, 6A, 10X, 3A, 9X, 9A
1050 IMAGE 1X, 1D, 2D, 3(2X, 1D, 4D), 3(2X, 4E)
1060 IMAGE 25T, 80A
1065 IMAGE 4T, 24A, 4D, 3D, 3A
1070 IMAGE 4D, 9D, 9D, 14D, 14D, 14D, 14D, 14D
1080 IMAGE 4T, 23A, 4E, 16A
1090 IMAGE 4T, 34A, 4D, 4D
1100 IMAGE 4T, 34A, 3D, 4D
1110 IMAGE 4T, 24A, 2D, 3D, 16A
1120 PRINT USING 1060: "PLANAR BLAST WAVE PROBLEMJJ"
1125 PRINT " ";
1128 PRINT P2
1130 INPUT " ";
1140 INPUT E1
1150 INPUT " ";
1160 INPUT X1
1170 INPUT " ";
1180 INPUT G1
1190 INPUT R1
1200 INPUT " ";
1230 INPUT N
1250 INPUT " ";
1260 DELETE T
1270 DIM T(N)
1280 FOR J=1 TO N
1290 PRINT "J ";
1300 INPUT T(J)
1310 NEXT J
1330 DELETE D

```

THE ENERGY PER UNIT AREA IN ERGS PER SQ CM= " ;
THE DIMENSIONLESS PARAMETER JO= " ;
THE RATIO OF SPECIFIC HEATS = " ;
THE INITIAL DENSITY IN GM PER CUBIC CM= " ;
THE NUMBER OF TIMES= " ;
PLEASE INPUT TIMES IN INCREASING ORDER"

```

1340 DIM D(N,6)
1350 DELETE P1
1360 DIM P1(N,6)
1370 PAGE
1380 I=1
1390 PRINT USING 1060:"PLANAR BLAST WAVE PROBLEMJJJ"
1395 PRINT USING 1065:"THE PROBLEM NUMBER IS ",P2,"J"
1400 PRINT USING 1090:"THE ENERGY PER AREA IS ",E1," ERGS PER SQ CMJ"
1410 PRINT USING 1090:"THE DIMENSIONLESS PARAMETER JO IS ",X1
1420 PRINT USING 1100:"THE RATIO OF SPECIFIC HEATS IS ",G1
1430 PRINT USING 1110:"THE INITIAL DENSITY IS ",R1," GM PER CUBIC CM"
1440 T1=T(I)
1450 PRINT USING 1010:"JJJJTHE PROBLEM TIME IS ",T1
1460 W1=9*T1*T1*E1*G1
1470 W2=8*X1*R1
1480 W3=W1/W2
1490 B=1/3
1500 R=W3*B
1510 W4=E1*G1
1520 W5=2*X1*R*R1
1530 B1=1/2
1540 U1=(W4/W5)*B1
1550 PRINT USING 1020:"JSHOCK FRONT RADIUS IS ",R," CMJ"
1560 PRINT USING 1030:"SHOCK FRONT VELOCITY IS ",U1," CM PER SECJ"
1570 E2=1
1580 R2=E2*R
1590 E2=E2+1.0E-3
1600 IF E2-1<0 THEN 1650
1610 F=0.8333
1620 G=1.167
1630 H=6
1640 GO TO 1880
1650 IF E2-0.8<0 THEN 1700
1660 F=0.611
1670 G=0.631

```

```

1680 H=1.766
1690 GO TO 1880
1700 IF E2-0.6<0 THEN 1750
1710 F=0.437
1720 G=0.496
1730 H=0.669
1740 GO TO 1880
1750 IF E2-0.4<0 THEN 1800
1760 F=0.2866
1770 G=0.461
1780 H=0.225
1790 GO TO 1880
1800 IF E2-0.2<0 THEN 1850
1810 F=0.143
1820 G=0.455
1830 H=0.039
1840 GO TO 1860
1850 F=0
1860 G=0.455
1870 H=0
1880 U=U1*F
1890 R3=R1*H
1900 P=E1*G/(2*R1*R)
1910 IF E2-1<0 THEN 1930
1920 PRINT USING 1040:"ETA","F","G","H","RADIUS","VEL","PRESSURE"
1930 PRINT USING 1050:E2,F,G,H,R2,U,P
1950 L=E2*5+1
1960 D(I,L)=R2
1970 P(I,L)=P
1980 E2=E2-1.0E-3
1990 E2=E2-0.2
2000 IF E2+1.0E-4=>0 THEN 1580
2010 I=I+1
2020 IF I-N-1<0 THEN 1440
2024 PRINT " JDO YOU WANT A GRAPH?; YES=1,N=0";

```

```

2026 INPUT G2
2030 IF G2=0 THEN 2830
2040 PAGE
2050 VIEWPORT 20,110,20,75
2060 F1=P1(N,1)
2070 F2=INT(LGT(F1))
2080 N2=10↑F2
2090 N3=10↑(INT(LGT(P1(1,6))) + 1)
2093 IF D(N,6) > 100 THEN 2100
2095 A1=(INT(D(N,6)/10)+1)*10
2097 GO TO 2110
2100 A1=(INT(D(N,6)/100)+1)*100
2110 WINDOW 0,A1,LGT(N2),LGT(N3)
2120 REMARK DRAW AXIS LINES
2130 AXIS 1000,0
2140 REM DRAW VERTICAL AXIS WITH LOG SCALE
2150 T2=A1*0.01
2160 H=LGT(N2)
2170 FOR I=10↑H TO 10↑(H+1) STEP 10↑H
2180 MOVE 0,LGT(I)
2190 DRAW T2,LGT(I)
2200 NEXT I
2210 H=H+1
2220 IF H<LGT(N3) THEN 2170
2230 T3=(LGT(N3)-LGT(N2))*0.02
2232 IF D(N,6) > 100 THEN 2240
2234 H=10
2236 GO TO 2250
2240 H=100
2250 MOVE H,LGT(N2)
2260 DRAW H,T3+LGT(N2)
2262 IF H=100 THEN 2270
2264 H=H+10
2266 GO TO 2280
2270 H=H+100

```


APPENDIX B
HYDROCODE CALCULATION DATA
REPORTS PRODUCED DURING THIS
TECHNICAL EFFORT

TABLE B-1. HYDROCODE CALCULATION DATA REPORTS PRODUCED DURING THIS TECHNICAL EFFORT

Calculation number	UNM/CERF report number	Hydrocode	Problem modeled	Features
905.0050	AST-33	HULL	HEST explosion cavity	Single explosive plane/real air
905.0021	AST-34	SAP		Single explosive plane/ideal gas
905.0020	AST-35			Single explosive plane/ideal gas
906.1090	AST-36		Shock tunnel	Normal reflection of 600 lb/in ² shock
906.0040	AST-37		Sample shock tube	Diffusion limitation evaluation
906.0040	AST-39			Modified detonating cord pattern
905.0060	AST-40	HULL	HEST explosion cavity	Modified detonating cord pattern with buffer zone
905.0090	AST-41			Modified detonating cord pattern with buffer zone
908.0010	AST-42		DABS test facility	Airblast loading on typical target structure
905.0030	AST-43		HEST explosion cavity	Basic detonating cord pattern
905.0070	AST-43		HEST explosion cavity	Basic detonating cord pattern
908.0011				
908.0021				
908.0031				
908.0041	AST-44			
908.0051		SAP	Shock tunnel	Parametric study of blast wave characteristics as a function of cell size and charge density.
908.0061				
908.0051				

TABLE B-1. CONTINUED.

Calculation number	UNM/CERF report number	Hydrocode	Problem modeled	Features
905.0010	AST-35	HULL	HEST explosion cavity	Single explosive plane
905.0020				Single explosive plane with γ -law equation of state
905.0030				Single explosive plane with γ -law equation of state
905.0021	SAP--Eulerian	Single explosive plane with heavy gas boundary		
905.0022	APOD--Lagrangian	Single explosive plane with heavy gas boundary		
905.0031	AST-22	SAP--Eulerian		Single explosive plane with heavy gas boundary
905.0041	AST-21			Single explosive plane with heavy gas boundary
905.0041	AST-23			Single explosive plane with real air equation of state
905.0051	AST-24			Single explosive plane with real air equation of state
905.1080	AST-25	HULL		Sweeping wave with transmissive entry
906.1010	AST-29	HULL	Sweeping wave with reflective entry	
906.1011	AST-30	SAP--Lagrangian	Incident wave	
906.1020	AST-38	HULL	Sweeping wave with transmissive entry	
906.1021	AST-30	SAP--Lagrangian	HAVE HOST T-series	Incident wave
906.1031				HEST explosive cavity
906.1041				Incident wave
906.1051				Incident wave
906.1061				Incident wave
906.1061				Incident wave
906.1071				Incident wave

TALBE B-1. CONCLUDED.

Calculation number	UNM/CERF report number	Hydrocode	Problem modeled	Features
906.1081	AST-26	SAP--Lagrangian	HAVE HOST T-series	Incident wave with energy deposit
906.1081	AST-26			Reflected wave with energy deposit
906.5081	AST-28			Incident wave with burn

APPENDIX C
PROGRAM SHOK2B

OUTLINE FOR PROGRAM SHOK2B
SHOCK TUBE INTERIOR BALLISTICS

Note: Region subscripts refer to Figure 56.

Given: $P_1, P_4, \rho_1, \rho_4, \epsilon_1, \epsilon_4, T_1, T_4,$ and TIME

1. Solve for $\gamma_1, \gamma_2, a_1, a_4$

$$\text{where } \gamma = \frac{P}{\rho \epsilon} + 1$$

$$a = \sqrt{\frac{(\gamma P)}{\rho}}$$

2. Iterative solution* for P_2

$$\text{where } \frac{P_4}{P_1} = \frac{P_2}{P_1} \left[1 - \frac{(\gamma_4 - 1) \left(\frac{a_1}{a_4}\right) \left(\frac{P_2}{P_1} - 1\right)}{\sqrt{2\gamma_1} \cdot \sqrt{2\gamma_1 + (\gamma_1 + 1) \left(\frac{P_2}{P_1} - 1\right)}} \right]^{\frac{-2\gamma_4}{(\gamma_4 - 1)}}$$

3. Complete solution for states in Regions 2 and 3

$$\text{where } P_3 = P_2$$

$$U_1 = U_4 = 0$$

$$U_2 = U_3 = \left[\frac{2a_4}{(\gamma_4 - 1)} \right] \left[1 - \left(\frac{P_3}{P_4}\right) \frac{(\gamma_4 - 1)}{\gamma_4} \right]$$

$$\rho_3 = \rho_4 \left(\frac{P_3}{P_4}\right)^{\frac{1}{\gamma_4}}$$

*Iuzzolino, H.J., "Subroutine ZEROIN," Air Force Weapons Laboratory, Kirtland Air Force Base, New Mexico, September 1970.

$$\rho_2 = \rho_1 \left(\frac{1 + \left[\frac{P_2 (\gamma_1 + 1)}{P_1 (\gamma_1 - 1)} \right]}{\left(\frac{\gamma_1 + 1}{\gamma_1 - 1} \right) + \frac{P_2}{P_1}} \right)$$

$$T_3 = T_4 \left[\frac{\left(\frac{P_2}{P_1} \right)}{\left(\frac{P_4}{P_1} \right)} \right] \frac{(\gamma_4 - 1)}{\gamma_4}$$

$$T = \frac{T P}{P} \left[\frac{\left(\frac{\nu_1 - 1}{\nu_1 + 1} \right) + \frac{P_1}{P_2}}{1 + \frac{P_1 (\nu_1 - 1)}{P_2 (\nu_1 + 1)}} \right]$$

$$a_3 = a_4 \cdot \sqrt{\frac{T_3}{T_4}}$$

$$a_2 = a_1 \cdot \sqrt{\frac{T_2}{T_1}}$$

Assume $\gamma_2 = \gamma_1$ and $\gamma_3 = \gamma_4$

$$\epsilon_2 = \frac{P_2}{[(\gamma_2 - 1) \rho_2]}$$

$$\epsilon_3 = \frac{P_3}{[(\gamma_3 - 1) \rho_3]}$$

4. Solve for primary shock speed and position

where $C_S = a_1 \sqrt{\left[\frac{(\gamma_1 - 1)}{2\gamma_1} \right] + \left[\frac{P_2 (\gamma_1 + 1)}{2 P_1 \gamma_1} \right]}$

$$X_S = C_S \cdot \text{TIME}$$

5. Solve for position of contact surface

$$\text{where } X_c = U_2 \cdot \text{TIME}$$

6. Solve for position of head and tail of expansion wave

$$\text{where } X_t = \left[(\gamma_+ + 1) \left(\frac{U_2}{2} \right) - a_+ \right] \cdot \text{TIME}$$

```

PROGRAM SHOK2B (INPUT, OUTPUT)
COMMON F(4),G(4),A(4),D(4),T(4),E(4),U(4)
EXTERNAL FN
TIME=.003
P(4)=1.F8 $ D(4)=2.665E-3 $ E(4)=5.6E10 $ T(4)=1782.
P(1)=1.F6 $ D(1)=1.225E-3 $ E(1)=2.0675E9 $ T(1)=295.
G(1)=G(2)=P(1)/(E(1)*E(1))+1.
G(3)=G(4)=P(4)/(D(4)*T(4))+1.
A(4)=SQRT(G(4)*P(4)/D(4))
A(1)=SQRT(G(1)*P(1)/D(1))
RE=2. $ AE=1.E-5 $ X=0. $ Y=P(4)
CALL ZERCIN(X,Y,FN,PE,AF,IFL)
IF(IFL.NE.0)STOP 77
P(2)=P(3)=X
U(1)=U(4)=0.
U(2)=U(3)=(2.*A(4)/(G(4)-1.))*((1.-(P(3)/P(4)))*((G(4)-1.)/
+ (2.*G(4))))
D(3)=D(4)*(P(3)/P(4))*((1./G(4))
D(2)=D(1)*((1.+(G(1)+1.)/(G(1)-1.))*((P(2)/P(1)))/
+ ((G(1)+1.)/(G(1)-1.))+((P(2)/P(1))))
E(2)=P(2)/((G(2)-1.)*D(2))
E(3)=P(3)/((G(3)-1.)*D(3))
T(3)=T(4)*((P(2)/P(1))/(P(4)/P(1)))*((G(4)-1.)/G(4))
T(2)=T(1)*((1.+(G(1)-1.)/(G(1)+1.))*((P(2)/P(1)))/
+ (1.+(G(1)-1.)/(G(1)+1.))*((P(1)/P(2))))
A(3)=A(4)*SQRT(T(3)/T(4))
A(2)=A(1)*SQRT(T(2)/T(1))
PRINT1
1 FORMAT(1H1,15X,8PPRESSURE,10X,5HGAMMA,4X,11HSOUND SPEED,5X,
+ 7HDENSITY,4X,11HTEMPERATURE,7X,8HVELOCITY,9X,6HENERGY)
2 FORMAT(/110,7E15.6)
CS=A(1)*SQRT((G(1)-1.)/(2.*G(1) + ((G(1)+1.)/(2.*G(1))*((P(2)/
+ P(1)))))
XS=CS*TIME
XC=J(2)*TIME
XRT=((G(4)+1.)*U(2)/2.)-A(4)*TIME
XRH=-A(4)*TIME
3 FORMAT(/14X,11HSHOCK SPEED,13X,2HXS,13X,2HXC,12X,3HXRT,12X,3HXRH)

```

```
PRINT 3
PRINT 4,CS,XS,XC,XRT,XRH
4 FORMAT(/10X,5E15.5)
END
```

```
FUNCTION FN(X)
COMMON P(4),G(4),A(4),D(4),T(4),E(4),U(4)
PWR=-2.*G(4)/(G(4)-1.)
FN=X*(1.-((G(4)-1.)*(A(1)/A(4))*(X/P(1)-1.)))/
+ (SQRT(2.*G(1))*SQRT(2.*G(1)+(G(1)+1.)*(X/P(1)-1.)))
+ **PWR-P(4)
RETURN
END
```

```

SUBROUTINE ZEROIN(X,Y,F,RE,AE,IFLAG)
LATEST CHANGE -- 21 SEPTEMBER 1970.
THE STATEMENT 'EXTERNAL F' MUST APPEAR IN THE CALLING PROGRAM.
RE=RELATIVE ERROR. AE=ABSOLUTE ERROR. CANNOT TAKE AE=0 IF THE
ORIGIN IS IN THE INTERVAL (X,Y).
IFLAG=0 IF ROOT CALCULATED, =1 IF NO ROOT FOUND IN INTERVAL,
=-1 IF TOO MANY FUNCTION EVALUATIONS.
THE FUNCTION SIGN(A1,A2) EQUALS ABS(A1) TIMES SIGN OF A2.

```

```

INITIALIZE

```

```

A=X
FA=F(X)
X=Y
B=Y
FB=F(B)
KOUNT=2
NANS=0

```

```

SET UP INTERPCLATION HERE.

```

```

1 C=A
FC=FA

```

```

SET UP EXTRAPOLATION HERE.
C,B BRACKET A ROOT. TEST AND INTERCHANGE IF NECESSARY TO MAKE FB
.LE. FC SC B IS THE BETTER APPROXIMATION.

```

```

2 IF(ABS(FC).LT.ABS(FB)) GO TO 20

```

```

TEST WHETHER FINISHED.

```

```

3 TOL=RE*ABS(X)+AE
AVG=(C+B)*0.5
IF(ABS(AVG-B).LE.TOL) GO TO 21

```

```

C
C
C
C
C
C
C
C
C
C
C
C
C
C
C

```

```

C
C
C

```

```

C
C
C
C
C

```

```

C
C
C

```

```

C C CALCULATE NEW ITERATE IMPLICITLY AS B+P/Q WHERE WE ARRANGE P.GE.0.
C C IMPLICIT FORM IS USED TO PREVENT OVERFLOW.
C C
P=(B-A)*FB
IF(P.GE.0.0) GO TO 4
Q=FB-FA
P=-P
GC TO 5
4 Q=FA-FB
C C UPDATE A
C C
5 A=B
FA=FB
TEST FOR TOO SMALL A CHANGE.
IF(P.LE.ABS(Q)*TCL) GC TO 10
ROOT OUGHT TO BE BETWEEN AVG AND B.
IF(P.LT.(AVG-B)*Q) GC TO 11
IF NOT BETWEEN, USE AVG.
B=AVG
LBL=7HAVERAGE
6 X=B
FB=F(X)
KOUNT=KOUNT+1
NANS=NANS+1
PRINT 500, NANS, LBL, B, FB
FCRMT(115,9X,AB,E27.20,E16.4)
IF (FB .EQ. 0.) GO TO 21
IF(KOUNT.GT.500) GO TO 23
C C DECIDE WHETHER NEXT STEP IS INTERPOLATION OR EXTRAPCLATION.
C C
IF(SIGN(1.0,FB).EQ.SIGN(1.0,FC)) GO TO 1

```

```

C      GO TO 2
C      REJECT CHANGES THAT ARE TOO SMALL.
C
10  P=SIGN(TOL,C-B)+B
    IFL=8HMIN STEP
    GO TO 6
C
C      HERE FOR NORMAL EXTRAPOLATION.
C
11  B=P/Q+B
    LEL=6HSECANT
    GO TO 6
C
C      INTERCHANGE C AND B, ALSO SET NEW A=NEW C.
C
20  A=B
    FA=FB
    B=C
    X=R
    FB=FC
    C=A
    FC=FA
    GO TO 3
C
C      HERE WHEN FINISHED. SET IFLAG.
C
21  Y=C
    IF(FB*FC.GT.0.0) GO TO 22
    IFLAG=0
    RETURN
22  IFLAG=1
    RETURN
23  IFLAG=-1
    Y=C
    RETURN
    END

```

DISTRIBUTION LIST

Assistant to the Secy. of Def.
Atomic Energy
Washington, D.C. 20301
(D. Cotter)
(ATSD (AE))

Undersecretary of Def. For Rsch. & Engrg.
Washington, D.C. 20301
(S and SS (OS))
(AD/SW)

Def. Advanced Rsch. Proj. Agency
1400 Wilson Blvd., Arlington, VA 22209
(Tech. Lib.)
(PMO)
(STO)
(G. Bulin)
(Director)

Defense Tech. Info. Ctr.
Alexandria, VA 22314
12 cy (DDRE)

Defense Intelligence Agency
Washington, D.C. 20301
(DT)
(DI-7E)
(A. Alexander)
(DI-AST-3)

Defense Nuclear Agency
Washington, D.C. 20305
(STSP)
(TITL)
(SPSS, G. Ullrich)
(SPSS, B. Swedock)

Field Command, Defense Nuclear Agency
Kirtland AFB, NM 87115
(FCT)
(FCTMD, B. Bestgen)
(FCTMC, B. Ristvet)

Field Command, Defense Nuclear Agency
Livermore Div., Livermore, CA 94550
(FCPRI)

Interservice Nuclear Wpns. School
Kirtland AFB, NM 87115
(Document Control)

Joint Strat. Tgt. Planning Staff
Offutt AFB, Omaha, NB 68113
(STINFO Library)

Weapon Systems Eval. Group
Washington, D.C. 20305
(Document Control)

HQ USAF, Washington D.C. 20330
(INATA)
(PRE)
(PREV)
(RDPQ)
(RDPQN)
(RDQSM)
(SAFAL, H. Cooper)

AFESC, Tyndall AFB, FL 32403
(RDCF, J. Hawn)

HQ, AFSC, Andrews AFB, Washington, D.C.
20334
(DLW)
(DLCAW)
(Tech. Lib.)

AFWL, Kirtland AFB, NM 87117
(SUL)
(NTE, M. Plamondon)
(NTESB)
(NTES, R. Henny)
(NTED, Lt Williams, Off. Record Cy.)
(NTY)
(HO, R. Minge)

HQ Space Div., P.O. Box 92060, Worldway
Postal Ctr., Los Angeles, CA 90009
(XRTB)

BMO, Norton AFB, CA 92409
(MNNH, M. Delveccio)
(MNNH, D. Gage)

HQ Space Div., P.O. Box 92060, Worldway
Postal Ctr., Los Angeles, CA 90009
(DYS)

Foreign Technology Div., Wright-Patterson
AFB, OH 45433
(NICD Library)

AFML, Wright-Patterson AFB, OH 45433
(Tech. Lib.)

AF Geophysics Lab., Hanscom AFB, MA 01731
(SUOL Rsch. Lib.)

AF Tech. Appl. Ctr, Patrick AFB, FL 32925
(TAP)
(B. Webster)

AF Off. of Sci. Rsch., Bolling AFB, DC 20332
(L. Ormend)
(W. Best)

AF Inst. of Tech., Wright-Patterson AFB,
OH 45433
(Library)

AU, Maxwell AFB, AL 36112
(AUL/LDE)

Vela Seismological Ctr., DAF, 312 Montgomery
St., Alexandria, VA 22314
(W. Ullrich)

USAF Academy, Colorado Springs, CO 80840
(DFSLB)

DCS for Rsch., Dev., & Acq., DA, Washington,
DC 20310
(Tech. Lib.)

Chief of Engrs., DA, Washington, DC 20314
(DAEN-RDM)
(DAEN-MCE-D)

DCS for Ops. & Plans, DA, Washington, DC
20310
(Tech. Lib.)

NATO School (SHAPE), APO New York, NY 09172
(U.S. Documents Officer)

Harry Diamond Labs., DA, Adelphi, MD 20783
(DELHD-NP)
(DELHD-TI)

U.S. Army Engr. Waterways Exper. Sta.
Vicksburg, MS 39180
(Tech. Lib.)
(J. Jackson)
(L. Ingram)
(W. Flathau)
(R. Walker)

U.S. Army Mat. & Mechanics Rsch. Ctr.
Watertown, MA 02172
(Tech. Lib.)

U.S. Army Engr. Ctr., Ft. Belvoir, VA 22060
(ATSEN-SY-L)

U.S. Army Mat. Dev. & Readiness Cmd.
Alexandria, VA 22333
(Tech. Lib.)

U.S. Army Nuclear & Chem. Agency
Springfield, VA 22150
(Library)
(W. Simms.)

U.S. Army Comb. Arms Comb. Dev. Acty.
Ft. Leavenworth, KS 66027
(G. Steger)

BMD Advanced Tech. Ctr., Huntsville, AL 35807
(CRDABH-S)
(ICRDABH-X)

Redstone Scientific Info. Ctr., U.S. Army
Missile Cmd., Redstone Arsenal, AL 35809
(Ch., Documents)

U.S. Army Ballistic Rsch. Labs., Aberdeen
Proving Ground, MD 21005
(E. Baicy)
(W. Taylor)
(J. Keefer)

U.S. Army Engr. Div., Huntsville, AL 35807
(HNDED-SR)

U.S. Army Engr. Div., Ohio River, Cincinnati,
OH 45201
(Tech. Lib.)

U.S. Army Mobility Equip. R&D Ctr.
Ft. Belvoir, VA 22060
(Tech. Lib.)

U.S. Army Training & Doctrine Cmd., Ft. Monroe
Ft. Monroe, VA 23651
(K. Auveduti)

U.S. Army Mat. Cmd., Dover, NJ 07801
(DRCPM-NUC)

Department of the Army, Washington, DC 20315
(Ch. of Eng. (ENGMC-EM))

Chief of Naval Material, Washington, DC 20360
(MAT 0323)

Chief of Naval Ops., Washington, DC 20350
(OP 981)

Chief of Naval Research, Arlington, VA 22217
(N. Perrone)
(Tech. Lib.)

Civil Engineering Lab., Naval Construction
Battalion Ctr., Port Hueneme, CA 93041
(S. Takahashi)
(Tech. Lib.)

David W. Taylor Naval Ship R&D Ctr.
Bethesda, MD 20084
(Library)

Naval Facilities Engr. Cmd.
Washington, DC 20390
(Tech. Lib.)
(Code 04R)
(Code 03A)

Naval Postgraduate School, Monterey, CA
93904
(Tech. Lib.)

Naval Research Laboratory, Washington, DC
20375
(Tech. Lib.)

Naval Ship Engr. Ctr., Washington, DC 20362
(Tech. Lib.)

Naval Surface Weapons Center
Silver Spring, MD 20910
(Navy Nuc. Prgms.)

Naval Surface Weapons Center
Dahlgren, VA 22448
(Tech. Lib.)

Naval Weapons Evaluation Facility
Kirtland AFB, NM 87117
(Tech. Lib.)

NWO (Code 753), China Lake, CA 93557
(Tech. Lib.)

Strategic Systems Project Office, Dept. of
the Navy, Washington, DC 20376
(Tech. Lib.)

Development Center, Fire Support Branch
Dept. of the Navy, Quantico, VA 22134
(L. Gapenski)

Naval Ship R&D Center, Bethesda, MD 20084
(Library)

Naval Ship R&D Ctr., Underwater Explosive
Rsch. Div., Portsmouth, VA 23709
(Tech. Lib.)

Office of Naval Rsch. Branch Office
Pasadena, CA 91101
(E. Weinburg)

Department of Energy, Div. of Hq. Services
Lib. Br. G-043, Washington, DC 20545
(Class. Tech. Lib.)

Department of Energy, Nevada Operations
Office, Las Vegas, NV 89114
(Tech. Lib.)

Department of Energy, Albuquerque Ops. Off.
Albuquerque, NM 87115
(Class. Tech. Lib.)

Oak Ridge National Laboratory, Oak Ridge,
TN 37830
(Tech. Lib.)

Sandia National Laboratories, Kirtland AFB,
NM 87185
(Info. Dist. Div.)
(L. Vortman)

Sandia National Laboratories, Livermore
Laboratory, Livermore, CA 94550
(Tech. Lib.)

Lawrence Livermore National Laboratory
Livermore, CA 94550
(Tech. Info. Dept. L-3)
(M. Nordyke)

Los Alamos National Scientific Laboratory
Los Alamos, NM 87545
(Reports Lib.)
(G. Stillman)

Central Intelligence Agency
Washington, DC 20505
(J. Ingley)

Dept. of the Interior, Bureau of Mines
Denver, CO 80225
(Tech. Lib.)
(L. Obert)

U.S. Geological Survey, Washington, DC 20244
(E. Chao)

U.S. Geological Survey, Menlo Park, CA 94025
(E. Jackson)

U.S. Geological Survey, Flagstaff, AZ 86001
(D. Roddy)

Aerospace Corp., Los Angeles, CA 90009 (Tech. Info. Services)	IIT Research Institute, Chicago, IL 60616 (Tech. Lib.)
Agabian Associates, El Segundo, CA 90245 (M. Agabian)	Kaman AvIDyne, Burlington, MA 01803 (F. Criscione)
Applied Theory, Inc., Los Angeles, CA 90024 (J. Trulio)	Kaman Sci. Corp., Colorado Springs, CO 80933 (Lib.)
BDM Corp., Albuquerque, NM 87119 (J. Leach)	Karagozian and Case, Los Angeles, CA 90042 (Lib.)
BDM Corp., McLean, VA 22101 (Tech. Lib.)	Lockheed Missiles and Space Co., Inc. Sunnyvale, CA 94088 (Tech. Lib.)
Boeing Co., Seattle, WA 98124 (Aerospace Lib.) (B. Dyrdaahl)	Lockheed Missiles and Space Co., Inc. Palo Alto, CA 94304 (T. Geers)
California Research and Tech., Inc. Woodland Hills, CA 91364 (Tech. Lib.) (K. Kreyenhagen)	McDonnell Douglas, Huntington Beach, CA 92647 (R. Halprin)
Civil Systems, Inc., Albuquerque, NM 87110 (J. Bratton)	Merritt CASES, Inc., Redlands, CA 92373 (J. Merritt)
Civil Systems, Inc., Midland, TX 79702 (S. Melzer)	Mission Research Corp., Santa Barbara, CA 93101 (C. Longmire)
University of Denver, Colorado Seminary Denver, CO 80210 (J. Wisotski)	Nathan M. Newmark, Consult. Engrg. Services University of Illinois, Urbana, IL 61801 (N. Newmark)
General American Trans. Corp., Niles, IL 60648 (M. Balcerzak)	Pacific-Sierra Research Corp., Santa Monica, Ca 90404 (H. Brode)
GE-TEMPO, Albuquerque, NM 87110 (L. Kennedy)	Pacifica Technology, Del Mar, CA 92014 (R. Allen)
GE-TEMPO, Center for Advanced Studies Santa Barbara, CA 93102 (J. Shoutens) (DASIAC)	Physics International Co., San Leandro, CA 94577 (Tech. Lib.) (F. Sauer)
Higgins, Auld and Assoc., Albuquerque, NM 87112 (N. Higgins)	Rand Corp, Santa Monica, CA 90406 (Tech. Lib.)
J. H. Wiggins Co., Redondo Beach, CA 90277 (J. Collins)	R & D Associates, Marina Del Rey, CA 90291 (R. Port) (J. Lewis) (J. Carpenter)

Science Applications, Inc., La Jolla, CA
92038

(Tech. Lib.)

Science Applications, Inc., Mc Lean, VA
22102

(J. Cockyane)

Southwest Research Institute, San Antonio,
TX 78284

(W. Baker)

SRI International, Menlo Park, CA 94025

(Tech. Lib.)

(B. Gasten)

Systems, Science and Software, Inc.
La Jolla, CA 92038

(T. Cherry)

(Tech. Lib.)

Teledyne Brown Engineering (SETAC)

Huntsville, AL 35807

(M. Patel)

Terra Tek, Inc., Salt Lake City, UT 84108

(Tech. Lib.)

Tetra Tech., Inc., Pasadena, CA 91107

(Tech. Lib.)

University of Illinois, Champaign, IL 61820

(S. Hendron)

TRW Defense and Space Sys. Group
Redondo Beach, CA 90278

(B. Sussholtz)

(P. Dai)

(N. Lipner)

(Tech. Info. Center)

TRW Defense and Space Systems Group, San
Bernardino Ops., San Bernardino, CA 92402

(B. Fay)

(G. Hulcher)

University of Oklahoma, Dept. of Info. and
Computing Science, Norman, OK 73069

(J. Thompson)

Eric H. Wang, Civil Engineering Rsch. Fac.
Albuquerque, NM 87131

(N. Baum)

(J. Berglund)

(G. Leigh)

(D. Calhoun)

Weidlinger Assoc. Consulting Engrs.

New York, NY 10022

(M. Baron)

Weidlinger Assoc. Consulting Engrs.

Menlo Park, CA 94025

(J. Isenberg)